

# ECOLE POLYTECHNIQUE FÉDÉRALE DE LAUSANNE

## MASTER THESIS

---

# Evaluation of Optical Aberrations using Phase Diversity

---

*Author:*  
Jordan VOIRIN

*Supervisors:*  
Dr. Laurent JOLISSAINT  
Dr. Jean-Paul KNEIB

*A thesis submitted in fulfillment of the requirements  
for the degree of Master in Applied Physics*

*in the*

**Astrophysics laboratory  
Basic Sciences**

March 15, 2018



## Declaration of Authorship

I, Jordan VOIRIN, declare that this thesis titled, "Evaluation of Optical Aberrations using Phase Diversity" and the work presented in it are my own. I confirm that:

- This work was done wholly or mainly while in candidature for a research degree at this University.
- Where any part of this thesis has previously been submitted for a degree or any other qualification at this University or any other institution, this has been clearly stated.
- Where I have consulted the published work of others, this is always clearly attributed.
- Where I have quoted from the work of others, the source is always given. With the exception of such quotations, this thesis is entirely my own work.
- I have acknowledged all main sources of help.
- Where the thesis is based on work done by myself jointly with others, I have made clear exactly what was done by others and what I have contributed myself.

Signed:

Date:



*"For the sake of persons of... different types, scientific truth should be presented in different forms, and should be regarded as equally scientific, whether it appears in the robust form and the vivid coloring of a physical illustration, or in the tenuity and paleness of a symbolic expression. "*

James Clerk Maxwell



ECOLE POLYTECHNIQUE FÉDÉRALE DE LAUSANNE

## *Abstract*

Physics  
Basic Sciences

Master in Applied Physics

### **Evaluation of Optical Aberrations using Phase Diversity**

by Jordan VOIRIN

This thesis deals with the aberrations present in an optical system and their corrections. Indeed, nowadays the telescopes are so big that they are limited by the Earth's atmosphere turbulence and their own defects. Sophisticated method are developed to take into account the aberrations and correct them. We study a retrieval method called phase diversity that uses the image given by the system to correct the aberrations present on the optical path.

The first part of our work is the test and use of a phase diversity algorithm developed by Mugnier, Blanc, and Idier (2006) at ONERA. The algorithm regarding the noise level in the images and the different parameters that could influence, behaves adequately. However, the usage of the phase diversity in comparison with a simulated calibrated aberration and another wavefront sensor highlighted problems with our optical bench and its simulation.

The second part presents the development and test of our phase diversity algorithm. The algorithm is based on a analytical approach unlike the ONERA phase diversity, which is based on a statistical approach. Our algorithm gives good results, however it shows a limited validity domain. A recursive approach is then proposed and tested to increase the validity domain with success up to an RMS wavefront error of  $\sim \frac{\lambda}{4}$ .

In conclusion, we tested the ONERA phase diversity algorithm successful. But its use highlighted technical problems of our setup. We then developed our own phase diversity algorithm in order to have a method that we fully understand and control. Using a recursive approach we are able to increase by a factor three the validity domain.



## *Acknowledgements*

I would first like to thank my thesis supervisor Dr. Laurent Jolissaint of the industrial automation institute at the School of Management and Engineering (HEIG-VD) of Yverdon-Les-Bains.

I would also like to thank the expert : Dr. Jean-Paul Kneib, Director of the astrophysics laboratory of the Ecole Polytechnique Federale de Lausanne (EPFL). Without his passionate participation and input, the validation survey could not have been successfully conducted.

I would also like to thank my colleagues Audrey Bouxin, Scientific collaborator at HEIG-VD and Jeremie Baudet, Scientific collaborator at HEIG-VD for their precious help and inputs during this project.

Finally, I must express my very profound gratitude to my family and to my girlfriend for providing me with unfailing support and continuous encouragement throughout my years of study and through the process of researching and writing this thesis. This accomplishment would not have been possible without them. Thank you.



# Contents

<b>Declaration of Authorship</b>	<b>iii</b>
<b>Abstract</b>	<b>vii</b>
<b>Acknowledgements</b>	<b>ix</b>
<b>Introduction</b>	<b>1</b>
<b>1 Theoretical background</b>	<b>5</b>
1.1 Scalar Diffraction Theory . . . . .	5
1.1.1 Scalar Field and Helmholtz equation . . . . .	5
1.1.2 Rayleigh-Sommerfeld integral . . . . .	5
1.1.3 Fresnel approximation . . . . .	6
1.1.4 Fraunhofer approximation . . . . .	7
1.1.5 Converging lens introduction . . . . .	7
1.2 Imaging system . . . . .	8
1.2.1 Impulse Response (IR) . . . . .	8
1.2.2 Optical Transfer Function (OTF) . . . . .	8
1.2.3 Image formation . . . . .	10
1.3 Aberrations . . . . .	11
1.3.1 Sources of aberration . . . . .	11
1.3.2 Zernike polynomials . . . . .	12
1.4 Phase retrieval . . . . .	14
1.4.1 Shack-Hartmann . . . . .	14
1.4.2 Phase Diversity . . . . .	15
<b>2 Phase Diversity Experiment</b>	<b>17</b>
2.1 ONERA algorithm . . . . .	17
2.1.1 Algorithm description . . . . .	17
2.1.2 Implementation . . . . .	18
2.2 Experimental Setup . . . . .	18
2.2.1 Light source . . . . .	19
2.2.2 Entrance pupil . . . . .	20
2.2.3 Pupil imaging system . . . . .	20
2.2.4 Detectors . . . . .	20
2.3 Data Acquisition . . . . .	20
2.3.1 Ximea Camera . . . . .	20
2.3.2 Shack-Hartmann WFS . . . . .	21
2.4 Results . . . . .	23
2.4.1 ONERA Phase Diversity test . . . . .	23
2.4.2 Parallel plane plate . . . . .	29
2.4.3 Shack-Hartmann comparison . . . . .	30
2.4.4 Discussion . . . . .	32

<b>3 Analytical phase diversity algorithm</b>	<b>35</b>
3.1 Analytical algorithm . . . . .	35
3.1.1 Algorithm description . . . . .	35
3.1.2 Implementation . . . . .	38
3.2 Results . . . . .	38
3.2.1 Algorithm test . . . . .	38
3.2.2 Recursive approach . . . . .	43
3.2.3 Discussion . . . . .	44
<b>Conclusion</b>	<b>47</b>
<b>A Python Code</b>	<b>49</b>
A.1 Phase Diversity analytical algorithm code . . . . .	49
A.1.1 phaseDiversity3PSFs.py . . . . .	49
A.1.2 fs.py . . . . .	51
A.1.3 myExceptions.py . . . . .	54
A.1.4 zernike.py . . . . .	54
A.1.5 phasor.py . . . . .	55
A.1.6 PSF.py . . . . .	56
A.2 Acquisition Code: Ximea Camera . . . . .	57
A.2.1 AlignementScriptXimeaCamera.py . . . . .	57
A.2.2 AcquisAndSaveXimea.py . . . . .	60
A.2.3 functionsXimea.py . . . . .	62
<b>B IDL Code</b>	<b>65</b>
B.1 ONERA phase diversity . . . . .	65
B.1.1 Diversity.pro . . . . .	65
B.2 Shack-Hartmann Acquisition Code . . . . .	73
B.2.1 readAndAverageSHdata.pro . . . . .	73
B.2.2 readSHWFSdata.pro . . . . .	74
<b>C Optical Component Datasheets</b>	<b>77</b>
C.1 Pigtailed laser diode . . . . .	78
C.1.1 Power supply modification . . . . .	79
C.2 Converging lens A220TM-A, f = 11 mm . . . . .	79
C.3 Pinhole 10 $\mu\text{m}$ . . . . .	81
C.4 Converging lens AL100200, f = 200 mm . . . . .	82
C.5 Converging lens AC254-100-A, f = 100 mm . . . . .	83
C.6 Ximea Camera, MQ013MG-E2 . . . . .	84
C.7 Shack-Hartmann wavefront sensor, WFS150-5C . . . . .	85
<b>Bibliography</b>	<b>87</b>

# List of Figures

1	Adaptive optics schema . . . . .	2
2	DAG 4m telescope . . . . .	3
1.1	Diffraction Schemas . . . . .	6
1.2	Schema of a imaging instrument, (Goodman, 1988, Chapter 6.1) . . . . .	8
1.3	PSF of a perfect imaging system composed by a 3.6 mm pupil and a focal length of 80 mm at a wavelength of 637.5 nm. The size, N, of the PSF is 400 pixels and the pixel size is 5.3 $\mu m$ . . . . .	9
1.4	OTF of a perfect imaging system composed by a 3.6 mm pupil and a focal length of 80 mm at a wavelength of 637.5 nm. . . . .	9
1.5	Gaussian reference sphere vs. aberrated Wavefront . . . . .	11
1.6	Comparison of perfect PSF and PSF with aberrations of an imaging system composed by a 3.6 mm pupil and a focal length of 80 mm at a wavelength of 637.5 nm. The size, N, of the PSF is 400 pixels and the pixel size is 5.3 $\mu m$ . . . . .	12
1.7	Representation of the 21 first Zernike polynomials . . . . .	13
1.8	Shack-Hartmann principle . . . . .	15
1.9	Schema of the phase diversity principle. The images from left to right are : the phase arriving on the exit pupil, the focused image and the defocused ( $2\pi$ ) image. . . . .	16
2.1	Experimental Setup Schema . . . . .	19
2.2	Wavefront curvature . . . . .	19
2.3	Source schema and pinhole effect on the beam. . . . .	20
2.4	Example of the results of an alignment procedure . . . . .	22
2.5	Shack-Hartmann Software GUI, with the beam view on the top left, the spot field in the middle and the reconstructed wavefront on the top right. . . . .	22
2.6	Noise level as a function of the number of averaging images acquired with $\sim 300 \mu s$ exposition time. The noise level is computed as the mean of the standard deviation of every pixel divided by the maximum of the focused PSF. . . . .	23
2.7	Results of the phase retrievals computed with the 25 different noise levels. The phase retrievals are done with a $j_{max} = 30$ . . . . .	24
2.8	Reconstructed wavefronts for two different numbers of averaging images, 10 and 3500, and their difference are on the first, second and third column respectively. The two first line are modal retrieval with $j_{max} = 30$ and $j_{max} = 200$ and the last line is the zonal retrieval. . . . .	26
2.9	Zernike coefficients $a_j$ as a function of $j$ for the 227 retrievals done for 231 different $j_{max}$ from 4 to 231. . . . .	27

2.10	Results of the $\Delta z$ measurement error test. The plots represent the results of the 125 phase retrievals run with all the permutations of errors, $[-2\sigma_{\Delta z}, -1\sigma_{\Delta z}, 0, 1\sigma_{\Delta z}, 2\sigma_{\Delta z}]$ with $\sigma_{\Delta z} = 5e-3$ mm, on the three PSFs position $\Delta z$ . . . . .	27
2.11	Zemax simulation of our optical system with the parallel plane plate introducing astigmatism. . . . .	28
2.12	Plexiglas parallel plane plate used to introduce calibrated aberrations. The width is equal to 14 mm and the refractive index is $n = 1.49$ . . . . .	28
2.13	Zernike coefficient of the vertical astigmatism $a_6$ as a function of the angle of the plexiglas parallel plane plate. The dashed line correspond to the Zemax simulation result, the blue line to the modal retrieval method, the red line to the zonal retrieval and the green line to the Shack-Hartmann reconstruction . . . . .	29
2.14	Zernike coefficient of the horizontal coma $a_8$ as a function of the angle of the plexiglas parallel plane plate. The dashed line correspond to the Zemax simulation result, the blue line to the modal retrieval method , the red line to the zonal retrieval and the green line to the Shack-Hartmann reconstruction. . . . .	30
2.15	Phase screen introduction. . . . .	31
2.16	Zernike coefficients retrieved as a function of $j$ . The red and blue lines correspond to the zonal and modal retrieval method respectively. The black line represent the Shack-Hartmann results. $j_{min} = 4$ and $j_{max} = 66$ . . . . .	31
2.17	Reconstructed wavefront by the Modal and Zonal method of the phase diversity on 66 Zernike mode on the first line and reconstructed wavefront by the Shack-Hartmann on 66 mode as well, on the second line. . . . .	32
3.1	Example of simulated phases and their PSFs to test the analytical algorithm, $j_{min} = 4$ and $j_{max} = 30$ . On the phases plot, first line, the image is not entirely shown, only from pixel 132 to 268 out of 400 pixels, for clarity. The PSFs are zoomed x10 (pixels 180 to 220) in order to be able to compare the spots. From left to right the PSFs are the defocused one, $-\delta\phi$ , the focused one and the other defocused one, $\delta\phi$ . The wavefront RMS error is set to 30 nm. The imaging system simulates the one we have on the optical bench composed by a 3.6 mm pupil and a focal length of 80 mm at a wavelength of 637.5 nm. The size, $N$ , of the PSF is 400 and the pixel size is $5.3 \mu m$ . . . . .	39
3.2	Zernike coefficient $a_j$ in nm as a function of $j$ . The blue line represents the true $a_j$ 's and the red line the retrieved ones. The phase and the 3 PSFs used to run the retrieval are the ones presented in Figure 3.1. $j_{min} = 4$ and $j_{max} = 30$ . . . . .	39
3.3	Zernike coefficient $a_j$ in nm as a function of $j$ . The blue thick line represents the true $a_j$ 's, the wavefront has a RMS error of 30 nm. The other lines are the retrieved Zernike coefficients with different $j_{max}$ values. . . . .	41
3.4	Noise study results. Noise level is 0.001. The wavefront RMS error is 30 nm. . . . .	42
3.5	Validity domain study results. . . . .	42

3.6 Zernike coefficient as a function of $j$ . The thick blue line represents the true $a_j$ 's, the dashed line the retrieved ones after the 6 iterations. The other coloured thin lines represent the retrieved coefficient at each iteration. . . . .	43
3.7 Results of the recursive approach . . . . .	44
C.1 LED driver . . . . .	80



# List of Abbreviations

<b>CCD</b>	Charge-Coupled Device
<b>CMOS</b>	Complementary Metal–Oxide–Semiconductor
<b>DAG</b>	Dogu Anadolu Gozlemevi, Eastern Anatolia Observatory
<b>ELT</b>	Extremly Large Telescope
<b>FWHM</b>	Full Width Half Maximum
<b>GUI</b>	Graphic User Interface
<b>HEIG-VD</b>	Haute Ecole d'Ingénierie et de Gestion du canton de Vaud School of Management and Engineering
<b>IR</b>	Impulse Response
<b>JMAP</b>	Joint Maximum <i>A Posteriori</i>
<b>NCPA</b>	Non Common Path Aberration
<b>ONERA</b>	Office Nationale d'Etude et de Recherche Aerospatiale French National Aerospace Research Center
<b>OTF</b>	Optical Transfer Function
<b>P2V</b>	Peak To Valley
<b>PSF</b>	Point Spread Function
<b>RMS</b>	Root Mean Square
<b>RMSE</b>	Root Mean Square Error
<b>VLT</b>	Very Large Telescope
<b>WFS</b>	WaveFront Sensor



# Introduction

This master thesis treats one of the major challenges in astronomy and in optics in general, the aberrations and their corrections. We will study and develop a method to identify the static aberrations present in an optical system using the data produced by it.

Ground based observation is as old as the first men. But since the Galilei Galileo telescope in 1609, the resolution power of the telescopes is far greater. Many inventions lead to the construction of the largest telescope ever built, the Very Large Telescope (VLT). Now that we are able to build enormous telescopes with mirror diameter up to 8m, soon to be bitten by the Extremely Large Telescope (ELT) with its 18m primary mirror diameter, the limitation of the resolution is not the diameter anymore, but the inhomogeneities of the Earth's atmosphere. Indeed, the turbulence present in the atmosphere creates a turbulent distribution of refractive index due to the distribution of temperature principally. This alters the optical path of the light through the atmosphere which finally deteriorates the images given by the telescope.

In the 1980's, systems to correct aberrations in telescopes called an active optics system were developed. It consists of actuators placed under the telescope mirrors capable of correcting the telescope deformation due to the effect of wind, temperature, gravity, vibration, etc... Those systems works at around 1 Hz , which is not fast enough to correct for the turbulence of the atmosphere (100-1000 Hz) but they are essential in the construction of large telescopes. The state-of-the-art technique is the adaptive optics, developed to take into account the effects of the atmosphere. This technique monitors the aberrations present in the wavefront and corrects them in real time. The schema of principle is shown in Figure 1. It uses a wavefront sensor to characterize its deformation and then passes the information to a deformable mirror to correct it. It is called an adaptive optic loop. It works well, but the drawback of this method is that it does not correct the aberrations up to the scientific detector. Those uncorrected aberrations are called Non-Common Path Aberration (NCPA), they are generally static or slowly evolving over time. The adaptive optic also requires a complex optical system before the scientific detector. The beam is split in two parts. One arm goes to the scientific detector and the other is used in the adaptive optic loop.

We present here a method called phase diversity that uses images of the scientific detector to deduct the aberrations present in the wavefront. In our case, the phase diversity is used to correct the static aberrations that deform the wavefront. Our work is inspired by the phase diversity idea that was first introduced by Gonsalves (1982). The idea is to use one focused and one defocused image to retrieve the aberrations. Two images at least are needed due to the property of light acquisition. There is an indetermination, because the detector is only sensitive to the intensity of light and not the light wave itself. This indetermination is raised adding a phase diversity. Unlike adaptive optic system, the phase diversity requires nearly no additional optical component depending on how it is implemented. The final aim of

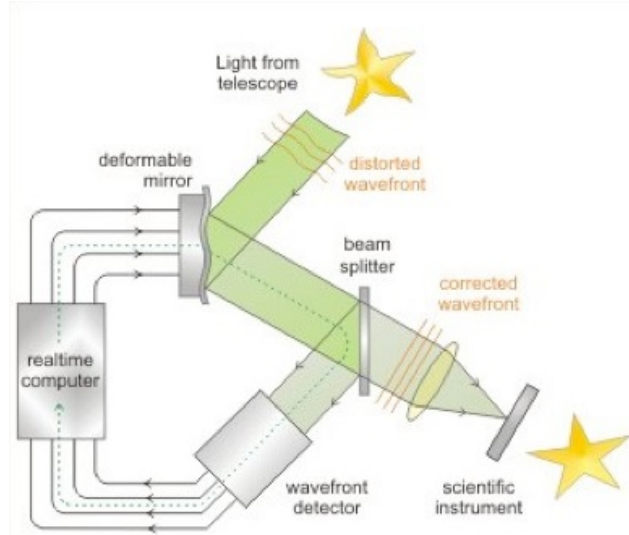


FIGURE 1: Adaptive optics schema  
source : Institut National of Astrophysics, Bologna Observatory, 2018,  
<http://www.bo.astro.it/ter5/ter5/ao.html>.

this project would be to integrate the developed phase diversity into the design of the DAG (Dogu Anadolu Gozlemevi) telescope in Turkey, see Figure 2.

This report is organized in three main chapters. First, a review of the necessary theoretical background is reminded, going from the scalar theory of diffraction to the description of phase retrievals methods. Then we present an experiment performed at the optic laboratory at HEIG-VD. The ONERA (Office National d'Etudes et de Recherches Aerospatiales) algorithm of phase diversity is tested and used in comparison with a Shack-Hartmann wavefront sensor. And finally, the development of an analytical phase diversity algorithm is presented and tested with simulated Point Spread Functions (PSFs).

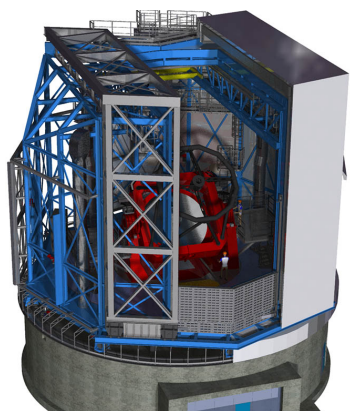


FIGURE 2: DAG 4m telescope  
source : EIE group, 2018,  
<http://www.eie.it/en/progetti/dag-dogu-anadolu-gozlemevi>.



## Chapter 1

# Theoretical background

In this chapter, the basic theory of our work is presented. First, the light propagation formalism is reminded through the scalar diffraction theory based on the book written by Goodman (1988). Then the general properties of an imaging system are described. And finally we present the wavefront aberration theory and two different methods to identify and correct the aberrations.

## 1.1 Scalar Diffraction Theory

### 1.1.1 Scalar Field and Helmholtz equation

A monochromatic wave, at position  $P$  and time  $t$ , can be represented by a scalar field  $u(P, t)$  written as :

$$u(P, t) = A(P) \exp[-j2\pi\nu t - j\phi(P)], \quad (1.1)$$

where  $A(P)$  and  $\phi(P)$  are the amplitude and phase, respectively, of the wave at position  $P$  and  $\nu$  is the wave frequency.

The spatial part of eqt. (1.1), also called phasor in the literature,

$$U(P) = A(P) e^{-j\phi(P)}, \quad (1.2)$$

must verify the Helmotz equation :

$$(\nabla^2 + k^2)U = 0, \quad (1.3)$$

where  $k$  is the wave number given by

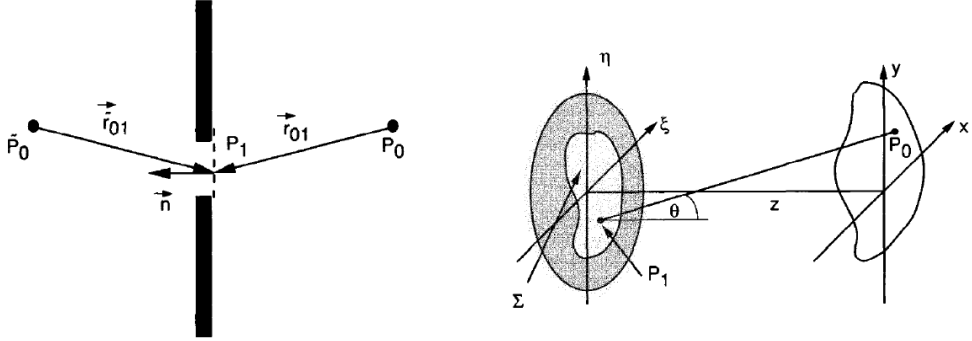
$$k = 2\pi n \frac{\nu}{c} = \frac{2\pi}{\lambda}, \quad (1.4)$$

and  $\lambda$  is the wavelength in the dielectric medium.

### 1.1.2 Rayleigh-Sommerfeld integral

Rayleigh and Sommerfeld developed a formalism using the Helmholtz equation and Green's Theorem to compute the induced diffraction by a plane screen. Let's suppose that we have a monochromatic source at  $\tilde{P}_0$  on the left of a plane screen with aperture  $\Sigma$ , the Rayleigh-Sommerfeld formula allows to compute the complex amplitude at  $P_0$  on the right of the plane screen (see Figure 1.1a).

$$U(P_0) = \frac{1}{j\lambda} \iint_{\Sigma} U'(P_1) \frac{\exp(jkr_{01})}{r_{01}} \cos(\mathbf{n}, \mathbf{r}_{01}) \mathbf{d}\mathbf{s} \quad (1.5)$$



(A) Rayleigh-Sommerfeld formulation of diffraction by a plane screen,  
 (Goodman, 1988, Chapter 3.5).  
 (B) Diffraction geometry, (Goodman, 1988, Chapter 4.1).

FIGURE 1.1: Diffraction Schemas

$U'(P_1)$  is the wave field on the screen and  $\cos(\mathbf{n}, \mathbf{r}_{01})$  is the cosine of the angle between the aperture plane normal toward the source and the vector  $\mathbf{r}_{01} = \mathbf{P}_0\mathbf{P}_1$  given by

$$r_{01} = \sqrt{z^2 + (x - \xi)^2 + (y - \eta)^2}. \quad (1.6)$$

We can rewrite eqt. (1.5) using  $\cos(\mathbf{n}, \mathbf{r}_{01}) = \cos(\theta) = \frac{z}{r_{01}}$  and the coordinate systems  $(\xi, \eta)$  and  $(x, y)$ , see Figure 1.1b,

$$U(x, y) = \frac{z}{j\lambda} \iint_{-\infty}^{\infty} U(\xi, \eta) \frac{\exp(jkr_{01})}{r_{01}^2} d\xi d\eta. \quad (1.7)$$

We can integrate from  $-\infty$  to  $\infty$ , using  $U(\xi, \eta) = P(\xi, \eta)U'(\xi, \eta)$  where  $P(\xi, \eta)$  is the pupil function. The latter equals to one in the pupil and zero outside.

### 1.1.3 Fresnel approximation

To reduce eqt. (1.7), also known as the Huygens-Fresnel principle, one can approximate the distance  $r_{01}$  using the taylor expansion of the square root :

$$r_{01} = z \sqrt{1 + \frac{x - \xi}{z} + \frac{y - \eta}{z}} \approx z \left[ 1 + \frac{1}{2} \left( \frac{x - \xi}{z} \right)^2 + \frac{1}{2} \left( \frac{y - \eta}{z} \right)^2 \right] \quad (1.8)$$

To obtain the Fresnel approximation, one has to replace  $r_{01}$  by eqt. (1.8) in eqt. (1.7). At the denominator, only the first term  $z$  is kept, since the introduced error is small. But in the exponential everything is kept. Then the final expression is given by,

$$U(x, y) = \frac{e^{jxz}}{j\lambda z} \iint_{-\infty}^{\infty} U(\xi, \eta) \exp \left\{ j \frac{k}{2z} [(x - \xi)^2 + (y - \eta)^2] \right\} d\xi d\eta. \quad (1.9)$$

In this form, the Fresnel approximation can be seen as a convolution between  $U(\xi, \eta)$  and  $h(x, y) = \frac{e^{jxz}}{j\lambda z} \exp \left[ j \frac{k}{2z} (x^2 + y^2) \right]$ .

Another form is found by developing  $[(x - \xi)^2 + (y - \eta)^2]$ ,

$$U(x, y) = \frac{e^{jkz}}{j\lambda z} e^{j\frac{k}{2z}(x^2+y^2)} \iint_{-\infty}^{\infty} \left\{ U(\xi, \eta) e^{j\frac{k}{2z}(\xi^2+\eta^2)} \right\} e^{-j\frac{2\pi}{\lambda z}(x\xi+y\eta)} d\xi d\eta, \quad (1.10)$$

this is the Fourier transform of the complex field in the pupil multiplied by a quadratic phase exponential.

#### 1.1.4 Fraunhofer approximation

In addition to the Fresnel approximation, we can introduce another approximation using the condition,

$$z >> \frac{k(\xi^2 + \eta^2)_{max}}{2}. \quad (1.11)$$

If eqt. (1.11) is satisfied the Fresnel approximation simplifies, since the quadratic phase factor in  $(\xi, \eta)$  is approximately one on the entire pupil, as

$$U(x, y) = \frac{e^{jkz}}{j\lambda z} e^{j\frac{k}{2z}(x^2+y^2)} \iint_{-\infty}^{\infty} U(\xi, \eta) e^{-j\frac{2\pi}{\lambda z}(x\xi+y\eta)} d\xi d\eta. \quad (1.12)$$

For instance, at a wavelength of 637.5 nm and a pupil diameter of 3.6 mm the Fraunhofer approximation constrains  $z$  to be greater than 63 meters to be valid.

#### 1.1.5 Converging lens introduction

The Fraunhofer conditions are severe as shown above, but one can reduce the distance  $z$  by observing the focal plane of a converging lens. Indeed, using the paraxial approximation, i.e. small angles with respect to the optical axis, the lens transmission function is given by,

$$\begin{aligned} t_l(\xi, \eta) &= \exp[jkn\Delta_0] \exp\left[-jk(n-1)\frac{\xi^2 + \eta^2}{2}\left(\frac{1}{R_1} - \frac{1}{R_2}\right)\right] \\ &= \exp\left[-j\frac{k}{2f}(\xi^2 + \eta^2)\right], \end{aligned} \quad (1.13)$$

where  $n$  is the refractive index of the lens material,  $R_1$  and  $R_2$  are the curvature's radii of the front and back surface of the lens, respectively, and  $f$  is the lens focal length defined as,

$$\frac{1}{f} \equiv (n-1)\left(\frac{1}{R_1} - \frac{1}{R_2}\right). \quad (1.14)$$

We can define  $U_l(\xi, \eta) = U(\xi, \eta)t_l(\xi, \eta)$ , which represents the complex amplitude passing through a lens. Finally, replacing  $U(\xi, \eta)$  by  $U_l(\xi, \eta)$  in Fresnel approximation and setting the observing distance to the focal length of the converging lens, we recover the Fraunhofer approximation,

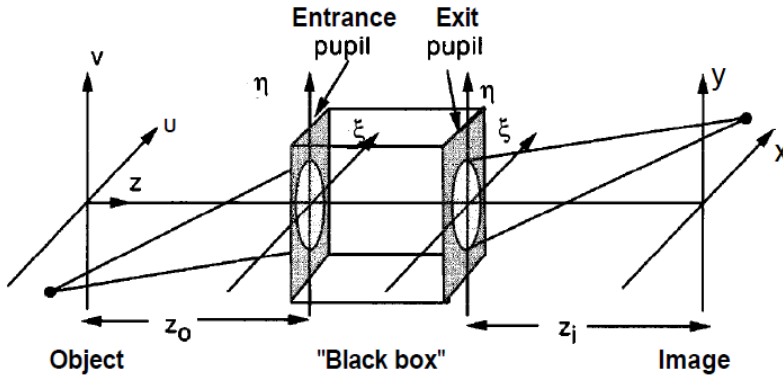


FIGURE 1.2: Schema of a imaging instrument, (Goodman, 1988, Chapter 6.1)

$$\begin{aligned} U(x, y) &= \frac{e^{jkz}}{j\lambda z} e^{j\frac{k}{2}(x^2+y^2)} \mathcal{F} \left\{ U(\xi, \eta) \exp \left[ j\frac{k}{2}(\xi^2 + \eta^2) \left( \frac{1}{z} - \frac{1}{f} \right) \right] \right\} \\ &\stackrel{z=f}{=} \frac{e^{jkz}}{j\lambda z} e^{j\frac{k}{2}(x^2+y^2)} \mathcal{F} \{ U(\xi, \eta) \}. \end{aligned} \quad (1.15)$$

## 1.2 Imaging system

An imaging system, such as a telescope, is used to acquire images of an object as perfectly as possible, generally working with high magnification to observe far object with details. An optical system, forming an instrument, is composed by lenses, mirrors, etc... and a detector (can be the human eye). A complex optical system can be reduced to a pupil,  $P(\xi, \eta)$ , and a focal length,  $f$ . The diffraction of the wave can be determined by the Fraunhofer approximation as long as the paraxial approximation is valid, see subsection 1.1.5. And the observed image of an incoherent object at the system's focal plane is proportional to the square modulus of the phasor  $U(x, y)$ ,

### 1.2.1 Impulse Response (IR)

The impulse response or PSF,  $h(x, y; u, v)$ , of an optical system is the field amplitude induced at coordinates  $(x, y)$  by a unit-amplitude point source at object coordinates  $(u, v)$ . An example of PSF for a incoherent point source object is shown in Figure 1.3. Using the linearity of the wave propagation, we can write the imaged amplitude as a superposition integral,

$$U(x, y) = \iint_{-\infty}^{\infty} h(x, y; u, v) U(u, v) du dv. \quad (1.16)$$

### 1.2.2 Optical Transfer Function (OTF)

The optical transfer function, OTF, is defined as the Fourier transform of the impulse response,

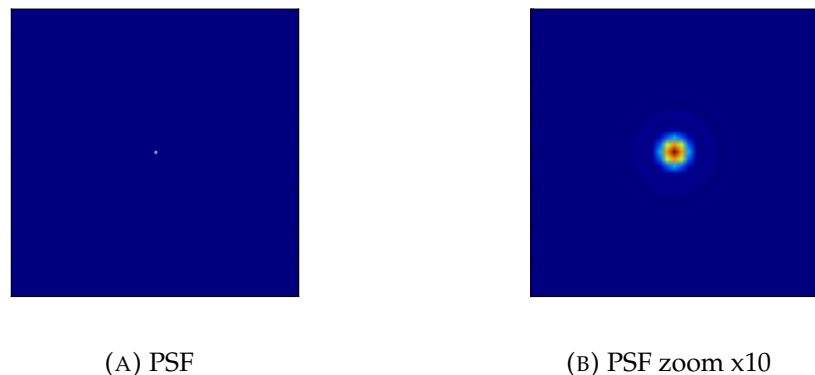


FIGURE 1.3: PSF of a perfect imaging system composed by a 3.6 mm pupil and a focal length of 80 mm at a wavelength of 637.5 nm. The size,  $N$ , of the PSF is 400 pixels and the pixel size is 5.3  $\mu\text{m}$ .

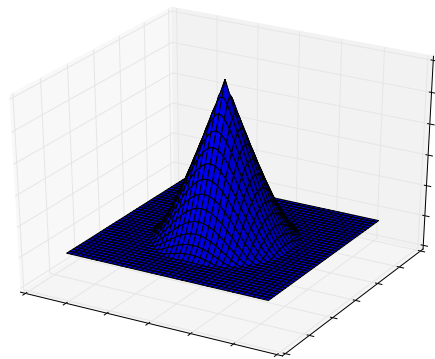


FIGURE 1.4: OTF of a perfect imaging system composed by a 3.6 mm pupil and a focal length of 80 mm at a wavelength of 637.5 nm.

$$\tilde{h}_{optical}(\xi, \eta) = \mathcal{F}\{h_{optical}(x, y)\}, \quad (1.17)$$

where  $\xi$  and  $\eta$  are the conjugate variables of  $x$  and  $y$  with respect to the Fourier transform.

An example for an incoherent point source is shown in Figure 1.4 and it correspond to the OTF of the PSF shown in Figure 1.3. For incoherent illumination, using the Fourier transform properties it can also be given by the autocorrelation of the pupil function as we will see in section 1.2.3,

$$\tilde{h}_{optical}(\xi, \eta) = (P \otimes P)(\xi, \eta). \quad (1.18)$$

### 1.2.3 Image formation

A detector only senses the energy distribution produced by an electromagnetic wave. Therefore, an image is given by the square modulus of the complex amplitude at the focal plane,

$$i(x, y) = |U(x, y)|^2 = |\iint_{-\infty}^{\infty} h(x, y; u, v) U(u, v) du dv|^2. \quad (1.19)$$

This integral simplifies differently depending on the type of object we are observing.

For a **coherent object**, Goodman (1988, Chapter 6.2) showed that the imaging is linear in complex amplitude, thus eqt. (1.19) becomes,

$$i(x, y) = |\iint_{-\infty}^{\infty} h(x - \tilde{u}, y - \tilde{v}) U(\tilde{u}, \tilde{v}) d\tilde{u} d\tilde{v}|^2, \quad (1.20)$$

where ( $\tilde{u} = Mu, \tilde{v} = Mv$ ) are the normalized object coordinates and  $M$  is the magnification of the imaging system. The image is given by the squared modulus of the convolution of the impulse response and the object complex amplitude.

For an **incoherent object**, Goodman (1988, Chapter 6.2) showed that the imaging is linear in intensity,

$$i(x, y) = \iint_{-\infty}^{\infty} |h(x - \tilde{u}, y - \tilde{v})|^2 o(\tilde{u}, \tilde{v}) d\tilde{u} d\tilde{v} = (h_{optical} \otimes o)(x, y), \quad (1.21)$$

where  $o(x, y) = |U(x, y)|^2$ . We can recognize the convolution of an object with an intensity impulse response,  $h_{optical}(x, y) = |h(x, y)|^2$ .

In this thesis, we study star-like radiation which are object with an incoherent emission. Stars are point source objects given their distances. The image that an optical system gives of a point source is called the point spread function, PSF, or impulse response, IR, of the system, see Figure 1.3. A point source is characterized by an infinite distance to the instrument and therefore the wave is planar, which means that the phasor is reduced to  $U(\xi, \eta) = P(\xi, \eta)$ . The PSF or IR is given by,

$$h_{optical}(x, y) = |\mathcal{F}\{P(\xi, \eta)\} (x, y)|^2 \quad (1.22)$$

The domain where the impulse response is invariant under translation is called the **isoplanatic domain**.

In presence of aberrations, which will be discussed in section 1.3, the wavefront is deformed with respect to the perfect planar or spheric form. The pupil function at the exit of the imaging system is modified as following,

$$\mathcal{P}(\xi, \eta) = P(\xi, \eta)e^{-j\phi_{Ab}(\xi, \eta)}, \quad (1.23)$$

where  $\phi_{Ab}(\xi, \eta)$  is the dephasing caused by the aberrations present between the object and the image planes. Replacing the new pupil function in eqt. (1.22), we obtain the PSF of an imaging system having aberrations on the optical path.

## 1.3 Aberrations

The aberrations present on the optical path between the object and the image plane decrease the quality of the resulting image. Indeed, they induce fluctuations of the amplitude and phase of the wave in the pupil plane. Since the amplitude fluctuations are negligible with respect to the phase fluctuations, we focus only on the latter. In figure 1.5, one can see the aberration's effect on an hypothetical spherical wavefront at the exit pupil of an imaging system. And in Figure 1.6, one can see the effect of aberrations on the PSF of an imaging system. The PSF is blurred due to the defocus and we can well recognize the astigmatism introduced as the PSF's shape tends towards an ellipse. The Strehl ratio is often used to quantify the importance of the aberrations, it is given by the following expression,

$$SR = \frac{\int \tilde{h}_{optical}(\xi, \eta) d\xi d\eta}{\int \tilde{h}_{perfect}(\xi, \eta) d\xi d\eta}, \quad (1.24)$$

where  $\tilde{h}_{perfect}(\xi, \eta)$  is the OTF of the perfect system with the same pupil as the optical system with the OTF  $\tilde{h}_{optical}(\xi, \eta)$ .

### 1.3.1 Sources of aberration

The phase fluctuations introduced by aberrations are due to different kind of perturbations on the optical path. In ground based astronomy, the main source of aberrations is the **atmosphere**. Indeed, the atmosphere's temperatures fluctuations coupled with turbulent airflows are at the origin of the refractive index's variations. Those variations induce different optical paths, in other words they generate perturbations on an electromagnetic wave passing through the atmosphere. The theory of the Atmospheric Turbulence is beyond the scope of this work, but we redirect the interested reader to Obukhov (1949), V.I. Tatarski (1961), and Kolmogorov (1968).

The other source of aberrations are the **defects of the instrument** itself. The flaws can limit the resolution and decrease the quality of a diffraction-limited imaging system. The defects can have multiple origins as described by Blanc (2002). The first one is a **defect during the fabrication process**, such as mirror polishing. This kind

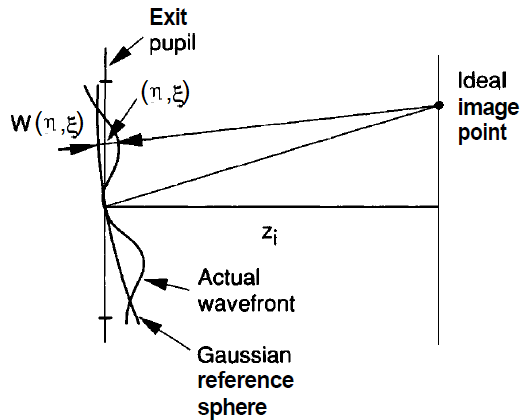


FIGURE 1.5: Gaussian reference sphere vs. aberrated Wavefront, (Goodman, 1988, Chapter 6.4). The dephasing is equal to the wave number multiplied by the aberration function,  $\phi_{Ab}(\xi, \eta) = kW(\xi, \eta)$ .

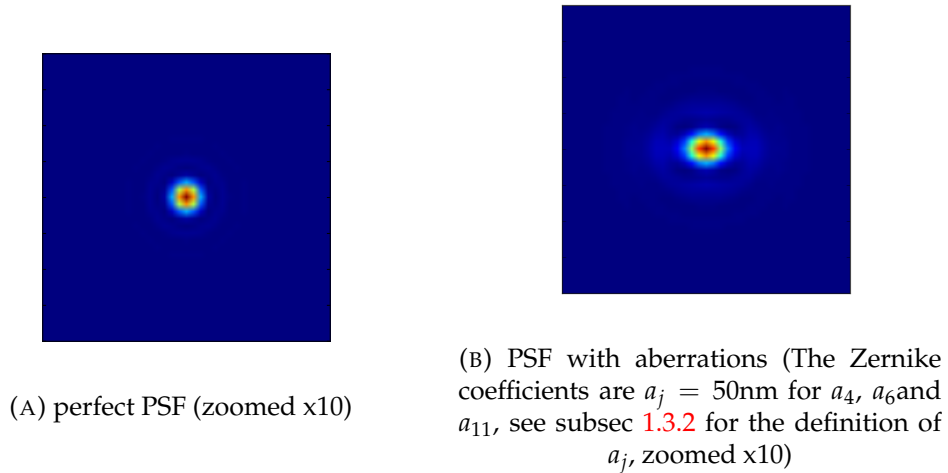


FIGURE 1.6: Comparison of perfect PSF and PSF with aberrations of an imaging system composed by a 3.6 mm pupil and a focal length of 80 mm at a wavelength of 637.5 nm. The size, N, of the PSF is 400 pixels and the pixel size is  $5.3 \mu\text{m}$ .

of defect is constant over time and of high spatial frequency. Perturbation of the electromagnetic wave can also be due to **misalignment of the optical instrument's components**. For instance, during the first stages of operation of the Hubble telescope, the mirrors were not correctly aligned and the resulting images were blurry. These defects are of low spatial frequencies and vary slowly over time. Finally, there are defects due to **mechanical stresses of the instrument**. The mirrors have to be held in place by different mechanical components. And under the influence of the gravity, a mirror deformation can arise resulting in an aberrations introduction. This kind of defect also evolves slowly through time but has a large spatial frequency domain.

We focus on a method to correct the effects of the instrument flaws. The method is particularly suited since it does not require a different path than the path to the scientific instrument, which means that we can correct the aberrations on the entire optical path.

### 1.3.2 Zernike polynomials

In order to study the aberrations present in an imaging system, F. Zernike (1934) introduced an orthonormal basis on which we can decompose the phase on a circular pupil, such as a telescope pupil. Those polynomials are the product of a trigonometric function and a radial polynomial function (Noll, 1976).

$$Z_j(\mathbf{r}) = R_n^m(r)\Theta_n^m(\theta), \quad (1.25)$$

where  $r = \frac{r'}{R_{pup}}$  is the normalized radius on the unit circle and  $\theta$  is the azimuthal angle on the unit circle.  $j$  correspond to the Zernike index in the Noll order, a specific  $j$  corresponds only to one couple  $(n, m)$ . The values of  $n$  and  $m$  satisfy the conditions  $|m| \leq n$  and  $n - |m| = \text{even}$ .

The trigonometric function is given by,

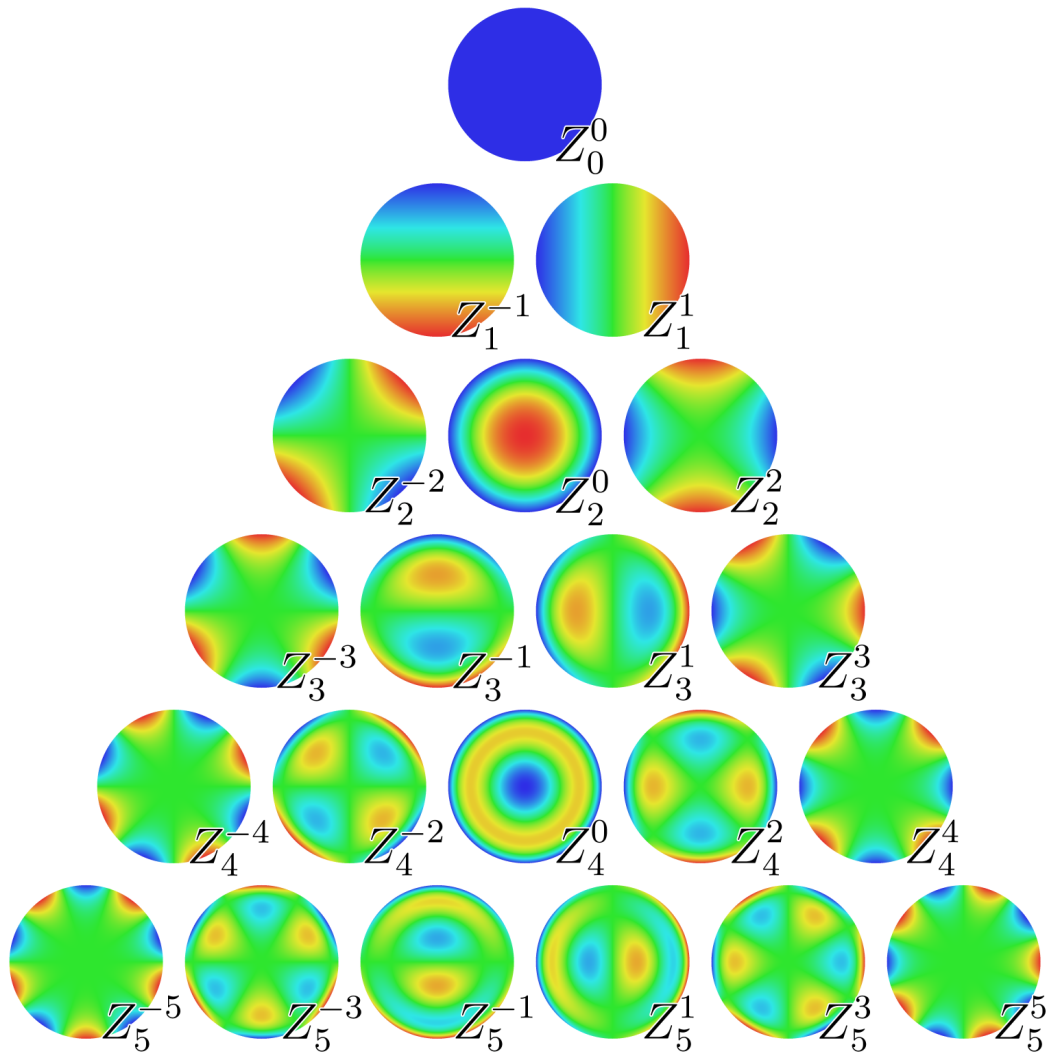


FIGURE 1.7: Representation of the 21<sup>st</sup> Zernike polynomials (Wikipe-  
dia, 2018)

$$\Theta_n^m(\theta) = \begin{cases} \sqrt{n+1} & \text{if } m = 0, \\ \sqrt{2(n+1)}\cos(m\theta) & \text{if } m \neq 0 \text{ and } i \text{ even,} \\ \sqrt{2(n+1)}\sin(m\theta) & \text{if } m \neq 0 \text{ and } i \text{ odd,} \end{cases} \quad (1.26)$$

and the radial function is given by,

$$R_n^m(r) = \sum_{s=0}^{(n-m)/2} \frac{(-1)^s (n-s)!}{s![(n+m)/2-s]![(n-m)/2-s]!} r^{n-2s}. \quad (1.27)$$

The decomposition of the phase onto the Zernike polynomials is given by,

$$\phi(\mathbf{r}) = \sum_{i=1}^{+\infty} a_i Z_i(\mathbf{r}), \quad (1.28)$$

where the  $a_i$ 's are the Zernike coefficients. And we characterize a wavefront by its root mean squared error (RMS error or RMSE) which is given by,

$$\sigma_\phi = \sqrt{\frac{1}{S} \int_S \phi^2(\mathbf{r}) d\mathbf{r}} = \sqrt{\sum_{i=2}^{+\infty} a_i^2}, \quad (1.29)$$

where  $S$  is the surface of the pupil.

## 1.4 Phase retrieval

The phase retrieval is a complicated process since the detectors are only sensitive to the intensity of a wave and not the wave itself, which prevents us to obtain a direct relation between phase and image. Thus, we only have an indirect measurement of the wavefront. Nevertheless, it is important to be able to estimate the aberrations of a system in order to correct them in real-time (Adaptive Optics systems) or in post-processing (Image restoration).

There are a couple of ways to characterize the form of a wavefront, i.e. to determine the amplitude of the aberrations present in an imaging system. Some uses the optical geometric approximation, which says that locally the light rays are perpendicular to the wavefront. These achromatic methods measure the gradient of the wave surface, such as Shack-Hartmann (Hartmann, 1900; Shack and Platt, 1971; Fontanella, 1985), Curvature sensing (Roddier, 1988) and Pyramid sensing (Ragazzoni, 1996). Another kind of methods is called interferometric or focal plane methods. They use the interference patterns of the pupil to determine the form of the wavefront. The **Phase Diversity** is part of those kind of methods. It was first proposed by Gonsalves (1982). The most popular methods nowadays are the Shack-Hartmann, the curvature sensing and the phase diversity. We explain the principle of a Shack-Hartmann sensor and phase diversity in the two next subsections.

### 1.4.1 Shack-Hartmann (Hartmann, 1900; Shack and Platt, 1971)

The Shack-Hartmann wavefront sensor measures the gradient of an aberrant phase. Figure 1.8 shows the principle. A micro-lenses array samples the wavefront passing through the pupil in a conjugated plane of the entrance pupil. Each micro-lens produces a dot on a CCD placed at the foci of the micro-lenses. The deformations of the wavefront induce a displacement of the dot with respect to a reference position

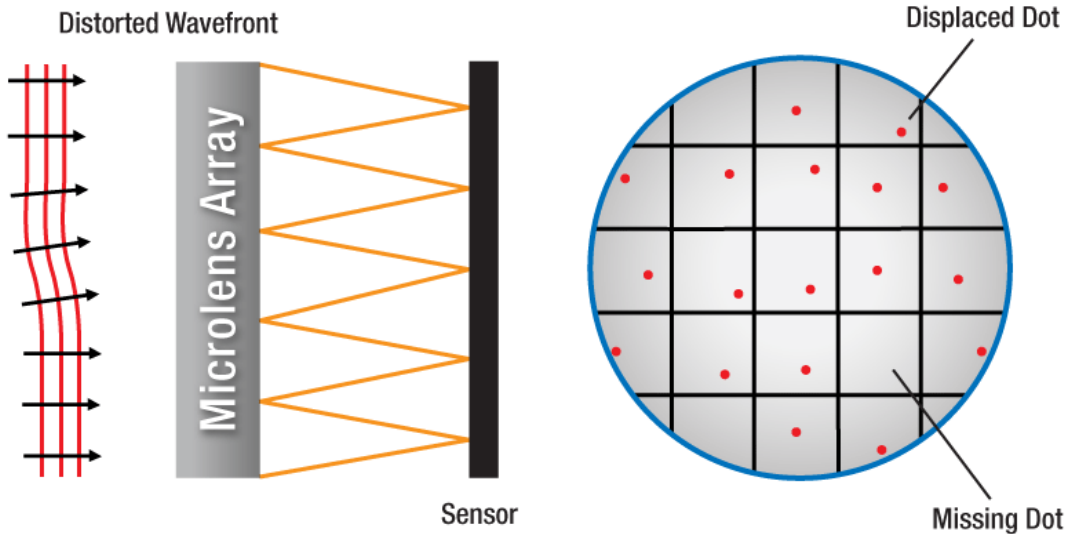


FIGURE 1.8: Shack-Hartmann principle (Thorlabs, 2018)

obtained with a perfectly planar or spherical wavefront. By measuring these displacements,  $\Delta x$  and  $\Delta y$ , it gives directly the local slope of the wavefront (Fontanella, 1985),

$$\frac{2\pi \Delta s}{\lambda f} = \frac{1}{S} \iint_S \frac{\delta\phi(x, y)}{\delta s} dx dy, \quad (1.30)$$

where  $s$  is either  $x$  or  $y$  and  $S$  is the surface of a micro-lens and  $f$  is the focal length of the micro-lenses. The wavefront is reconstructed by integrating over all the local slope measurements. The advantage of this technique is that it does not require a lot of computation since it is a direct measurement. But it requires an important optical system to acquire the data. It is used in many fields, especially in adaptive optics systems to correct the atmospheric turbulence.

#### 1.4.2 Phase Diversity

The phase diversity was first implemented by R. A. Gonsalves in 1976 (Gonsalves, 1976; Gonsalves, 1982) to retrieve the phase of a wavefront coming from a point source. It uses two images, one at the focal plane and another one with a diversity introduced, such as a defocus, in order to recover the phase of the wavefront.

Unlike Shack-Hartmann wavefront reconstruction, which is a pupil plane technique, the phase diversity uses data acquired at the focal plane. Using the non-linear relation between the phase of the wavefront and the image,

$$i(x, y) = (h_{optical} \otimes o)(x, y), \text{ with } h_{optical}(x, y) = \left| \left[ \mathcal{F} \left\{ A(\xi, \eta) e^{j\phi(\xi, \eta)} \right\} \right] (x, y) \right|^2, \quad (1.31)$$

one can determine the phase, i.e. the aberrations present in the imaging system, by solving an inverse problem. The major difficulty of this technique is that, as one can see in eqt. (1.31), there is not a unique solution to the problem at hand. This indetermination comes from the fact that the available detectors can only sense the

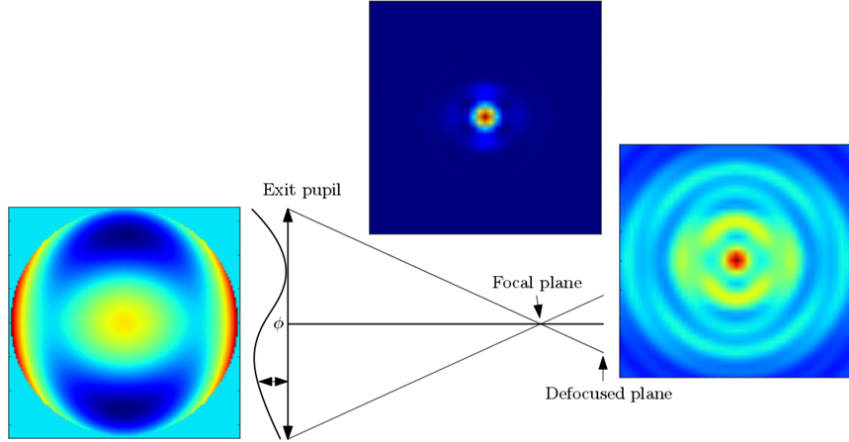


FIGURE 1.9: Schema of the phase diversity principle. The images from left to right are : the phase arriving on the exit pupil, the focused image and the defocused ( $2\pi$ ) image.

intensity of the wave, and not the wave itself, which is the modulus squared of the phasor as exposed in section 1.2. Thus,  $\phi(\xi, \eta)$  and  $\phi'(\xi, \eta) = -\phi(-\xi, -\eta)$  give the same PSF. More specifically by decomposing the phase in its even and odd part and using the autocorrelation properties ( $\Gamma_A = \Gamma_{A'}$  with  $A'(t) = A^*(-t)$ ), with only one image, one cannot determine the sign of the phase even part. This leads to the introduction of a phase diversity to raise the indetermination. The idea is to add a known aberration  $\delta\phi$  to the system and to use two images to retrieve the phase of the wavefront.

Figure 1.9 shows the principle of the phase diversity. Two images are acquired, one at the focal plane and another with a defocus. We introduce the defocus by sliding the detector along the z-axis, others use a beamsplitter and another detector (Mugnier, Blanc, and Idier, 2006). We notice that having a more complex system, such has a deformable mirror, one could introduce any other even aberration such as an astigmatism, the only requirement is that the diversity introduced must have an even radial and azimuthal order.

The phase diversity is a technique that is sensitive to chromatism, because it is based on diffraction. The non-linear relation that links the image and the phase depends also on the object. This makes the inverse problem to solve more complicated, but it allows to retrieve the phase, the object or both, when the object is unknown (most of the time). Furthermore, it is very simple optically, in other words it does not require complex optical components to acquire the data, one just uses the detector in place. Thus it depends directly on the images, without any NCPA between the adaptive optic system and the scientific detector.

The final application of the phase diversity algorithm is to correct for static aberrations in an optical system. We know the object, since it is a point source that we introduce with a laser or choose in the sky (a star).

## Chapter 2

# Phase Diversity Experiment

In this chapter, the experiment set up in the optical laboratory at HEIG-VD is described. This experiment is used to reconstruct wavefronts with unknown static aberrations introduced using phase screens. First, the behaviour of the phase diversity algorithm put in place by Mugnier, Blanc, and Idier (2006) at ONERA is tested with respect to numbers of averaging images, in other words noise level, numbers of Zernike coefficients retrieved, etc... Then the algorithm is tested using a calibrated aberration introduced by a parallel plane plate in the beam and the results are compared to a Zemax simulation. And finally, we introduce random static aberrations in the pupil with a phase screen and try to compare the phase diversity results with the Shack Hartman wavefront sensor results.

## 2.1 ONERA algorithm, Mugnier, Blanc, and Idier (2006)

In this section, we briefly present the phase diversity algorithm developed at ONERA by Mugnier, Blanc, and Idier (2006).

### 2.1.1 Algorithm description

As explained in section 1.4.2, the phase diversity determines the wavefront's phase, as well as the unknown object when needed, using two images of the same object with a phase diversity between each image. This gives the following equations system (Mugnier, Blanc, and Idier, 2006, p.11),

$$\mathbf{i}_f = \mathbf{h}_f * \mathbf{o} + \mathbf{n}_f \quad (2.1)$$

$$\mathbf{i}_d = \mathbf{h}_d * \mathbf{o} + \mathbf{n}_d, \quad (2.2)$$

where the bold letters means that it is the sampled quantities, the indexes f and d means respectively focused and defocused and  $\mathbf{n}$  regroups the photon and detector noises present on the image. Using the data available, this algorithm approaches the problem at hand with a statistic point of view. It estimates jointly the aberrations and the object (Paxman, Schulz, and Fienup, 1992), which consists in computing the joint maximum *a posteriori* (JMAP) estimator (Mugnier, Blanc, and Idier, 2006, p.17),

$$\begin{aligned} (\hat{\mathbf{o}}, \hat{\boldsymbol{\phi}})_{MAP} &= \arg \max_{\mathbf{o}, \boldsymbol{\phi}} p(\mathbf{i}_f, \mathbf{i}_d, \mathbf{o}, \boldsymbol{\phi}; \boldsymbol{\theta}) \\ &= \arg \max_{\mathbf{o}, \boldsymbol{\phi}} p(\mathbf{i}_f | \mathbf{o}, \boldsymbol{\phi}; \boldsymbol{\theta}_n) p(\mathbf{i}_d | \mathbf{o}, \boldsymbol{\phi}; \boldsymbol{\theta}_n) p(\mathbf{o}; \boldsymbol{\theta}_o) p(\boldsymbol{\phi}; \boldsymbol{\theta}_{\boldsymbol{\phi}}), \end{aligned} \quad (2.3)$$

where  $p(\mathbf{i}_f, \mathbf{i}_d, \mathbf{o}, \boldsymbol{\phi}; \boldsymbol{\theta})$  is the joint probability density function of the two images  $(\mathbf{i}_f, \mathbf{i}_d)$ , the object  $\mathbf{o}$  and the phase  $\boldsymbol{\phi}$ . It can also depend on a set of hyperparameters  $\boldsymbol{\theta} = (\boldsymbol{\theta}_n, \boldsymbol{\theta}_o, \boldsymbol{\theta}_\phi)$ .  $p(\mathbf{i}_k | \mathbf{o}, \boldsymbol{\phi}; \boldsymbol{\theta}_n)$  is the likelihood of the image  $\mathbf{i}_k$ .  $p(\mathbf{o}; \boldsymbol{\theta}_o)$  and  $p(\boldsymbol{\phi}; \boldsymbol{\theta}_\phi)$  are the *a priori* probability density functions of  $\mathbf{o}$  and  $\boldsymbol{\phi}$ .

They assume that the noise is white and stationary with a variance  $\sigma^2$  on each image. They take Gaussian prior probability distributions for the object and for the phase which they decompose on the Zernike polynomial basis,  $\boldsymbol{\phi}(\mathbf{a})$ , with  $\mathbf{a}$  the vector containing the Zernike coefficients from  $a_4$  to  $a_{j_{max}}$ , see Mugnier, Blanc, and Idier (2006, p.18-19) for the detailed expressions. Finally, the phase and the object are retrieved by maximizing the joint probability density function  $p(\mathbf{i}_f, \mathbf{i}_d, \mathbf{o}, \mathbf{a}; \boldsymbol{\theta})$  or by minimizing the logarithm of the latter. Thus the criterion to minimize is given by,

$$\begin{aligned} L_{JMAP}(\mathbf{o}, \mathbf{a}, \boldsymbol{\theta}) &= -\ln p(\mathbf{i}_f, \mathbf{i}_d, \mathbf{o}, \mathbf{a}; \boldsymbol{\theta}) \\ &= N^2 \ln \sigma^2 + \frac{1}{2} \ln \det(R_0) + \frac{1}{2} \ln \det(R_a) \\ &\quad + \frac{1}{2\sigma^2} (\mathbf{i}_f - H_f \mathbf{o})^t (\mathbf{i}_f - H_f \mathbf{o}) + \frac{1}{2\sigma^2} (\mathbf{i}_d - H_d \mathbf{o})^t (\mathbf{i}_d - H_d \mathbf{o}) \\ &\quad + \frac{1}{2} (\mathbf{o} - \mathbf{o}_m)^t R_o^{-1} (\mathbf{o} - \mathbf{o}_m) + \frac{1}{2} \mathbf{a}^t R_a^{-1} \mathbf{a} + A, \end{aligned} \quad (2.4)$$

where  $N^2$  is the number of pixels in the image,  $\mathbf{o}_m$  and  $R_o$  are the mean object and its covariance matrix,  $R_a$  is the covariance matrix of the aberrations,  $H_k$  is the matrix representing the discrete convolution by the sampled  $\mathbf{h}$  and  $A$  is a constant.

In order to simplify and fasten the computation, they rewrite the criterion replacing  $\mathbf{o}$  by its estimator  $\hat{\mathbf{o}}(\mathbf{a}, \boldsymbol{\theta})$  obtained by cancelling the derivative of  $L_{JMAP}$  with respect to  $\mathbf{o}$ , and they move to the Fourier domain, see eqt. (24) of Mugnier, Blanc, and Idier (2006, p.21).

### 2.1.2 Implementation

The implementation of the algorithm was done by Mugnier, Blanc, and Idier (2006), the code is called Deco\_ConjMarg. Dr. Laurent Jolissaint wrote the IDL code to run the ONERA phase diversity, it is called Diversity.pro and visible in Appendix B.1.1. The code takes as input an array of at least two PSFs, one focused and one defocused, the displacement  $\Delta z$  of the PSFs with respect to the focus position, the wavelength of the incoming light, the focal distance of the system, the pixel size in arc second, the threshold of the minimization and the mode of reconstruction. It takes also the pupil diameter, pupil central obscuration diameter if needed and finally  $j_{max}$ . The code can run in two different mode, *Modal* and *Zonal*. The modal method reconstruct the phase using the Zernike basis. The zonal mode uses the pixels of the phase as the basis to reconstruct and the projection on the Zernike is done after the reconstruction. Both method uses the JMAP estimator.

## 2.2 Experimental Setup

The design of the experiment was already done by Bouxin (2017). The system is built according to her plans and specifications. Figure 2.1 shows the schema of the experimental setup.

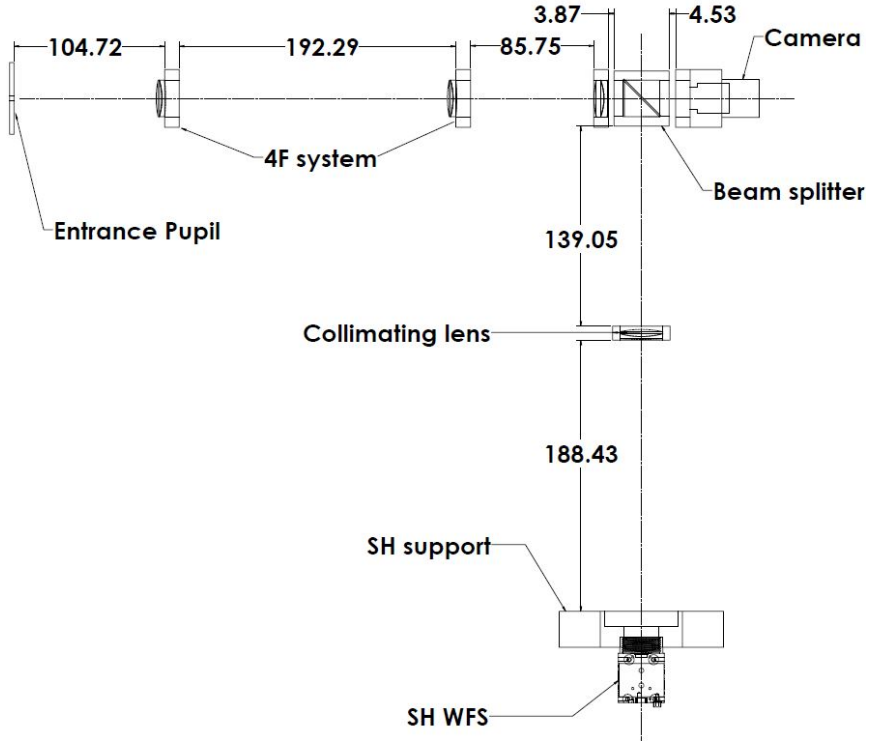


FIGURE 2.1: Experimental setup schema with the relevant distances, (Bouxin, 2017).

The experiment is mounted on a pressurized legs optical table. The assembly contains six main components : a light source, an entrance pupil, an imaging system, a converging lens to focus the beam on the camera, a camera and a wavefront sensor.

### 2.2.1 Light source

Regarding the final application of the phase diversity, the light source has to simulate a distant star aberration-free wavefront. A distant star wavefront is considered planar since the object distance,  $z$ , is far greater than the telescope size,  $r$ , see Fig. 2.2. The source of our experiment must then be characterized by a planar wavefront.

In order to obtain such a planar wavefront at the entrance pupil, the light source consist of a "pigtailed laser diode", a  $f=11\text{mm}$  converging lens, a pinhole and a  $f=200\text{ mm}$  converging lens, see Table 2.1. The pigtailed laser diode emits a Gaussian beam centred at  $637.5\text{ nm}$  slightly diverging. The converging lens concentrates the beam at the center of the  $10\mu\text{m}$  pinhole to filter the noise. The second converging lens collimates the beam, obtaining a collimated beam with a planar wavefront, see Fig. 2.3a and 2.3b.

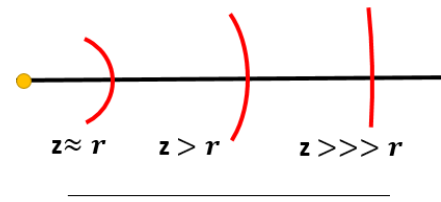


FIGURE 2.2: Wavefront curvature for different point source's distances,  $z$ .  $r$  represents the characteristic size of the arc of interest.

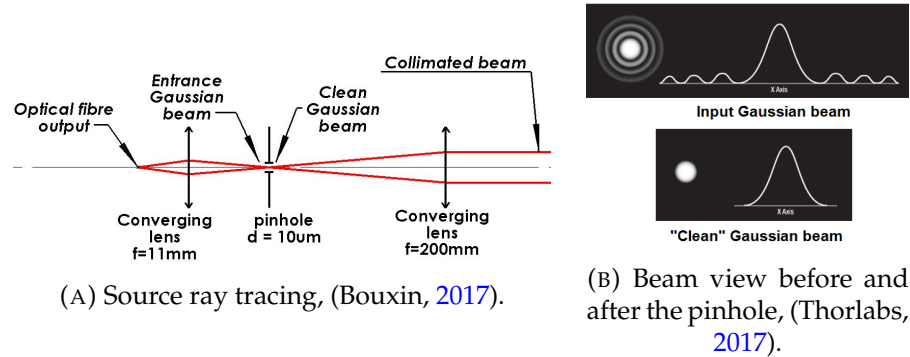


FIGURE 2.3: Source schema and pinhole effect on the beam.

## 2.2.2 Entrance pupil

The entrance pupil of our optical system is a circular aperture of 3.2 mm diameter placed after the collimating lens of the light source. It is milled in a metal plate and centred in his support, to avoid positioning with a XY table. The diameter is chosen in available material to fit in the different detector's surfaces.

## 2.2.3 Pupil imaging system

The phase diversity technique requires PSFs images as input, which means that the beam has to be focused onto the detector surface. To analyse the aberrations in the pupil plane, one needs to focus an image of the beam passing through the entrance pupil. The simplest assembly to achieve this goal is the 4F system, which consists of two converging lenses of focal 100 mm. The two lenses are separated by 200 mm, see Fig. 2.1. This places the image of the entrance pupil 100 mm after the second converging lens.

## 2.2.4 Detectors

The image of the entrance pupil, obtained with the 4F system, is focused onto a CMOS Ximea camera by a  $f = 80$  mm converging lens to acquire the PSFs for the phase diversity wavefront retrieval. The camera has a surface composed by 1280x1024 pixels of  $5.3 \mu\text{m}$ , see Appendix C.6. It is mounted on sliding support in order to be able to acquire in/out-of-focus images. A beam splitter is placed in the converging beam to separate it in two. The second beam is collimated and a Shack-Hartman WFS is placed on the entrance pupil image plane, to check the results of the phase diversity wavefront retrieval. The Shack-Hartman WFS has a 39 X 31 lenslets grid and a CCD with a resolution of 1280x1024 pixels of  $4.65 \mu\text{m}$ , see Appendix C.7.

## 2.3 Data Acquisition

### 2.3.1 Ximea Camera

The ONERA algorithm takes at least one focused and one defocused PSFs as inputs, as described in section 2.1.2. The PSFs are acquired using a python script which uses an open-source library to control the ximea camera, pyXimea<sup>1</sup>, available on GitHub. The acquisition is done following these steps. The first step in order

<sup>1</sup><https://github.com/pupil-labs/pyximea>

TABLE 2.1: Optical Components

#	Components	Model	Reference
1	Pigtailed laser diode	Thorlabs, LPS-635-FC	C.1
2	Converging lens, $f = 11$ mm	Thorlabs, A220TM-A	C.2
3	Pinhole, $10 \mu\text{m}$	Thorlabs, P10S	C.3
4	Converging lens, $f = 200$ mm	Thorlabs, AL100200	C.4
5	3.2 mm Hole milled in metal sheet	...	...
6	Converging lens, $f = 100$ mm	Thorlabs, AC254-100-A	C.5
7	Converging lens, $f = 80$ mm		
8	Camera CMOS	Ximea, MQ013MG-E2	C.6
9	Converging lens, $f = 100$ mm		
10	Shack-Hartman WFS	Thorlabs, WFS150-5C	C.7

to acquire PSFs is to determine the position of the camera's focus point using the python script `AlignementScriptXimeaCamera.py`, see Appendix A.2.1. This script let's you acquire consecutively PSFs at different camera's positions and computes their FWHM. It finally returns the minimum FWHM and the camera's position, see Figure 2.4a and 2.4b.

Once the focus point position of the camera is determined, the acquisition of the data is possible. The acquisition script is called `AcquisAndSaveXimea.py`, see Appendix A.2.2.

The user needs to set the main parameters before acquiring. There are the number of images on which to average, the size of the final PSFs, the position of the focus point on the sliding system and the initial guess to fit the 2D Gaussian on the PSF to find its center. The initial guess can be made using the Ximea camera software, called `xiCamTool`, with which one gets a live image of the camera.

Then the running program asks the user what he needs to do after having made a sound. The first thing the user needs to do is to place the camera at the focus point and turn on the LED in order to set the optimal exposure time to avoid saturation.

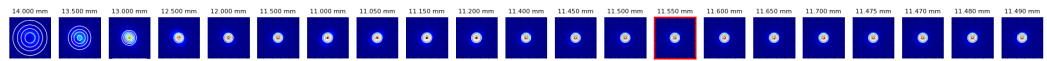
Then the acquiring sequence begins, the program ask the user to shut down and turn on the source to get the dark images and the PSF, respectively. The user needs to manually displace the camera to get the defocused PSFs. The program computes the positions to get a  $2\pi$  P2V defocus dephasing. The PSFs are finally saved in `.fits` file.

Many functions, used in the two scripts described above, are coded in the script `functionsXimea.py`, see Appendix A.2.3.

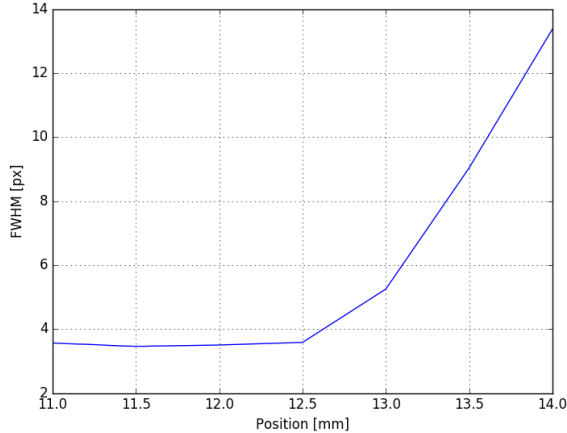
### 2.3.2 Shack-Hartmann WFS

The Shack-Hartmann wavefront sensor is delivered with a software which does the numerical integration to compute the wavefront. The GUI shows the spot field (focal points), the beam view (irradiance on the CCD), the wavefront measured or reconstructed (where you can choose the Zernike coefficients to consider for the integration up to  $j_{max} = 66$ ) and the Zernike coefficients.

The acquisition is done with the company software. The data of interest are the Zernike coefficients and the reconstructed wavefront computed following the principle described in section 1.4.1. There are a few parameters that the user can set : the exposure time (there is also an auto set), the number of averaging images (1 up to 300) and the focus points reference of the micro-lenses array.



(A) PSFs taken during the alignment procedure, each image is taken at another camera position.



(b) FWHM of the PSFs as a function of the camera's position. The minimum is at 11.55 mm

FIGURE 2.4: Example of the results of an alignment procedure

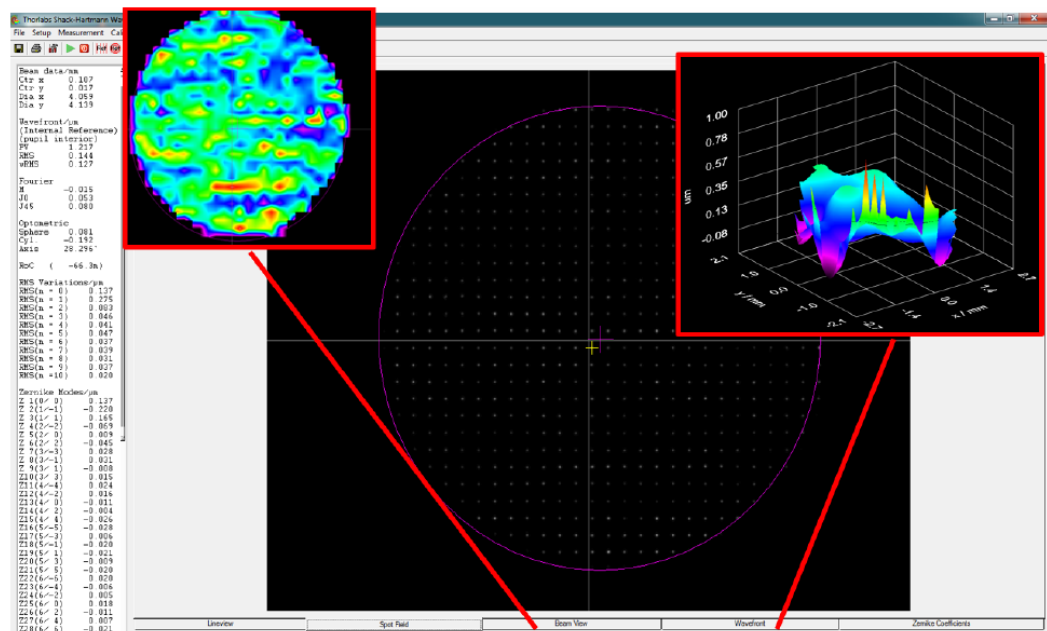


FIGURE 2.5: Shack-Hartmann Software GUI, with the beam view on the top left, the spot field in the middle and the reconstructed wavefront on the top right.

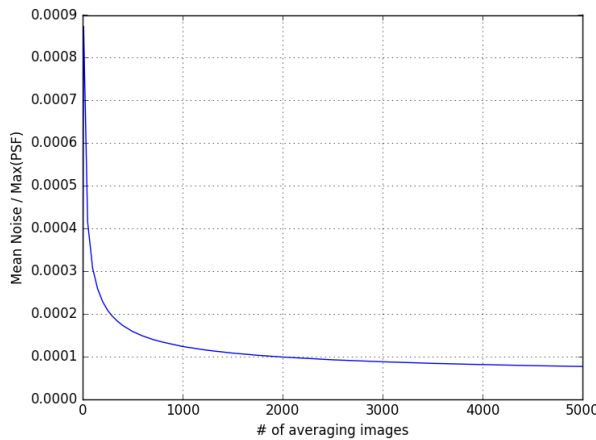


FIGURE 2.6: Noise level as a function of the number of averaging images acquired with  $\sim 300 \mu\text{s}$  exposition time. The noise level is computed as the mean of the standard deviation of every pixel divided by the maximum of the focused PSF.

The data are saved manually in a *.csv* file. We coded an IDL script to read and average the Shack-Hartmann data, in order to be able to analyse them and compare the results with the phase diversity, see Appendix B.2.1 and B.2.2.

## 2.4 Results

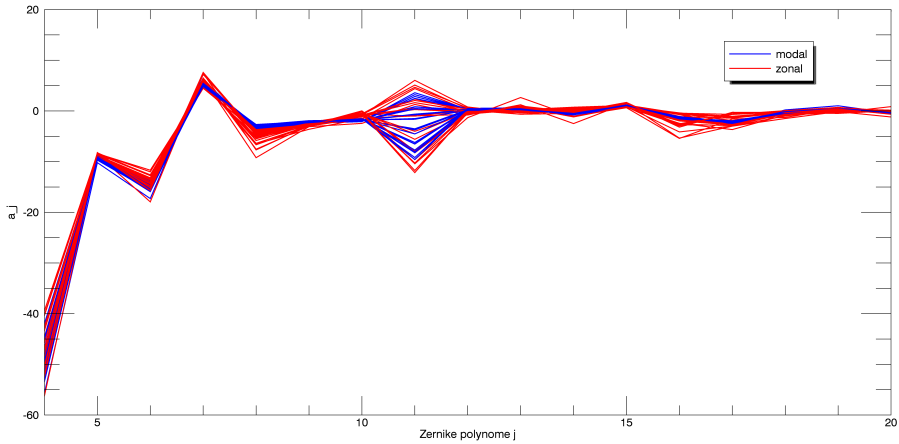
This section presents the results of the phase diversity experiment, with the introduction of different sources of aberrations. We will first present the results of the ONERA algorithm test, then we will compare the phase diversity retrieval with a calibrated aberration and finally we introduce random static aberrations using a phase screen and compare the results with the Shack-Hartmann wavefront sensor results.

### 2.4.1 ONERA Phase Diversity test

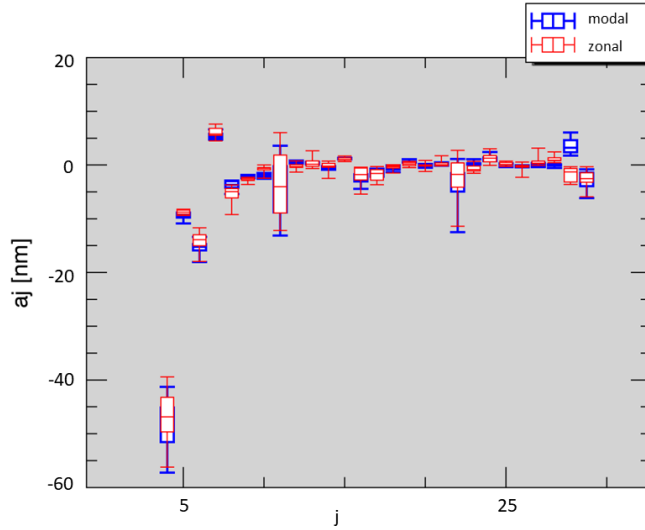
This test's motivation is to better understand the behaviour of the ONERA phase diversity algorithm with respect to the different parameters that could influence its results, such as the noise present in the PSFs, the number of Zernike coefficients returned for the modal mode and the error on the position of the Ximea camera.

To study the noise, we acquire PSFs with 25 different numbers of averaging images going from 10 to 5000. The noise level is defined as the ratio between the mean pixel standard deviation and the PSF maximum. The Ximea detector has a noise curve visible in Figure 2.6. The noise curve is computed with the noise level of the focused PSFs. It follows an exponential law with the number of averaging images. The noise level varies from  $\sim 1e - 3$  to  $\sim 8e - 5$ , for 10 and 5000 images respectively. Having the noise curve of the detector, we can study empirically how it influences the phase diversity results.

Figures 2.7a and 2.7b presents the results of the 25 different retrievals. As one can see there is some spread due to the different noise levels present in the PSFs given to the algorithm. The biggest standard deviation on a Zernike coefficient is smaller than 6 nm. And there can be up to 20 nm of maximal difference between the  $a_j$ 's as



(A) Zernike coefficients  $a_j$  as a function of  $j$  the Zernike index of the 25 modal and zonal phase retrievals, in blue and red respectively.



(B) Boxplot of the 25 Zernike coefficients  $a_j$  of the different phase retrievals computed with the different averaging numbers of images as a function of the Zernike index  $j$ .

FIGURE 2.7: Results of the phase retrievals computed with the 25 different noise levels. The phase retrievals are done with a  $j_{max} = 30$

one can see on Figure 2.7b. The spherical aberration,  $a_{11}$ , has the biggest standard deviation and range of values. This shows that the PSFs noise levels have an impact on the retrieval and that not all Zernike coefficients are affected in the same way. Two important points are the good correspondence between the modal and zonal retrievals and the relatively small spread of the Zernike coefficients.

Furthermore, looking at the reconstructed wavefronts in Figure 2.8, one can see the effects of noise in the PSFs and how important is the choice of  $j_{max}$  for the modal reconstruction. Indeed, for the wavefronts reconstructed using  $j_{max} = 30$ , the retrieved structures are similar with 10 or 3500 averaging images, however for  $j_{max} = 200$  there are more structures in the retrieval done on the PSFs with 10 averaging images than with 3500 images. This shows that the noise has a strong signal at high spatial frequencies. The zonal retrieval shows it clearly, the reconstruction is significantly different between 10 and 3500 averaging images. The averaging over a large number of acquisition smooth out the noise high frequencies that perturbs the reconstruction. Looking at the 25 reconstructed wavefronts with the zonal method, the noise threshold is at 3500 averaging images, corresponding to a noise level of 0.0009, above it the effect of the noise are reduced. Also as said above for the Zernike coefficients and still valid for the wavefront, the two retrieval methods give similar results, as one can compare the three retrievals with 3500 images on the left column of Figure 2.8. There are noisy structures present in the wavefront reconstructed on 200 Zernike coefficients, but the footprint of the beam is similar to the two other reconstructions.

In order to be sure that the number of Zernike coefficients retrieved only influences the wavefront reconstruction and not the  $a_j$ 's values, we compute them varying  $j_{max}$  from 4 to 231 and found that the spread is negligible, see Figure 2.9. This confirmation is expected since the Zernike polynomials are orthonormal, thus not correlated.

Finally, the last test is to control a measurement error  $\sigma_{\Delta z}$ 's impact, the error position of the Ximea camera, on the phase retrieval. To do so the phase retrieval is run with 125 different permutations of errors  $[-2\sigma_{\Delta z}, -1\sigma_{\Delta z}, 0, 1\sigma_{\Delta z}, 2\sigma_{\Delta z}]$  on the 3 PSFs positions.  $\sigma_{\Delta z}$  is set to represent the best precision we have on the position of the camera. As explained in section 2.2.4, the camera is mounted on a sliding element moved by a micro metric screw, so  $\sigma_{\Delta z} = 5e-3$  mm. Figures 2.10a and 2.10b present the results. The position error has nearly no effect on the phase retrieval, the median standard deviations are  $\sim 0.05$  nm and  $\sim 0.07$  nm for the modal and zonal methods respectively.

In conclusion, the ONERA algorithm tests show that first the two different methods, to retrieve the phase using the JMAP estimator, modal and zonal, give similar results. Then, we have seen that the noise levels present in the PSFs influence the retrieval, see Figures 2.7a, 2.7b and 2.8. We can consider the noise as an added aberration that touches all the Zernike coefficients. The spherical aberration is the most sensitive one. Also looking at the wavefronts, we see that there is a number of averaging images threshold at 3500 images for the zonal retrieval. Above this threshold the noise seems to be smooth and the retrieval loses the high spatial frequency components. The same thing is true for the modal retrieval, but the smoothing is not as effective at 3500 images. For the rest of this work each PSFs will be acquired with 5000 averaging images. Also we showed that the number of Zernike coefficients  $j_{max}$  does not alter the modal retrieval. And finally, the error on the position of the camera also has a negligible impact.

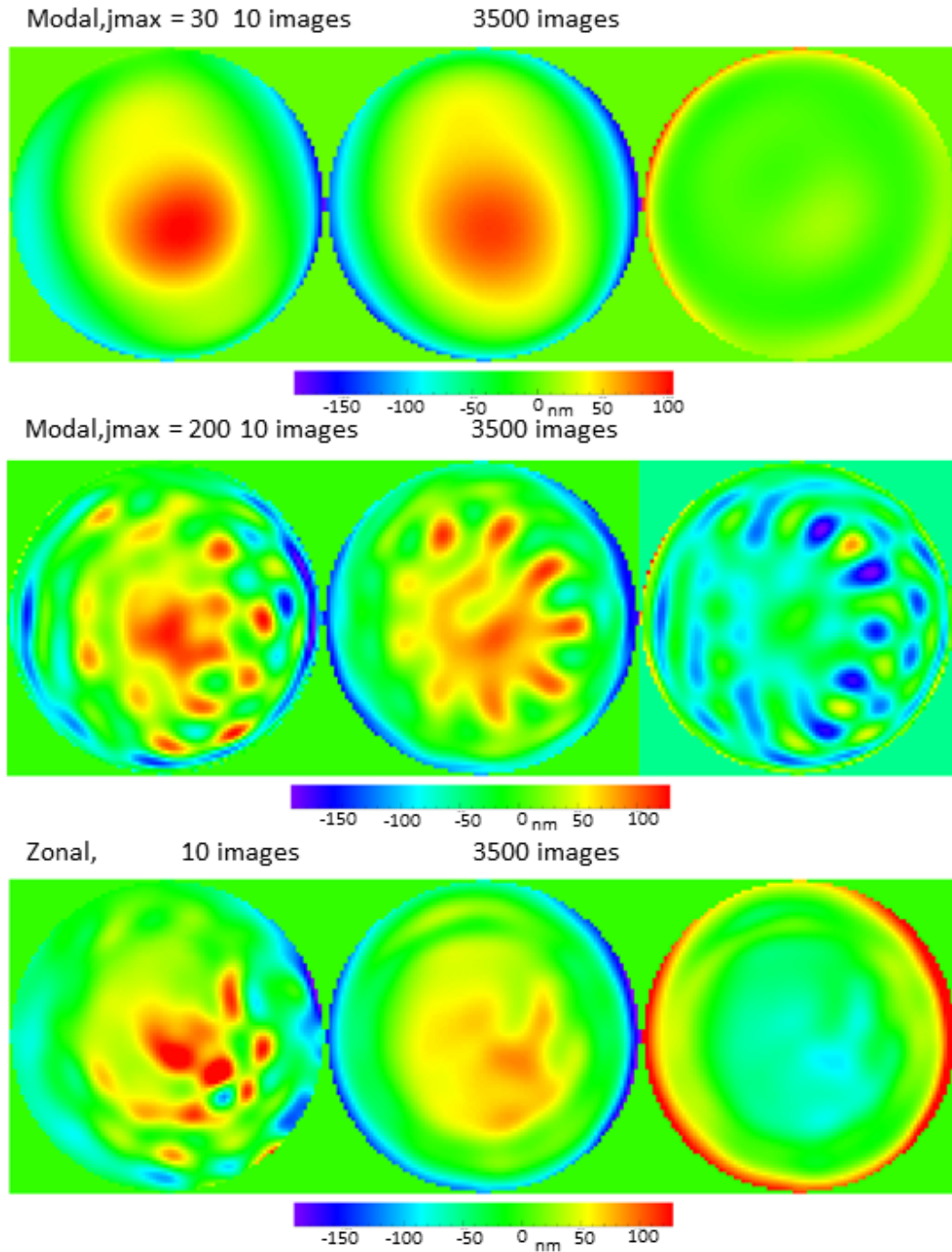


FIGURE 2.8: Reconstructed wavefronts for two different numbers of averaging images, 10 and 3500, and their difference are on the first, second and third column respectively. The two first line are modal retrieval with  $j_{max} = 30$  and  $j_{max} = 200$  and the last line is the zonal retrieval.

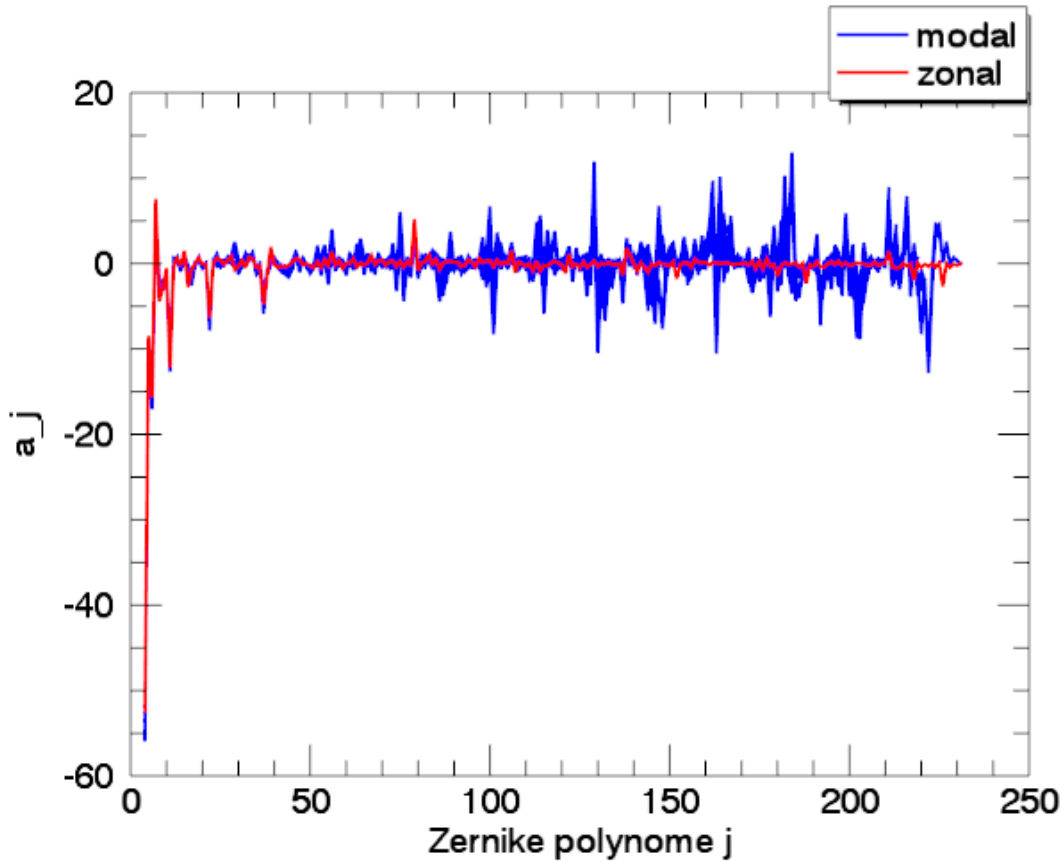
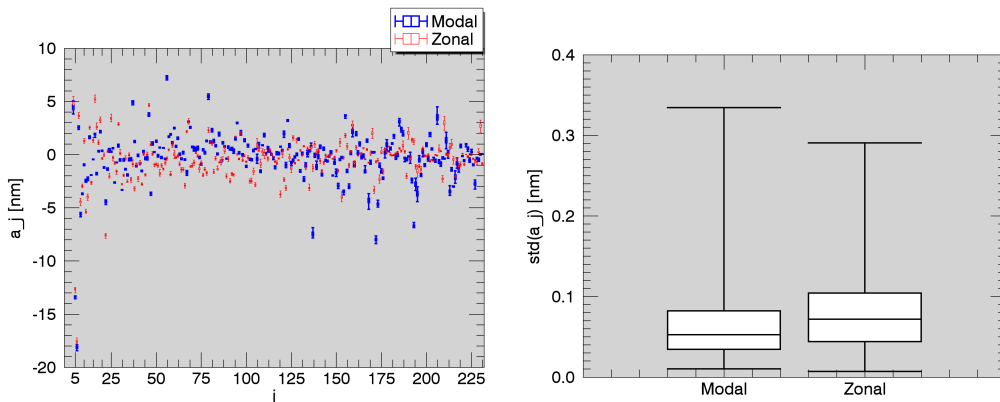


FIGURE 2.9: Zernike coefficients  $a_j$  as a function of  $j$  for the 227 retrievals done for 231 different  $j_{max}$  from 4 to 231.



(A) Boxplots of the 125  $a_j$ 's retrieved with the modal method (blue) and zonal method (red). The PSFs are acquired with 5000 averaging images.

(B) Boxplots of the 125 standard deviations on the Zernike coefficient for the modal and zonal method.

FIGURE 2.10: Results of the  $\Delta z$  measurement error test. The plots represent the results of the 125 phase retrievals run with all the permutations of errors,  $[-2\sigma_{\Delta z}, -1\sigma_{\Delta z}, 0, 1\sigma_{\Delta z}, 2\sigma_{\Delta z}]$  with  $\sigma_{\Delta z} = 5e-3$  mm, on the three PSFs position  $\Delta z$

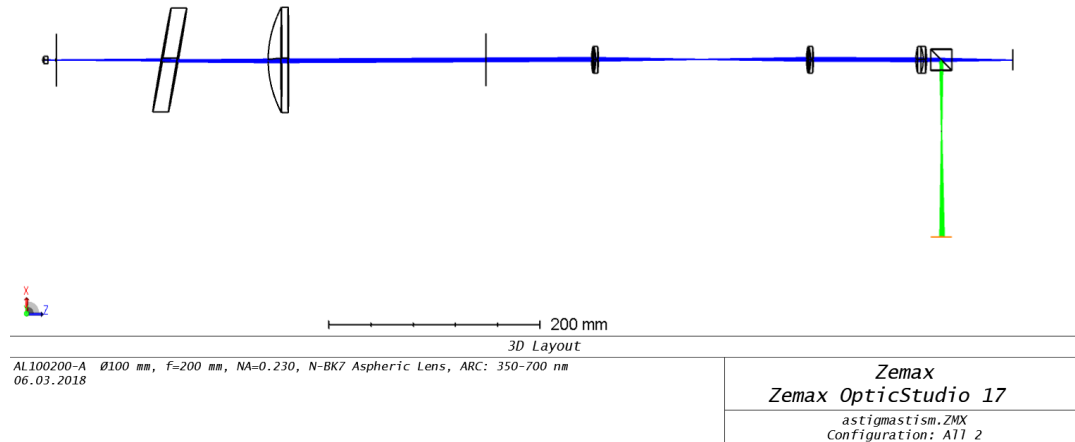


FIGURE 2.11: Zemax simulation of our optical system with the parallel plane plate introducing astigmatism.



FIGURE 2.12: Plexiglas parallel plane plate used to introduce calibrated aberrations. The width is equal to 14 mm and the refractive index is  $n = 1.49$ .

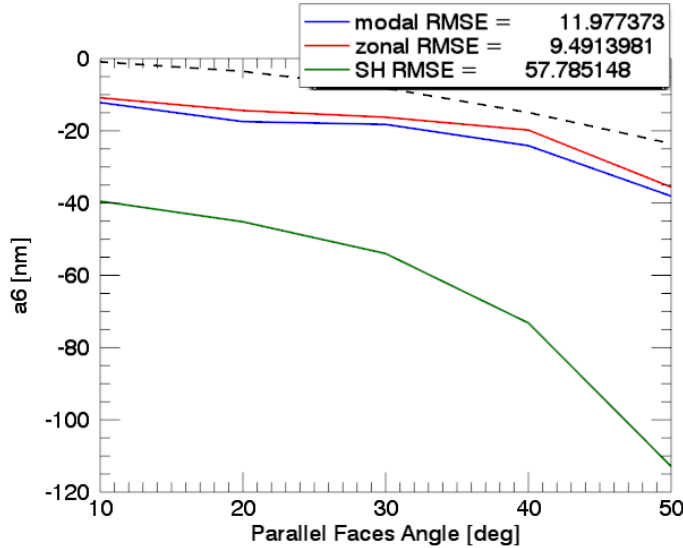


FIGURE 2.13: Zernike coefficient of the vertical astigmatism  $a_6$  as a function of the angle of the plexiglas parallel plane plate. The dashed line correspond to the Zemax simulation result, the blue line to the modal retrieval method, the red line to the zonal retrieval and the green line to the Shack-Hartmann reconstruction

#### 2.4.2 Parallel plane plate

Knowing how the algorithm behaves with respect to noise,  $j_{max}$ , etc... We compare its results to a calibrated aberration. The calibration is done by simulating the optical system using Zemax<sup>2</sup>. We introduce astigmatism using a plexiglas parallel plane plate with an angle with respect to the optical axis, see Figure 2.12. The astigmatism is due to the non symmetric incident angle on the left and right side of the optical axis with respect to  $x$ . This induces a difference in optical path between the symmetrical rays on the left and right side of the optical axis and thus induces an aberration, called the astigmatism.

In order to have the best correspondence between the simulation and the experiment, the results are computed as the difference between the Zernike coefficients retrieved with the parallel plane plate and the Zernike coefficients without the plate. Indeed, the Zemax simulation do not have alignment issues and other man introduced imperfections. So by subtracting the aberrations present in the system without the parallel plane plate, in theory we should remove any component that do not come from the plate itself in order to only retrieve the plate effect.

Figure 2.13 shows the vertical astigmatism Zernike coefficient  $a_6$  as a function of the parallel plane plate angle from  $10^\circ$  to  $50^\circ$ . The two coloured lines correspond to the two phase retrieval methods and the dashed line is the Zemax simulation of the parallel plane plate. As one can see, there is an offset of  $\sim 10 - 15$  nm between the simulation and the experiment, which correspond to an error of  $\sim \frac{\lambda}{64}$ . The behaviours of the simulation and the experiment are the same which is good, despite the overestimation of the astigmatism by the phase diversity retrievals. The system without the parallel plane plate has an astigmatism coefficient  $a_6 = 2.1$  nm. This might

<sup>2</sup><https://www.zemax.com/opticstudio>

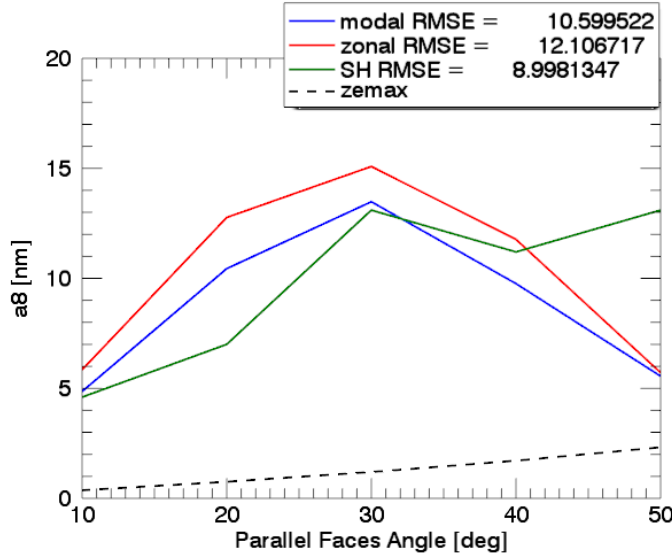


FIGURE 2.14: Zernike coefficient of the horizontal coma  $a_8$  as a function of the angle of the plexiglas parallel plane plate. The dashed line correspond to the Zemax simulation result, the blue line to the modal retrieval method , the red line to the zonal retrieval and the green line to the Shack-Hartmann reconstruction.

show that our system is not perfectly aligned, but it does explain the  $\sim 10 - 15$  nm offset.

The vertical coma, Zernike coefficient  $a_8$ , as a function of the parallel plane plate angle is shown in Figure 2.14. The optical system in presence of the parallel plane plate has a significant coma aberration, up to  $\sim 15$  nm according to the phase diversity. Without an aberration introduction, the system has a vertical coma coefficient  $a_8 = 6.4$  nm, which also supports the fact that our system is not perfectly aligned.

### 2.4.3 Shack-Hartmann comparison

We have compared the phase diversity to the Shack-Hartmann. The comparison is performed with random static aberrations introduced by a phase screen. A phase screen is a transparent plastic box, see Figure 2.15a, whose fabrication process gives it the property of static turbulent aberrations, see Figure 2.15b. Indeed, the plastic injection follows the typical flux that we can find in the atmosphere and the solidification fixes this distribution.

The results of the comparison are presented in Figures 2.16 and 2.17. According to both instruments, the phase screen introduces significant aberrations, but the comparison between the two does not seem to support any correlation between the two methods. Indeed, there is more than a 25 nm difference in average between the phase diversity and the Shack-Hartmann. Also the comparison of the wavefronts is not good. Furthermore, the comparison of the parallel plane plate results of the Shack-Hartmann, the phase diversity and the Zemax model reveals that there are differences between the three, see Figures 2.13 and 2.14. However, the vertical coma comparison between the phase diversity and the Shack-Hartmann is better, but it might be a coincidence.

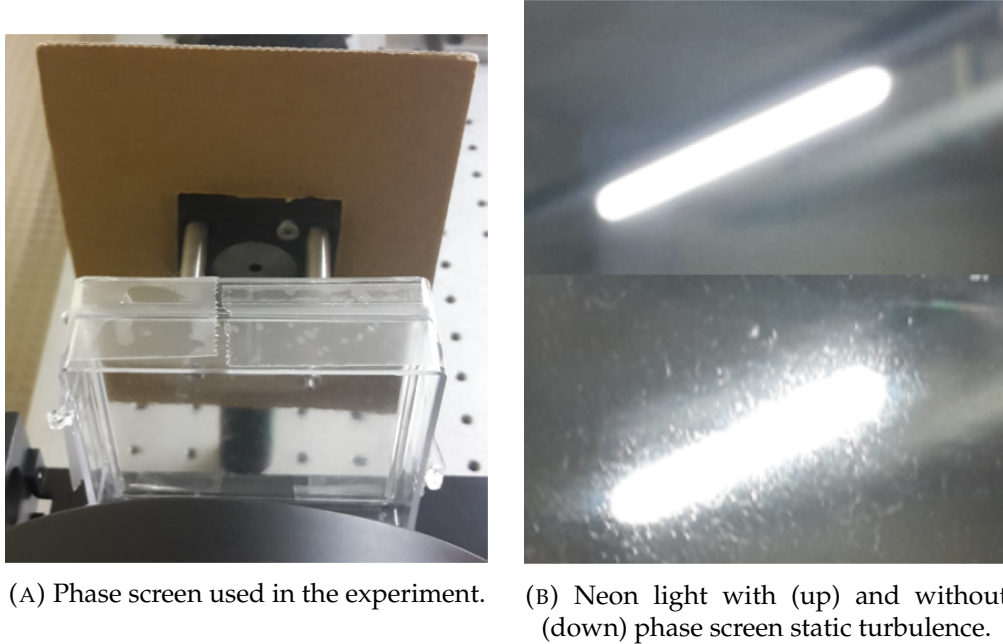
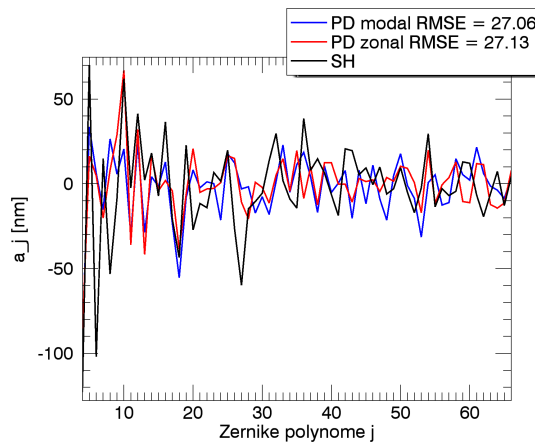


FIGURE 2.15: Phase screen introduction.

FIGURE 2.16: Zernike coefficients retrieved as a function of  $j$ . The red and blue lines correspond to the zonal and modal retrieval method respectively. The black line represent the Shack-Hartmann results. $j_{min} = 4$  and  $j_{max} = 66$ .

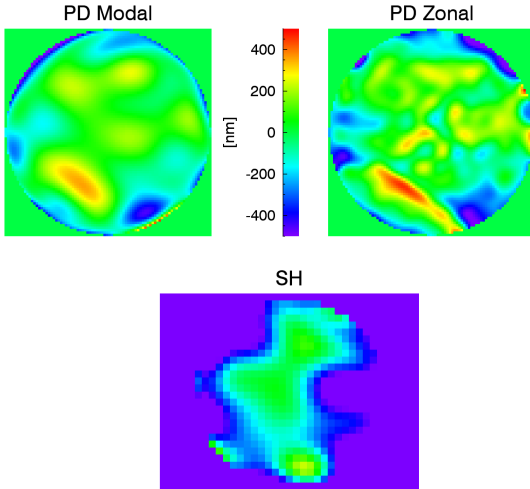


FIGURE 2.17: Reconstructed wavefront by the Modal and Zonal method of the phase diversity on 66 Zernike mode on the first line and reconstructed wavefront by the Shack-Hartmann on 66 mode as well, on the second line.

#### 2.4.4 Discussion

The algorithm test, section 2.4.1, is interesting. We have learned a lot of things about the properties and behaviour of the ONERA phase diversity algorithm. The noise present in the PSFs is important especially when trying to reconstruct the wavefronts. There seems to be a threshold above which the high spatial frequency component of the noise is neutralized. This threshold is at 3500 images corresponding to a noise level of  $\sim 0.00009 \frac{1}{\max(PSF)}$  as observed in the Zonal reconstruction. Also the number of Zernike over which the retrieval is done,  $j_{max}$ , does not really matters to recover the Zernike coefficient, but as seen in Figure 2.8, it has a significant influence on the reconstruction of the wavefronts due to the high spatial frequency component of the noise. Finally the test also confirms that a small error on the position of the camera would not perturb the phase retrieval.

The parallel plane plate experiment used to compare the phase diversity with a calibrated aberration does not work as expected. The retrieved astigmatism introduced by the Plexiglas plate follows the behaviour of the model qualitatively, but there is an offset that is not expected of  $\sim 10 - 15$  nm. Comparing the vertical coma from the model with the retrieved ones, we see that a significant amount of coma is present even though it is negligible in the Zemax model. The coma is interesting because it is typical in systems with alignment problems. In amateur telescopes with two mirrors, it arises when the secondary mirror is not correctly aligned on the primary mirror. Thus, we conclude that there is an alignment problem. The alignment problem probably comes from the complex setup collimating the beam after the pin-hole. To fix this problem in the future, one should use a f=200mm lens that goes onto the 4-rods mounting system and attach the source to the rods also. That way any aberrations due to a misalignment of the source with its collimating lens and the rest of the setup could be avoided.

Now, two problem still remains.

The calibrated aberration modelled by Zemax cannot be reproduced exactly in reality. Indeed, the offset is unexpected, because subtracting the results of the phase

retrieval on the PSFs acquired without introducing aberrations to the results with the parallel plane plate should have eliminated the aberrations present in the optical system. Either the Zemax model is not representing our system correctly; or the phase diversity algorithm does not respect the linearity of the image formation process. This argument would also mean that the Shack-Hartmann has a linearity problem. The most plausible explanation is the first one, but this must be confirmed as all the components introduced in the model correspond to the ones we have on the optical bench. An hypothesis supporting the second explanation could be that, since we retrieve a limited number of Zernike, non linear effects could arise as the available Zernike could retrieve a bigger amount of aberrations than they truly have.

The second problem is the fact that the phase diversity and the Shack-Hartmann are not similar. This might be due to a misalignment of the wavefront sensor, in other words it might not be on a plane conjugated with the pupil. The Shack-Hartmann is placed according to the distance on the schema (see Figure 2.1) and the position is refined by cancelling the defocus coefficient  $a_4$  to find the correct position. Thus, since the systems seems already to have alignment problems the position with no defocus might not be the correct one, explaining the difference between the two retrieval methods. A better way to check the conjugation between the planes would have been to put a rule on the milled entrance pupil and determine the position where it was sharp on the Shack-Hartmann.

Finally, in order to improve our results and be able to use correctly the ONERA phase diversity algorithm, we would need to be more prudent at the beginning. We should first have a solid way to describe the system independently, without the phase diversity. It was the idea behind the use of the Shack-Hartmann. But we went to quickly into trying the phase diversity algorithm and testing it. We need to first be sure of the data collected by the Shack-Hartmann and be able to recover the Zemax predictions with the Shack-Hartmann. Once we know how our system behaves and we have a clear way to characterize it, we can try to compare the phase diversity and the Shack-Hartmann. We could not do the experiment again, following all the indications proposed above, due to time limitations.



## Chapter 3

# Analytical phase diversity algorithm

After having tested and used the ONERA algorithm, we can pass to the main goal of this work, the development of our phase diversity algorithm. We describe the algorithm and its implementation. We present the results of its testing with simulated PSFs. A comparison between our algorithm and the ONERA algorithm is reported. And finally an approach to expand the validity domain of the method is presented, that could be used on a telescope equipped with a deformable mirror.

### 3.1 Analytical algorithm

#### 3.1.1 Algorithm description

This algorithm uses an analytical approach, developed by Dr. Laurent Jolissaint and refined by Jordan Voirin, to retrieve the phase of the wavefront **induced by a known point source object**. We assume the object known, because we want to correct the static aberrations present in the optical system to the scientific detector. Thus we use a point source to illuminate the optical system, either a star or a laser.

As we have seen in section 1.2, the PSF of an optical system correspond to the image of a point source,

$$PSF(x, y) = \frac{1}{S_p^2} | \left[ \mathcal{F} \left\{ P(\xi, \eta) A(\xi, \eta) e^{-j\phi(\xi, \eta)} \right\} \right] (x, y) |^2, \quad (3.1)$$

where  $P(\xi, \eta)$  is the exit pupil function,  $A(\xi, \eta)$  is the amplitude of the wave through the exit pupil,  $\phi(\xi, \eta)$  is the phase of the wavefront and  $S_p$  is the exit pupil surface. In the following, we omit the coordinates to simplify the notation. The unit of the PSF is directly the Strehl ratio. Under the assumption that we have weak aberrations, we can expand the exponential term,

$$\exp(-j\phi) \approx 1 - j\phi - \frac{\phi^2}{2} + O(\phi^3), \quad (3.2)$$

replacing the exponential by its expansion in eqt.(3.1) leads to,

$$S_p^2 PSF \cong | \mathcal{F} \left\{ PA(1 - j\phi - \frac{\phi^2}{2}) \right\} |^2 \quad (3.3)$$

Developing eqt. (3.3), keeping only the terms up to the second order, assuming that the amplitude through the pupil  $A(\xi, \eta)$  is constant and unitary since we have a point source object and using the well known complex relations,

$$\begin{aligned} a + a^* &= 2\Re\{a\} \\ a - a^* &= 2j\Im\{a\}, \end{aligned}$$

we obtain the following relation,

$$S_p^2 PSF \cong |\widetilde{P}|^2 + |\widetilde{P}\phi|^2 + 2\Im\{\widetilde{P}^*\widetilde{P}\phi\} - 2\Re\{\widetilde{P}^*\widetilde{P}\phi^2\} \quad (3.4)$$

Defining  $\Delta PSF$  as the difference between eqt. (3.4) for an arbitrary optical system and its perfect equivalent, we obtain the following expression,

$$\Delta PSF = S_p^2 PSF - S_p^2 PSF_{perfect} = |\widetilde{P}\phi|^2 + 2\Im\{\widetilde{P}^*\widetilde{P}\phi\} - 2\Re\{\widetilde{P}^*\widetilde{P}\phi^2\}, \quad (3.5)$$

where  $S_p^2 PSF_{perfect}$  is equal to  $|\widetilde{P}|^2$  for an equivalent perfect system with the same pupil. One can decompose  $\phi$  into its even and odd phase,  $\psi$  and  $\gamma$  respectively,

$$\phi = \psi + \gamma \quad (3.6)$$

Developing eqt. (3.5) after replacing  $\phi$  by its decomposition and using the properties of the Fourier transform of real and purely even or odd functions, we get the following expression,

$$\Delta PSF = |\widetilde{P}\psi|^2 + |\widetilde{P}\gamma|^2 + 2\Im\{\widetilde{P}^*\widetilde{P}\gamma\} - \Re\{\widetilde{P}^*\widetilde{P}\psi^2\} - \Re\{\widetilde{P}^*\widetilde{P}\gamma^2\} \quad (3.7)$$

We can decompose  $\Delta PSF$  into its even and odd components,

$$\Delta PSF_{even} = |\widetilde{P}\psi|^2 + |\widetilde{P}\gamma|^2 - \Re\{\widetilde{P}^*\widetilde{P}\psi^2\} - \Re\{\widetilde{P}^*\widetilde{P}\gamma^2\}, \quad (3.8)$$

$$\Delta PSF_{odd} = 2\Im\{\widetilde{P}^*\widetilde{P}\gamma\}, \quad (3.9)$$

This equation system shows that we can retrieve the odd part of the phase easily with eqt. (3.9). But eqt. (3.8) clearly reveals the indetermination of the phase retrieval with only one image, as the sign of the even part of  $\phi$  can not be determine. In order to raise this indetermination we need to introduce a phase diversity  $\delta\phi$ . We can modify the pupil function  $P$  in order to take into account this introduced diversity,

$$P_\delta \equiv Pe^{-j\delta\phi} = P(\cos(\delta\phi) - j\sin(\delta\phi)) = P(C - iS) \quad (3.10)$$

The expression of  $\Delta PSF_{\delta\phi}$ , which is the  $\Delta PSF$  at the defocus plane, is found by replacing  $P$  by  $P_\delta$  in eqt. (3.7), we give directly the expressions of the even and odd components by taking into account that the phase is only define on the pupil ( $P\phi = \phi$ ) to simplify the reading,

$$\begin{aligned} \Delta PSF_{\delta\phi,even} &= |\widetilde{C}\psi|^2 + |\widetilde{C}\gamma|^2 + |\widetilde{S}\psi|^2 + |\widetilde{S}\gamma|^2 - 2\widetilde{PC}^*\widetilde{S}\psi + 2\widetilde{PS}^*\widetilde{C}\psi \\ &\quad - \widetilde{PC}^*\widetilde{C}\psi^2 - \widetilde{PC}^*\widetilde{C}\gamma^2 - \widetilde{PS}^*\widetilde{S}\psi^2 - \widetilde{PS}^*\widetilde{S}\gamma^2 \end{aligned} \quad (3.11)$$

$$\begin{aligned} \Delta PSF_{\delta\phi,odd} &= 2\widetilde{C}\psi^*\Im\{\widetilde{S}\gamma\} + 2\Im\{\widetilde{C}\gamma^*\}\widetilde{S}\psi + 2\widetilde{PC}^*\Im\{\widetilde{C}\gamma\} + 2\widetilde{PS}^*\Im\{\widetilde{S}\gamma\} \\ &\quad + 2j\widetilde{PC}^*\widetilde{S}\psi\gamma - 2j\widetilde{PS}^*\widetilde{C}\psi\gamma. \end{aligned} \quad (3.12)$$

Eqt. (3.9), eqt. (3.11) and eqt. (3.12) allow the retrieval of the complete phase of the optical system under the assumption of weak aberrations. The numerical retrieval method uses the decomposition of the even and odd part of the phase on the Zernike polynomials,

$$\psi = \sum_{j \text{ is even}} a_j Z_j \quad (3.13)$$

$$\gamma = \sum_{j \text{ is odd}} a_j Z_j. \quad (3.14)$$

This allows to have a linear system of equations with respect to the Zernike coefficients  $a_j$  using eqts. (3.9) and (3.12), but a problem arises when the phase is purely even. The equations give an odd phase part equals to zero, as expected, but also an even phase part equals to zero. This comes from the fact that in eqt. (3.12), each term is multiplied by the odd phase component. And we cannot use eqts. (3.8) or (3.11), due to the squared modulus of the even and odd phase components, which renders our system of equation non-linear.

One way to get around this issue is to add another diversity, which is equal in amplitude to the first one but is inverted. So we have two diversities given by,

$$\delta\phi_+ = \delta\phi \text{ and } \delta\phi_- = -\delta\phi \quad (3.15)$$

Using the new diversity, eqt. (3.9) allows us to determine the odd part of the phase as before, but now for the even part of the phase we compute the difference between  $\Delta PSF_{\delta\phi_+, \text{even}}$  and  $\Delta PSF_{\delta\phi_-, \text{even}}$ . This gives us the following system of equations,

$$\Delta PSF_{\text{odd}} = 2\Im\{\widetilde{P}^*\widetilde{P}\widetilde{\gamma}\} \quad (3.16)$$

$$\Delta PSF_{\delta\phi_+, \text{even}} - \Delta PSF_{\delta\phi_-, \text{even}} = -4\widetilde{PC}^*\widetilde{S}\widetilde{\psi} + 4\widetilde{PS}^*\widetilde{C}\widetilde{\psi}, \quad (3.17)$$

which we can use to determine the complete phase of the wavefront. We can rewrite it using the decomposition of  $\psi$  and  $\gamma$  on the Zernike basis,

$$\Delta PSF_{\text{odd}} = \sum_{j \text{ is odd}} a_j 2\Im\{\widetilde{P}^*\widetilde{P}\widetilde{Z}_j\} \quad (3.18)$$

$$\Delta PSF_{\delta\phi_+, \text{even}} - \Delta PSF_{\delta\phi_-, \text{even}} = \sum_{j \text{ is even}} a_j \{-4\widetilde{PC}^*\widetilde{S}\widetilde{Z}_j + 4\widetilde{PS}^*\widetilde{C}\widetilde{Z}_j\}. \quad (3.19)$$

To solve these two equations and find the  $a_j$ 's, we use a linear regression method. We can rewrite the equations under a vectorial form to clarify the equations by flattening the images,

$$\overrightarrow{\Delta PSF}_{\text{odd}} = \underline{Z}_f \vec{a}_{\text{odd}} \quad (3.20)$$

$$\overrightarrow{\Delta PSF}_{\delta\phi_+, \text{even}} - \overrightarrow{\Delta PSF}_{\delta\phi_-, \text{even}} = \underline{Z}_d \vec{a}_{\text{even}}. \quad (3.21)$$

where  $\underline{Z}_f$  is the  $N^2 \times k_{\text{odd}}$  matrix regrouping all the terms of  $2\Im\{\widetilde{P}^*\widetilde{P}\widetilde{Z}_j\}$ ,  $k_{\text{odd}}$  is the number of odd Zernike polynomials between  $j_{\min}$  and  $j_{\max}$ , and  $\underline{Z}_d$  is the  $N^2 \times k_{\text{even}}$

matrix regrouping all the terms of  $\{-4\widetilde{PC}^*\widetilde{SZ}_j + 4\widetilde{PS}^*\widetilde{CZ}_j\}$ ,  $k_{even}$  is the number of even Zernike polynomials between  $j_{min}$  and  $j_{max}$ .

### 3.1.2 Implementation

The resolution of the equations as said above is done with a linear regression. The code is structured as following :

**The Class phaseDiversity3PSFs** is the main class of the program, see Appendix A.1.1. It takes as inputs : the 3 PSFs needed to retrieve the phase as exposed above (inFoc, outFocpos and outFocneg), the displacement of the detector with respect to its focused position ( $\Delta z$ ),

$$\Delta z = \frac{4\Delta\phi}{\pi} \lambda \left( \frac{D}{F} \right)^2, \quad (3.22)$$

where  $\Delta\phi$  is the Peak To Valley (P2V) dephasing that we want to introduce in the defocused image. In the following it will be equal to  $2\pi$ ,  $D$  is the pupil diameter and  $F$  the focal length of the optical system. It takes also as inputs the wavelength of the incoming light, the pixel size of the detector, the focal length of the optical system, the radius of the pupil and the boundary on  $j_{min} < j < j_{max}$  of the Zernike index.

The instantiation of all the elements of eqts. (3.20) and (3.21) is done by calling the class method `initiateMatrix1()` and `initiateMatrix2()`. These two methods compute the left and right members of the equations by calling methods present in the script `fs.py`.

**The script fs** is gathering functions needed to retrieve the phase of the wavefront, see Appendix A.1.2.  $\Delta PSF_{odd}$  and  $\Delta PSF_{\delta\phi_+, even} - \Delta PSF_{\delta\phi_-, even}$  are computed by the two methods `y1(params)` and `y2even(params)`. The matrix elements of  $\underline{Z}_f$  are computed by the method `f1j(params)` and the elements of  $\underline{Z}_d$  are computed by `f2jeven(params)`. Those two functions needs the Zernike polynomial basis which is coded in `zernike.py`, see Appendix A.1.4.

The linear regression is done after having initiated all the elements of the equations. We use the `numpy.linalg` class, especially its `lstsq` function<sup>1</sup>. This function takes a vector  $\vec{b}$  corresponding to the flattened  $\Delta PSF_{odd}$  or  $\Delta PSF_{\delta\phi_+, even} - \Delta PSF_{\delta\phi_-, even}$  and a matrix  $\underline{a}$  corresponding  $\underline{Z}_f$  or  $\underline{Z}_d$ . Then it determines the vector  $\vec{x}$  corresponding to the vector  $\vec{a}$  that minimizes the euclidean 2-Norm  $\|b - ax\|$  by computing the Moore-Penrose pseudo inverse of  $\underline{a}$ .

## 3.2 Results

This section presents the results of the test of the analytical algorithm of phase diversity developed in the frame of this project and described above.

### 3.2.1 Algorithm test

To test the new algorithm, we use simulated PSFs, see Figure 3.1. The simulated PSFs are computed using eqt. (3.1). We assume a unitary amplitude over the entire

---

<sup>1</sup>Documentation found at <https://docs.scipy.org/doc/numpy/reference/generated/numpy.linalg.lstsq.html#numpy.linalg.lstsq>

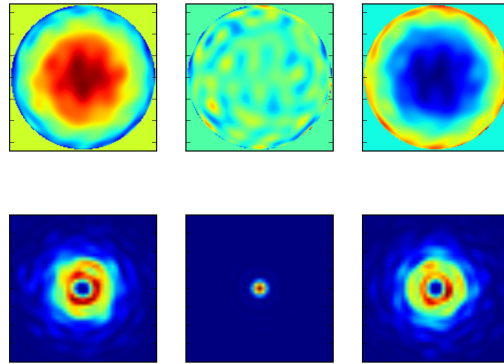


FIGURE 3.1: Example of simulated phases and their PSFs to test the analytical algorithm,  $j_{min} = 4$  and  $j_{max} = 30$ . On the phases plot, first line, the image is not entirely shown, only from pixel 132 to 268 out of 400 pixels, for clarity. The PSFs are zoomed  $\times 10$  (pixels 180 to 220) in order to be able to compare the spots. From left to right the PSFs are the defocused one,  $-\delta\phi$ , the focused one and the other defocused one,  $\delta\phi$ . The wavefront RMS error is set to 30 nm. The imaging system simulates the one we have on the optical bench composed by a 3.6 mm pupil and a focal length of 80 mm at a wavelength of 637.5 nm. The size,  $N$ , of the PSF is 400 pixels and the pixel size is 5.3  $\mu m$ .

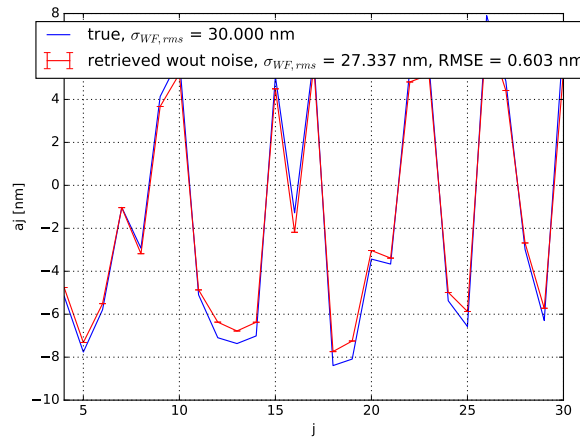


FIGURE 3.2: Zernike coefficient  $a_j$  in nm as a function of  $j$ . The blue line represents the true  $a_j$ 's and the red line the retrieved ones. The phase and the 3 PSFs used to run the retrieval are the ones presented in Figure 3.1.  $j_{min} = 4$  and  $j_{max} = 30$ .

pupil, as explained above and we construct the phase by attributing random values to Zernike coefficients from  $j_{min}$  to  $j_{max}$  and the two defocused PSFs have a  $2\pi$  P2V dephasing. The number of pixel is  $N = 400$  and the pixel size is  $5.3 \mu\text{m}$ , according to the Ximea Camera characteristics. The focal length of the exit pupil is 80 mm and its diameter is set to 3.2 mm. The system simulates the optical system we used in the phase diversity experiment. The implementation can be seen in Appendix A.1.6.

Using the PSFs shown in Figure 3.1, we are able to reconstruct the phase of the incoming wavefront onto the pupil. Figure 3.2 shows the true Zernike coefficients as well as the retrieved ones. The correspondence is good. There is a RMS error of 0.603 nm between the retrieved coefficient and the true ones. And the wavefront RMS error retrieved is 2.663 nm too small. This is due to the fact that our algorithm is based on an approximation that leads the retrieval to underestimate the aberrations present.

As for the ONERA algorithm, we want to know if  $j_{max}$  has an influence on the results. In order to study its effect, two different phases with  $j_{max} = 30$  and 200 are used. Retrievals are done for  $j_{max} = 10, 20, 30, 50, 100, 150, 200$ . The results are presented in Figures 3.3a and 3.3b. They are noteworthy for multiple aspects. First, we can see that  $j_{max}$  has a negligible influence on the overall retrieval. The RMSE is similar for all retrievals except for  $j_{max} = 200$  in Figure 3.3a and for  $j_{max} = 30$  and 50 in Figure 3.3b. This leads to the second interesting result. The phase diversity algorithm is more precise if  $j_{max}$  used for the retrieval is close to the one used to create the simulated PSFs. Indeed, when  $j_{max}$  used for the retrieval is smaller than the one used to create the PSFs, in other words when we retrieve less Zernike coefficients than the number of aberrations present in the wavefront, the results tend to overestimate the  $a_j$ 's. This might be due to the fact that there is not enough Zernike to retrieve the total wavefront RMS error. And when we retrieve more Zernike coefficients than the number of aberrations present in the wavefront, the results tends to underestimate the  $a_j$ 's which should be retrieved and overestimate the ones that should be equal to zero. This might be due to the fact that there is too many Zernike over which to spread all the aberrations.

Figures 3.2, 3.3a and 3.3b show the results of phase retrievals computed with noiseless PSFs. Given that in reality detectors have acquisition noises, we need to introduce noise into the simulated PSFs and study its effect on the retrieval. We assume that the noise is white Gaussian as it is simpler than adding Poisson noise and it is a good approximation. The random introduction of noise is done with a numpy function called `numpy.random.normal()`<sup>2</sup>.

Figure 3.4a and 3.4b presents the results of the 100 phase retrievals computed with the 100 different noisy PSFs. The comparison between the true Zernike coefficients and the retrieved ones is good. The mean RMSE of the 100 retrievals is equal to 0.910 nm, which is comparable to the one we have using noiseless PSFs. And the boxplots in Figure 3.4b show that the spread induce by the noise is clearly less than 1 nm,  $\bar{\sigma}_{ajs} = 0.23$  nm, which demonstrates that the noise does not affect significantly the retrieval. The results are similar for other wavefront RMS errors and different  $j_{max}$ 's.

Another important point to look at is the domain of validity of the phase retrieval method. Indeed as explained in section 3.1, the analytical development used is possible only by assuming weak phase aberrations in order to enable the expansion of the phase term. To constrain the validity domain, a serie of phase retrievals is computed on noiseless PSFs with random phase having a RMS wavefront error going

<sup>2</sup><https://docs.scipy.org/doc/numpy/reference/generated/numpy.random.html>

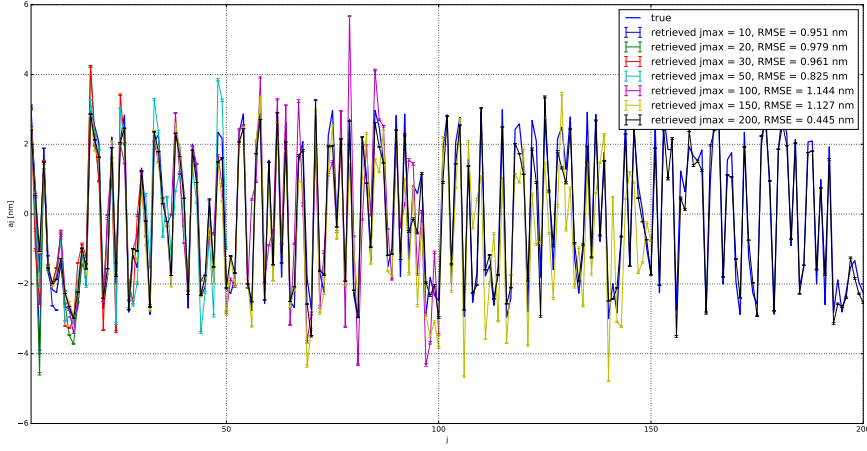
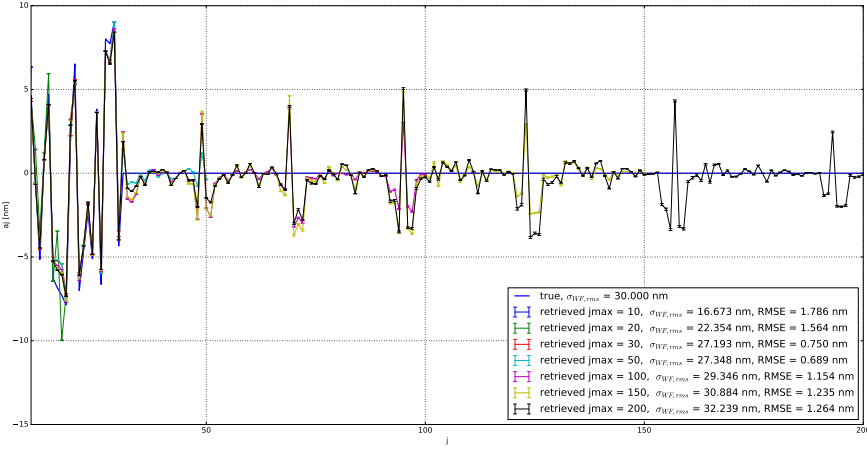
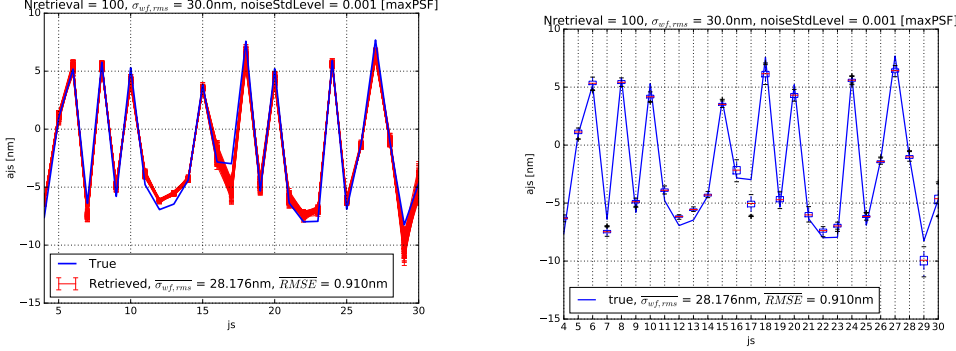
(A)  $j_{max}$  to create the PSFs is equal to 200.(B)  $j_{max}$  to create the PSFs is equal to 30.

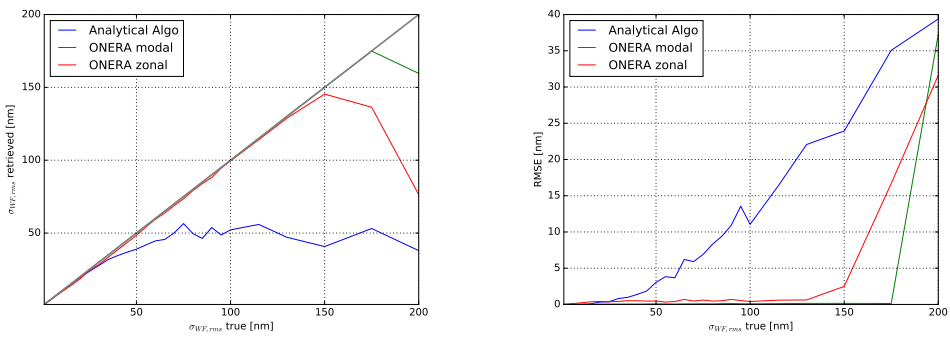
FIGURE 3.3: Zernike coefficient  $a_j$  in nm as a function of  $j$ . The blue thick line represents the true  $a_j$ 's, the wavefront has a RMS error of 30 nm. The other lines are the retrieved Zernike coefficients with different  $j_{max}$  values.



(A) Zernike coefficient as a function of  $j$ . The blue line represents the true  $a_j$ 's. The red lines correspond to the 100 different retrievals computed with the 100 noisy PSFs.  $j_{\min} = 4$  and  $j_{\max} = 30$ .

(B) Boxplots representing the statistics of the 100 Zernike coefficients as a function of  $j$ . The blue line represents the true ones.  $j_{\min} = 4$  and  $j_{\max} = 30$ .

FIGURE 3.4: Noise study results. Noise level is 0.001. The wavefront RMS error is 30 nm.



(A) RMS wavefront error retrieved as a function of the true one. The grey line is the one to one line. The blue line correspond to the analytical algorithm and the green and red lines correspond to the ONERA algorithm, modal and zonal retrieval respectively.  
 $j_{\min} = 4$  and  $j_{\max} = 30$ .

(B) RMSE of the Zernike coefficient retrieved with respect to the true ones as a function of the true RMS wavefront error. The blue line corresponds to the analytical algorithm and the green and red lines correspond to the ONERA algorithm, modal and zonal retrieval respectively.  
 $j_{\min} = 4$  and  $j_{\max} = 30$ .

FIGURE 3.5: Validity domain study results.

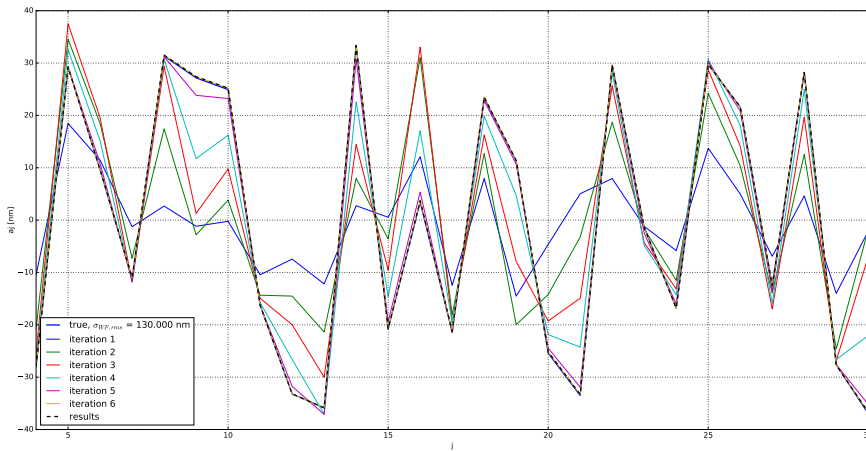


FIGURE 3.6: Zernike coefficient as a function of  $j$ . The thick blue line represents the true  $a_j$ 's, the dashed line the retrieved ones after the 6 iterations. The other coloured thin lines represent the retrieved coefficient at each iteration.

from 1 to 200 nm. The comparison between the wavefront RMS errors retrieved and the true ones is visible in Figure 3.5a. We focus first on the blue lines, which represent the analytical algorithm. As expected, the method is underestimating the phase aberrations due to the approximation on which the phase retrieval is based, see eqt. (3.3). The retrieval method is off by more than 10% and saturates at  $\sim 50$  nm when retrieving the aberrations of a wavefront having a true RMS wavefront error above 50 nm. Also the  $\sim 50$  nm threshold is the RMS wavefront error above which the RMSE of the retrieved Zernike becomes significant as seen in Figure 3.5b. To have an idea of the performance of the analytical algorithm, the ONERA algorithm modal and zonal RMS wavefront errors retrieved are also shown in Figure 3.5a. They are both far better than the analytical algorithm. They go up to  $\sim 150$  nm really accurately, but above the two retrieval methods also underestimate the RMS wavefront error. So the approximation limits considerably the range of validity of the method.

### 3.2.2 Recursive approach

The tests have shown that the analytical phase diversity algorithm works well for wavefront having weak aberrations up to 50 nm of RMS error. But in order to use it on a real optical system to correct the static aberrations present, the algorithm should be able to at least correct wavefront with 100-120 nm RMS error. Then an idea comes to mind to use the phase retrievals recursively as the aberration phenomenon is linear. Indeed, correcting the aberrations in the system using the deformable mirror present on the telescope, we could reduce the aberrations in the system recursively.

To simulate the deformable mirror, the retrieved Zernike coefficients at each iteration are subtracted to the ones used to compute the PSFs as a deformable mirror would remove the aberrations retrieved by the phase diversity. The results of the recursive approach on a wavefront having a RMS error of 130 nm are presented in Figure 3.6. The dashed line confounded with the thick blue line represent the final result of the recursive phase retrieval. The other thin lines present the different

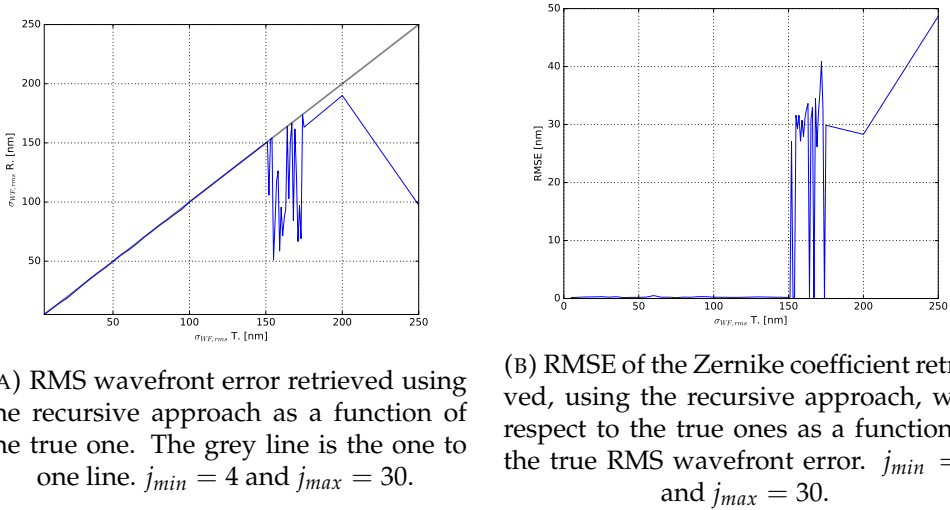


FIGURE 3.7: Results of the recursive approach

Zernike coefficients retrieved at each iteration. For a 130 nm RMS wavefront, the method needs 6 iterations to converge to the solution. The comparison between the wavefront RMS errors retrieved and the true ones as well as the RMSE as a function of the wavefront RMS error are visible in Figures 3.7a and 3.7b. The recursive phase diversity allows to extend the validity domain by 100 nm. The wavefront RMS errors retrieved is correct up to 150 nm and then the method does not converge. The RMSE shows it clearly as it is nearly zero and then explodes at 150 nm.

### 3.2.3 Discussion

The analytical algorithm works as expected. The phase retrieval is correctly done for weak aberrations using simulated PSFs, see Figure 3.2. The tests of our algorithm are also satisfying. As for the ONERA algorithm, the number of Zernike over which the reconstruction is done does not influence significantly the results. There is still an interesting behaviour intrinsic to the retrieval method. If the number of Zernike over which the reconstruction is done is smaller than the number of aberrations present in the PSFs, the algorithm tends to overestimate the Zernike coefficients to counter-balance the loss of components available. And in the opposite case, if there is more Zernike than the number of aberrations, then the non-zero coefficients are underestimated and the zero coefficients are overestimated. This might come from the fact that the zero coefficients are not equal not zero and take a part of the aberrations. These results are important because in reality we do not know the kind of aberrations present in the system and we have the confirmation that the retrieval will be trustworthy. The introduction of noise in the PSFs to simulate the effects of the detector does not influence significantly the retrieval, and the mean spread on the  $a_j$  values is 0.23 nm. So the algorithm works well and its behaviour is really good with respect to noise and  $j_{max}$ .

The only drawback of the algorithm is its validity domain. The approximation used to expand the phase exponential in the phasor limits significantly the range of RMS wavefront error that the algorithm can reconstruct. Figure 3.5a shows that it is usable for  $\sigma_{WF,rms} < 50$  nm. This is a third of the ONERA algorithm validity domain.

To increase the validity domain of the method, a new approach is considered. Since the telescope has a deformable mirror, the latter allows to correct the aberrations present in the system recursively, using the linearity of the phenomenon. Which means that we use the algorithm more than once to retrieve bigger aberrations. The recursive phase diversity simulation gives promising results as we triple the validity domain. Above 150 nm, non linear effects enter in play and disturb the retrieval. As a consequence the algorithm does not converge every time. This result is really good since we are now as good as the ONERA algorithm on simulated PSFs. We will use our algorithm, because it is based on simpler principles and we have total control over it.

The next step would be to test the algorithm using PSFs acquired on the optical bench and if possible introduce a deformable mirror to also test the recursive approach. But as explained in section 2.4.4, the experiment does not work as expected and some preliminary work needs to be undertaken before any phase diversity can be tested.



# Conclusion

The wavefront reconstruction is at the forefront of the astronomical instruments development nowadays. Having bigger and bigger telescopes will not bring a lot without methods to monitor and correct the perturbations introduced by the atmosphere. Both the VLT and the ELT as well as the DAG telescope use and will use wavefront sensing and reconstruction to correct most of the aberrations and improve the resolution up to the diffraction limit. At the moment, the phase diversity method is still not widely used but its advantages are recognized regarding the NCPA and its implementation simplicity.

We conducted an experiment to test the phase diversity algorithm developed at ONERA by Mugnier, Blanc, and Idier (2006). The algorithm's tests regarding noise level and  $j_{max}$  are interesting. We discovered that, as expected, the noise level in the PSFs is important especially in order to reconstruct wavefronts, and that  $j_{max}$  modifies significantly the wavefront retrieved.

We then computed a Zemax model of our optical system to introduce calibrated astigmatism with a parallel plane plate in Plexiglas. The results are not as expected. The astigmatism retrieved by the phase diversity follows the right behaviour qualitatively, but there is an offset. We also compared the vertical coma retrieved with the Zemax model, and once again the results were off. This shows that we might have an alignment problem.

Two problems remain, first the offset between the Zemax model of the parallel plane plate and the phase diversity. And then, the difference between the Shack-Hartmann and the phase diversity. The first problem shows that either the Zemax model does not simulate correctly the optical bench; or the ONERA phase diversity algorithm does not respect the linearity of the aberrations introduction. The second problem could be due to a misalignment of the Shack-Hartmann, because the alignment procedure we used is perturbed by the aberrations present in the system.

In the future, we would need to take a step back and be sure that we have a way to characterize the system aberrations before trying to use the phase diversity. The alignment of the source and the collimating f=200mm lens should be simpler using mounting system compatible with the 4-rods. And the Shack-Hartmann position could be checked using a rule placed at the entrance pupil.

After having tested the ONERA algorithm, the aim was to develop our own phase diversity. It works as expected. And the behaviour with respect to noise and  $j_{max}$  are satisfying. An interesting result is the overestimation and underestimation of the Zernike coefficients when the number of Zernike used by the retrieval is smaller and bigger, respectively, than the one used to create the simulated PSFs. This overestimation and underestimation might come from the fact that the algorithm counter-balances for the loss or gain of available Zernike components as there is a definite budget of aberrations to spread over a definite number of Zernike. The

validity domain of the method is limited as the method is based on a strong approximation. The method is usable up to a wavefront RMS error of 50 nm. Above the difference becomes too important to be trustworthy.

To increase the validity domain of the algorithm, a recursive approach has been tested. This method could be used on a system having a deformable mirror. The results are really satisfying and we succeeded to multiply by three the validity domain of the analytical phase diversity. This is similar to the validity domain of the ONERA algorithm, with the advantage that our algorithm is based on simpler principles and we understand fully the way it works.

Now, before implementing this algorithm on any telescope, we would need to first test it on real PSFs and characterize it as we did for the ONERA algorithm. This could be done after having improved the phase diversity experiment as said above.

In conclusion, this work was really interesting and I learned the hard way that in science research most of the time it does not go as planned. The experimental work was a challenge, as it was the first time I worked as much in a lab. The development of the phase diversity algorithm was a bit more common. But I learned a lot about discrete Fourier transform and their specificity. It has been a great experience. There is still a lot to do especially improving the laboratory experiment in order to correctly test the ONERA algorithm and more importantly test our own phase diversity on real data.

## Appendix A

# Python Code

### A.1 Phase Diversity analytical algorithm code

#### A.1.1 phaseDiversity3PSFs.py

---

```

1 #Class phaseDiversity object to retrieve the phase in the pupil from two
  psfs in/out of focus
2
3 import numpy as np
4 import fs
5 import myExceptions
6 import PSF as psf
7
8 class phaseDiversity3PSFs(object):
9
10    def
11        __init__(self,inFoc,outFocpos,outFocneg,deltaZ,lbda,pxsize,F,pupilRadius,jmin,jmax):
12    #
13    #      input:
14    #          inFoc,outFocpos,outFocneg are the 3 squared PSFs data, (focused,
15    #          defocused positiv and defocused negative)
16    #          deltaZ is the displacement of the detector to acquire the two
17    #          defocused PSFs
18    #          lbda is the wavelength of the incoming light
19    #          pxsize is the pixel size of the detector
20    #          F is the focal length of the imaging system
21    #          pupilRadius is the radius of the exit pupil
22    #          jmin and jmax gives the boundary on the js to retrieve
23
24        print 'phaseDiversity ...'
25
26    #PSF
27        self.inFoc = inFoc
28        self.outFocpos = outFocpos
29        self.outFocneg = outFocneg
30        shapeinFoc = np.shape(self.inFoc)
31        shapeoutFocpos = np.shape(self.outFocpos)
32        shapeoutFocneg = np.shape(self.outFocneg)
33        if shapeinFoc == shapeoutFocpos and shapeinFoc == shapeoutFocneg:
34            self.shape = shapeinFoc
35        else:
36            raise myExceptions.PSFsizeError('the shape of the in/out PSFs is
37                                         not the same',[shapeinFoc,shapeoutFocpos])
38        if shapeinFoc[0]==shapeinFoc[1] and np.mod(shapeinFoc[0],2)==0:
39            self.N = shapeinFoc[0]

```

```

36     else:
37         raise myExceptions.PSFsizeError('Either PSF is not square or
38                                         mod(N,2) != 0',shapeinFoc)
39
40     # properties
41     self.deltaZ = deltaZ
42     self.lbda = lbda
43     self.pxsize = pxsize
44     self.F = F
45     self.pupilRadius = pupilRadius
46     self.dxp = self.F*self.lbda/(self.N*self.pxsize)
47     self.rad = int(np.ceil(self.pupilRadius/self.dxp))
48     if 2*self.rad > self.N/2.:
49         raise myExceptions.PupilSizeError('Npupil (2*rad) is bigger than
50                                         N/2 which is not correct for the fft computation',[])
51
52     self.NyquistCriterion()
53     self.jmin = jmin
54     self.jmax = jmax
55     self.oddjs = fs.getOddJs(self.jmin,self.jmax)
56     self.evenjs = fs.getEvenJs(self.jmin,self.jmax)
57
58     # result computation
59     self.result = self.retrievePhase()
60
61     def NyquistCriterion(self):
62         deltaXfnyq = 0.5*self.lbda/(2*self.pupilRadius)
63         deltaXf = self.pxsize/self.F
64         if deltaXfnyq < deltaXf : raise myExceptions.NyquistError('the
65                                         system properties do not respect the nyquist criterion',[])
66
67     def retrievePhase(self):
68         y1,A1 = self.initiateMatrix1()
69         results1 = np.linalg.lstsq(A1,y1)
70         ajsodd = results1[0]
71         A1tA1inv= np.linalg.inv(np.matmul(np.transpose(A1),A1))
72         n_p = y1.size-1
73         ste1 = np.sqrt(results1[1]/n_p * np.diagonal(A1tA1inv))
74
75         deltaphi =
76             fs.deltaPhi(self.N,self.deltaZ,self.F,2*self.pupilRadius,self.lbda,self.dxp)
77         y2,A2 = self.initiateMatrix2(deltaphi)
78         results2 = np.linalg.lstsq(A2,y2)
79         ajseven = results2[0]
80         A2tA2inv= np.linalg.inv(np.matmul(np.transpose(A2),A2))
81         n_p = y2.size-1
82         ste2 = np.sqrt(results2[1]/n_p * np.diagonal(A2tA2inv))
83
84         js = np.append(self.oddjs,self.evenjs)
85         ajs = np.append(ajsodd,ajseven)
86         ajsSte = np.append(ste1,ste2)
87
88         Ixjs = np.argsort(js)
89         result = {'js': js[Ixjs], 'ajs': ajs[Ixjs], 'ajsSte': ajsSte[Ixjs]}
90             #,'wavefront':phase}
91         return result
92
93     def initiateMatrix1(self):

```

```

88     deltaPSFinFoc = self.CMPTEdeltaPSF()
89     y1 = fs.y1(deltaPSFinFoc)
90     A1 = np.zeros((self.N**2,len(self.oddjs)))
91     for ij in np.arange(len(self.oddjs)):
92         phiJ = fs.f1j(self.oddjs[ij],self.N,self.dxp,self.pupilRadius)
93         A1[:,ij] = phiJ
94     return y1,A1
95
96 def initiateMatrix2(self,deltaphi):
97     deltaPSFoutFocpos,deltaPSFoutFocneg = self.CMPTEdeltaPSF(self.deltaZ)
98     y2 =
99         fs.y2even(fs.getEvenPart(deltaPSFoutFocpos),fs.getEvenPart(deltaPSFoutFocneg))
100    A2 = np.zeros((self.N**2,len(self.evenjs)))
101    for ij in np.arange(len(self.evenjs)):
102        phiJ =
103            fs.f2jeven(self.evenjs[ij],self.N,deltaphi,self.dxp,self.pupilRadius)
104        A2[:,ij] = phiJ
105    return y2,A2
106
107 def CMPTEdeltaPSF(self,deltaZ=[]):
108     if not deltaZ:
109         PSF = psf.PSF([1],[0],self.N,self.dxp,self.pupilRadius)
110         return PSF.Sp**2*self.inFoc - PSF.Sp**2*PSF.PSF
111     else:
112         P2Vdephasing =
113             np.pi*self.deltaZ/self.lbda*(2*self.pupilRadius/self.F)**2/4.
114         a4 = P2Vdephasing/2./np.sqrt(3)
115         PSF = psf.PSF([4],[a4],self.N,self.dxp,self.pupilRadius)
116         return [PSF.Sp**2*self.outFocpos -
117             PSF.Sp**2*PSF.PSF,PSF.Sp**2*self.outFocneg -
118             PSF.Sp**2*PSF.PSF]

```

### A.1.2 fs.py

```

1 #functions to compute the matrix element of the system of equations Ax = b
2 import zernike as Z
3 import phasor as ph
4 import numpy as np
5
6 def f1j(j,N,dxp,pupilRadius): # 1: phij's of matrix A to find a_j odd
7     Zj = Z.calc_zern_j(j,N,dxp,pupilRadius)
8     FFTZj = scaledfft2(Zj,dxp)
9
10    Lp = N*dxp
11    xp = np.arange(-Lp/2,Lp/2,dxp)
12    yp = xp
13
14    [Xp,Yp]=np.meshgrid(xp,yp)
15
16    pupil = np.float64(np.sqrt(Xp**2+Yp**2)<=pupilRadius)
17    FFTPupil = scaledfft2(pupil,dxp)
18
19    return np.ravel(2 * np.real(FFTPupil) * np.imag(FFTZj))
20

```

```

21 def f2j(j,N,jsodd,ajsodd,deltaphi,dxp,pupilRadius): # 2: phij's of matrix A
22     # to find a_j even
23     #Get the jth zernike polynomials values on a circular pupil of radius rad
24     Zj = Z.calc_zern_j(j,N,dxp,pupilRadius)
25
26     #compute the different 2Dfft given in the equations of deltaPSF
27     cosZj = np.cos(deltaphi)*Zj
28     sinZj = np.sin(deltaphi)*Zj
29     FFTcosZj = scaledfft2(cosZj,dxp)
30     FFTsinZj = scaledfft2(sinZj,dxp)
31
32     #odd phase
33     oddPhasor = ph.phasor(jsodd,ajsodd,N,dxp,pupilRadius)
34     oddPhase = oddPhasor.phase
35     pupil = oddPhasor.pupil
36     cosOddPhase = pupil*np.cos(deltaphi)*oddPhase
37     sinOddPhase = pupil*np.sin(deltaphi)*oddPhase
38     FFTcosOddPhase = scaledfft2(cosOddPhase,dxp)
39     FFTsinOddPhase = scaledfft2(sinOddPhase,dxp)
40
41     #2Dfft of pupil function times sin(deltaPhi) and cos(deltaPhi)
42     pupilSin = pupil*np.sin(deltaphi)
43     pupilCos = pupil*np.cos(deltaphi)
44     FFTPupilSin = scaledfft2(pupilSin,dxp)
45     FFTPupilCos = scaledfft2(pupilCos,dxp)
46
47     FFTsinZjOddPhase = scaledfft2(sinZj*oddPhase,dxp)
48     FFTcosZjOddPhase = scaledfft2(cosZj*oddPhase,dxp)
49
50     return np.ravel(2*np.imag(np.conj(FFTcosZj) * FFTsinOddPhase + FFTsinZj
51                     * np.conj(FFTcosOddPhase)
52                     - np.conj(FTTPupilCos) * FFTsinZjOddPhase + np.conj(FTTPupilSin)
53                     * FFTcosZjOddPhase))
54
55 def f2jeven(j,N,deltaphi,dxp,pupilRadius): # 2: phij's of matrix A to find
56     # a_j even
57     #Get the jth zernike polynomials values on a circular pupil of radius rad
58     Zj = Z.calc_zern_j(j,N,dxp,pupilRadius)
59     Phasor = ph.phasor([1],[0],N,dxp,pupilRadius)
60     pupil = Phasor.pupil
61
62     #compute the different 2Dfft given in the equations of deltaPSF
63     cosZj = pupil*np.cos(deltaphi)*Zj
64     sinZj = pupil*np.sin(deltaphi)*Zj
65     FFTcosZj = scaledfft2(cosZj,dxp)
66     FFTsinZj = scaledfft2(sinZj,dxp)
67
68     #2Dfft of pupil function times sin(deltaPhi) and cos(deltaPhi)
69     pupilSin = pupil*np.sin(deltaphi)
70     pupilCos = pupil*np.cos(deltaphi)
71     FTTPupilSin = scaledfft2(pupilSin,dxp)
72     FTTPupilCos = scaledfft2(pupilCos,dxp)
73
74     return
75         np.ravel(-4*np.real(np.conj(FTTPupilCos)*FFTsInZj-np.conj(FTTPupilSin)*FFTcosZj))
76
77 def y1(deltaPSFinFoc): #1: yi's of y to find a_j odd
78     #compute the odd part of delta PSF
79     oddDeltaPSF = getOddPart(deltaPSFinFoc)

```

```

73     return np.ravel(oddDeltaPSF)
74
75 def y2(deltaPSFoutFoc,N,jsodd,ajsodd,deltaphi,dxp,pupilRadius): # 2: yi's
76     of y to find a_j even
77     oddDeltaPSF = getOddPart(deltaPSFoutFoc)
78     oddPhasor = ph.phasor(jsodd,ajsodd,N,dxp,pupilRadius)
79     oddPhase = oddPhasor.phase
80
81     pupilSin = oddPhasor.pupil*np.sin(deltaphi)
82     pupilCos = oddPhasor.pupil*np.cos(deltaphi)
83     FFTPupilSin = scaledfft2(pupilSin,dxp)
84     FFTPupilCos = scaledfft2(pupilCos,dxp)
85     cosOddPhase = oddPhasor.pupil*np.cos(deltaphi)*oddPhase
86     sinOddPhase = oddPhasor.pupil*np.sin(deltaphi)*oddPhase
87     FFTcosOddPhase = scaledfft2(cosOddPhase,dxp)
88     FFTsinOddPhase = scaledfft2(sinOddPhase,dxp)
89
90     return np.ravel(oddDeltaPSF -
91                     2*np.real(np.conj(FFTPupilCos))*np.imag(FFTcosOddPhase)
92                     - 2*np.real(np.conj(FFTPupilSin))*np.imag(FTTsInOddPhase))
93
94
95 #Other
96     functions-----
96 def flipMatrix(M):
97     #flip 2D matrix along x and y
98     dimM = (np.shape(M))[0]
99     Mflipped = np.fliplr(np.fliplr(M))
100    if np.mod(dimM,2)==0:
101        Mflipped = np.roll(Mflipped,1,axis=0)
102        Mflipped = np.roll(Mflipped,1,axis=1)
103    return Mflipped
104 def getOddPart(F):
105    oddF = (F - flipMatrix(F))/2.
106    return oddF
107 def getEvenPart(F):
108    evenF = (F + flipMatrix(F))/2.
109    return evenF
110 def getOddJs(jmin,jmax):
111    js = []
112    for j in np.arange(jmin,jmax+1):
113        [n,m] = Z.noll_to_zern(j)
114        if np.mod(m,2) == 1:
115            js.append(j)
116        else:
117            continue
118    return np.array(js)
119 def getEvenJs(jmin,jmax):
120    js = []
121    for j in np.arange(jmin,jmax+1):
122        [n,m] = Z.noll_to_zern(j)
123        if np.mod(m,2) == 0:
124            js.append(j)
125        else:
```

```

126         continue
127     return np.array(js)
128 def deltaPhi(N,deltaZ,F,D,wavelength,dxp):
129     Zj = Z.calc_zern_j(4,N,dxp,D/2.)
130     P2Vdephasing = np.pi*deltaZ/wavelength*(D/F)**2/4.
131     a4defocus = P2Vdephasing/2/np.sqrt(3)
132     return a4defocus*Zj
133 def cleanZeros(A,threshold):
134     A[np.abs(A) < threshold] = 0.
135     return A
136 def scaledfft2(f,dxp):
137     return np.fft.ifftshift(np.fft.fft2(np.fft.fftshift(f)))*dxp**2
138 def RMSE(estimator,target):
139     return np.sqrt(np.mean((estimator-target)**2))
140 def BIAS(estimator,target):
141     return np.mean((estimator-target))
142
143 def RMSwavefrontError(js,ajs):
144     if 1 in js:
145         return np.sqrt(np.sum(ajs**2)-ajs[js==1]**2)
146     else:
147         return np.sqrt(np.sum(ajs**2))

```

---

### A.1.3 myExceptions.py

```

1 class PSFsizeError(ValueError):
2     '''Raise when the size of the PSFs are not correct'''
3     def __init__(self, message, foo, *args):
4         self.message = message
5         self.foo = foo
6         super(PSFsizeError, self).__init__(message, foo, *args)
7
8 class NyquistError(ValueError):
9     '''Raise when the PSFs properties do not respect the nyquist criterion'''
10    def __init__(self, message, foo, *args):
11        self.message = message
12        self.foo = foo
13        super(NyquistError, self).__init__(message, foo, *args)
14
15 class PupilSizeError(ValueError):
16     '''Raise when Npupil is bigger than the size of the PSF N'''
17     def __init__(self, message, foo, *args):
18         self.message = message
19         self.foo = foo
20         super(PupilSizeError, self).__init__(message, foo, *args)

```

---

### A.1.4 zernike.py

```

1 import numpy as np
2
3 def calc_zern_j(j, N, dxp, pupilRadius):
4
5     Lp = N*dxp
6

```

```

7     if (j <= 0):
8         return {'modes':[], 'modesmat':[], 'covmat':0, 'covmat_in':0,
9             'mask':[[0]]}
10    if (N <= 0):
11        raise ValueError("N should be > 0")
12    if (dxp <= 0 or dxp >= N):
13        raise ValueError("dxp should be > 0 or < N")
14
15    xp = np.arange(-Lp/2,Lp/2,dxp)
16    yp = xp
17    [Xp,Yp]=np.meshgrid(xp,yp)
18    r = np.sqrt(Xp**2+Yp**2)
19    r = r*(r<=pupilRadius)/pupilRadius
20    pup = np.float64(np.sqrt(Xp**2+Yp**2)<=pupilRadius)
21    theta = np.arctan2(Yp,Xp)
22
23    Zj = zernike(j,r,theta)*pup
24    return Zj
25
26 def zernike(j,r,theta):
27     n,m = noll_to_zern(j)
28     nc = (2*(n+1)/(1+(m==0)))**0.5
29     #nc = (2*(n+1)/(1+(m==0)))**0.5
30     if (m > 0): return nc*zernike_rad(m, n, r) * np.cos(m * theta)
31     if (m < 0): return nc*zernike_rad(-m, n, r) * np.sin(-m * theta)
32     return nc*zernike_rad(0, n, r)
33
34 def zernike_rad(m, n, r):
35     if (np.mod(n-m, 2) == 1):
36         return r*0.0
37     wf = r*0.0
38     for k in range((n-m)/2+1):
39         wf += r**((n-2.0*k) * (-1.0)**k * fac(n-k) / ( fac(k) * fac(
40             (n+m)/2.0 - k ) * fac( (n-m)/2.0 - k ) ))
41     return wf
42
43 def noll_to_zern(j):
44     j = int(j)
45     if (j == 0):
46         raise ValueError("Noll indices start at 1, 0 is invalid.")
47     n = 0
48     j1 = j-1
49     while (j1 > n):
50         n += 1
51         j1 -= n
52     m = (-1)**j * ((n % 2) + 2 * int((j1+((n+1)%2)) / 2.0 ))
53     return (n, m)
54
55 def fac(n):
56     if n == 0:
57         return 1
58     else:
59         return n * fac(n-1)

```

### A.1.5 phasor.py

---

```

1 #class phasor
2 import numpy as np
3 import zernike as Z
4
5 class phasor(object):
6
7     def __init__(self,js=[1],ajs=[0],N=800,dxp=1,pupilRadius = 200):
8         self.js = js
9         self.ajs = ajs
10        self.N = N
11        self.dxp = dxp
12        self.pupilRadius = pupilRadius
13
14        self.pupil = self.constructPupil()
15
16        self.phase = self.constructPhase()
17        self.phasor = self.pupil*np.exp(-1j*self.phase)
18
19    def constructPhase(self):
20        phase = np.zeros((self.N,self.N))
21        for ij, j in enumerate(self.js):
22            Zj = Z.calc_zern_j(j,self.N,self.dxp,self.pupilRadius)
23            phase += self.ajs[ij]*Zj
24        return phase
25
26    def constructPupil(self):
27        Lp = self.N*self.dxp
28
29        xp = np.arange(-Lp/2,Lp/2,self.dxp)
30        yp = xp
31
32        [Xp,Yp]=np.meshgrid(xp,yp)
33
34        pup = np.float64(np.sqrt(Xp**2+Yp**2)<=self.pupilRadius)
35        return pup

```

---

### A.1.6 PSF.py

---

```

1 import numpy as np
2 import phasor as ph
3 import fs
4
5 class PSF(object):
6
7     def __init__(self,js=[1],ajs=[0],N=400,dxp=1.,pupilRadius = 67.):
8         self.phasor = ph.phasor(js,ajs,N,dxp,pupilRadius) #phasor in the
9             pupil
10        self.Sp = np.sum(self.phasor.pupil)*dxp**2 #pupil surface
11        self.FFTphasor = fs.scaledfft2(self.phasor.phasor,dxp) #fourier
12            transform of the phasor
13        self.PSF = np.abs(self.FFTphasor)**2/self.Sp**2 #PSF on the focal
14            plane
15        self.FFTpupil = fs.scaledfft2(self.phasor.pupil,dxp) #fourier
16            transform of the pupil function which gives the perfect PSF
17        self.perfectPSF = np.abs(self.FFTpupil)**2/self.Sp**2 #perfect PSF

```

---

---

```

14     self.deltaPSF = self.Sp**2*self.PSF-self.Sp**2*self.perfectPSF
      #deltaPSF

```

---

## A.2 Acquisition Code: Ximea Camera

### A.2.1 AlignementScriptXimeaCamera.py

---

```

1 ##Script to compute the FWHM of the beam on the camera averaging
2 #over "nbrImgAveraging" images and see which position minimizes it.
3
4 from ximea import xiapi
5 import numpy as np
6 from matplotlib import pyplot as plt
7 import scipy.optimize as opt
8 import datetime
9 import functionsXimea as fX
10 import seaborn as sns
11 import os
12 sns.set()
13 #%% instantiation
14
15 dataFolderPath = '...'
16 plotFolderPath = '...'
17 #create the matrix grid of the detector CCD
18 x = np.linspace(0,1280,1280)
19 y = np.linspace(0,1024,1024)
20 x, y = np.meshgrid(x, y)
21
22 #initial guess for the fit depending on the position of the beam in the CCD
23 initial_guess = [250, 481, 706, 3, 3] # [max PSF,y,x,sigmay,sigmax]
24
25 #number of image to average
26 nbrImgAveraging = 10
27
28 #%%data acquisition and treatment
29
30 #create instance for first connected camera
31 cam = xiapi.Camera()
32 #start communication
33 print('Opening camera...')
34 cam.open_device()
35 #settings
36 cam.set_imgdataformat('XI_MONO8') #XIMEA format 8 bits per pixel
37 cam.set_gain(0)
38 #create instance of Image to store image data and metadata
39 img = xiapi.Image()
40 #start data acquisition
41 print('Starting data acquisition...')
42 if cam.get_acquisition_status() == 'XI_OFF':
43     cam.start_acquisition()
44
45 cam.set_exposure(fX.determineUnsaturatedExposureTime(cam,img,[60,10000],1))
46
47 #instanciation for the while loop
48 answer ='y'

```

```

49 i=0
50 relativePos = []
51 data = []
52 data_fitted = []
53 FWHMx = []
54 FWHMy = []
55 x0 = []
56 y0 = []
57 sigmaX0 = []
58 sigmaY0 = []
59
60 while answer == 'y':
61
62     try:
63         relativePos.append(float(raw_input('What is the position on the
64             screw [mm] ? ')))
65     except ValueError:
66         print('Not a float number')
67
68     [tmpdata, stdData] = fX.acquireImg(cam, img, nbrImgAveraging)
69     data.append(tmpdata)
70     #Fit the img data on the 2D Gaussian to compute the FWHM
71     print('Fitting 2D Gaussian...')
72     popt, pcov = opt.curve_fit(fX.TwoDGaussian, (x,y), data[i].ravel(), p0 =
73         initial_guess)
74     print('Fitting done')
75
76     FWHMx.append(2*np.sqrt(2*np.log(2))*popt[3])
77     FWHMy.append(2*np.sqrt(2*np.log(2))*popt[4])
78     x0.append(popt[2])
79     sigmaX0.append(popt[4])
80     y0.append(popt[1])
81     sigmaY0.append(popt[3])
82
83     print 'Fig %d : (x,y) = (%3.2f,%3.2f), FWHM x = %3.2f, FWHM y = %3.2f'
84     %(i,x0[i],y0[i],FWHMx[i],FWHMy[i])
85
86     data_fitted.append(fX.TwoDGaussian((x, y),
87         popt[0],popt[1],popt[2],popt[3],popt[4]).reshape(1024, 1280))
88
89     #plot the beamspot
90     fig, ax = plt.subplots(1, 1)
91     ax.imshow(data[i], cmap=plt.cm.jet, origin='bottom',
92             extent=(x.min(), x.max(), y.min(), y.max()))
93     ax.contour(x, y, data_fitted[i], 5, colors='w', linewidths=0.8)
94     plt.xlim( (popt[2]-4*popt[4], popt[2]+4*popt[4]) )
95     plt.ylim( (popt[1]-4*popt[3], popt[1]+4*popt[3]) )
96     plt.show()
97
98     #ask if the person wants to acquire a new image to improve the alignment
99     pressedkey = raw_input('Do you want to acquire an other image [y (yes)
100         or n (no)]: ')
101
102     if (pressedkey =='n'):
103         answer = pressedkey
104
105     #increase i
106     i+=1

```

```

101 #stop data acquisition
102 print('Stopping acquisition...')
103 cam.stop_acquisition()
104
105 #stop communication
106 cam.close_device()
107
108 #convert list to np.array
109 relativePos = np.array(relativePos)
110 data = np.array(data)
111 FWHMx = np.array(FWHMx)
112 FWHMy = np.array(FWHMy)
113 x0 = np.array(x0)
114 y0 = np.array(y0)
115 sigmaX0 = np.array(sigmaX0)
116 sigmaY0 = np.array(sigmaY0)
117
118 #plot the FWHM vs. relPos
119 fig, ax = plt.subplots(1,1)
120 ind = np.argsort(relativePos)
121 ax.plot(relativePos[ind],(np.sqrt(FWHMx**2+FWHMy**2))[ind])
122 ax.set_xlabel('Position [mm]')
123 ax.set_ylabel('FWHM [px]')
124 ax.grid()
125 date = datetime.datetime.today()
126 if not os.path.isdir(plotFolderPath):
127     os.makedirs(plotFolderPath)
128 plt.savefig(plotFolderPath+date.strftime('%Y%m%d%H%M%S')+'FWHM_pos.pdf')
129 plt.savefig(plotFolderPath+date.strftime('%Y%m%d%H%M%S')+'FWHM_pos.png')
130
131 indOfMinFWHM = np.argmin(np.sqrt(FWHMx**2+FWHMy**2))
132
133 fig, axarr = plt.subplots(1,np.size(data,0))
134 #plot all the images besides each other
135 for iImg in ind:
136     axarr[iImg].imshow(data[iImg], cmap=plt.cm.jet,origin='bottom',
137                         extent=(x.min(), x.max(), y.min(), y.max()))
138     # axarr[iImg].contour(x, y, data_fitted[iImg], 5,
139     # colors='w', linewidths=0.8)
140     axarr[iImg].set_xlim( (x0[iImg]-12, x0[iImg]+12) )
141     axarr[iImg].set_ylim( (y0[iImg]-12, y0[iImg]+12) )
142     axarr[iImg].set_yticklabels('',visible=False)
143     axarr[iImg].set_xticklabels('',visible=False)
144     axarr[iImg].set_title('%.3f mm'%relativePos[iImg],fontsize=8)
145     if iImg == indOfMinFWHM:
146         axarr[iImg].set_frame_on(True)
147         for pos in ['top', 'bottom', 'right', 'left']:
148             axarr[iImg].spines[pos].set_edgecolor('r')
149             axarr[iImg].spines[pos].set_linewidth(2)
150     else:
151         axarr[iImg].set_frame_on(False)
152 plt.show()
153 date = datetime.datetime.today()
154
155 plt.savefig(plotFolderPath+date.strftime('%Y%m%d%H%M%S')+'ImgPSF.pdf')
156 plt.savefig(plotFolderPath+date.strftime('%Y%m%d%H%M%S')+'ImgPSF.png')

```

```

157
158
159 #save data
160 if not os.path.isdir(dataFolderPath):
161     os.makedirs(dataFolderPath)
162 date = datetime.datetime.today()
163 np.save(dataFolderPath+date.strftime('%Y%m%d%H%M%S')+'data.npy',data)
164 np.save(dataFolderPath+date.strftime('%Y%m%d%H%M%S')+'relativePos.npy',relativePos)

```

---

## A.2.2 AcquisAndSaveXimea.py

```

1 #%% Script to acquire images average over nbrImgAveraging images and save
2      them into fits file
3
4 from xiapi import xiapi
5 import datetime
6 import functionsXimea as fX
7 import winsound
8 import numpy as np
9 #%% instantiation
10 -----
11 #number of image to average
12 nbrImgAveraging = 5000
13 numberOffinalImages = 1
14
15 #Cropping information
16 sizeImg = 256
17
18 #Parameter of camera and saving
19 folderPathCropped = 'data//cropped/20/'
20 darkFolderPathCropped = '.data/dark//cropped/20/'
21 folderPathFull = 'data/full/'
22 darkFolderPathFull = '/data/dark//full/'
23 nameCamera = 'Ximea'
24 focusPos = 11.63
25
26 #Sound
27 duration = 1000 # millisecond
28 freq = 2000 # Hz
29
30 #initial guess for the fit depending on the position of the beam in the CCD
31 initial_guess = [250, 468, 954, 3, 3] # [max PSF,y,x,sigmay,sigmax]
32 -----
33 #%% data acquisition
34
35 #Opening the connection to the camera
36 cam = xiapi.Camera()
37 cam.open_device()
38 cam.set_imgdataformat('XI_MON08') #XIMEA format 8 bits per pixel
39 cam.set_gain(0)
40
41 img = xiapi.Image()

```

```

42 if cam.get_acquisition_status() == 'XI_OFF':
43     cam.start_acquisition()
44 #%% exposition
45 cond = 1
46 while bool(cond):
47     source = ''
48     winsound.Beep(freq, duration)
49     source = int(raw_input('Is the source turned on and at focus point
50         (usually %5.3f mm) (yes = 1) ? '%focusPos))
51     if source == 1:
52         cond = 0
53     else:
54         print 'Please turn on the source and place the camera on the focus
55             point (%5.3f mm)'%focusPos
56
57 if bool(source):
58     #Set exposure time
59     cam.set_exposure(fX.determineUnsaturatedExposureTime(cam,img,[1,10000],1))
60     #get centroid
61     centroid = fX.acquirePSFCentroid(cam,img,initial_guess)
62     print 'centroid at (%d, %d)'%(centroid[0],centroid[1])
63
64 #%%Acquire images at different camera position
65 acquire = 1
66 while bool(acquire):
67     cond = 1
68     while bool(cond):
69         dark = ''
70         winsound.Beep(freq, duration)
71         dark = int(raw_input('Is the source turned off (yes = 1) ? '))
72         if dark == 1:
73             cond = 0
74         else:
75             print 'Please shut down the source.'
76         winsound.Beep(freq, duration)
77         pos = float(raw_input('What is the position of the camera in mm focused
78             (%5.3f mm) dephase 2Pi (pos+ = %5.3f mm, pos- = %5.3f) ?
79             %(focusPos,focusPos+3.19,focusPos-3.19))')
80
81         if bool(dark):
82             print 'Acquiring dark image...'
83             # Acquire dark images
84             [darkData, stdDarkData] = fX.acquireImg(cam,img,nbrImgAveraging)
85             print 'Cropping'
86             [darkdataCropped, stddarkDataCropped] =
87                 fX.cropAroundPSF(darkData, stdDarkData, centroid, sizeImg, sizeImg)
88             print 'saving'
89             fX.saveImg2Fits(datetime.datetime.today(),darkFolderPathCropped,nameCamera,darkdataCropped)
90             fX.saveImg2Fits(datetime.datetime.today(),darkFolderPathFull,nameCamera,darkData, stdDarkData)
91
92         #Acquire images -----
93         cond = 1
94         while bool(cond):
95             source = ''
96             winsound.Beep(freq, duration)

```

```

94     source = int(raw_input('Is the source turned on (yes = 1) ? '))
95     if source == 1:
96         cond = 0
97     else:
98         print 'Please place turn on the camera'
99
100    if bool(source):
101        print 'Acquiring images...'
102        # Acquire focused images
103        for iImg in range(numberOfFinalImages):
104            imgNumber = iImg+1
105            print 'Acquiring Image %d'%imgNumber
106            [data, stdData] = fX.acquireImg(cam, img, nbrImgAveraging)
107            print 'Cropping'
108            [dataCropped, stdDataCropped] =
109                fX.cropAndCenterPSF(data-darkData, stdData+stdDarkData, sizeImg, initial_guess)
110            print 'Saving'
111            fX.saveImg2Fits(datetime.datetime.today(), folderPathCropped, nameCamera, dataCropped)
112            fX.saveImg2Fits(datetime.datetime.today(), folderPathFull, nameCamera, data-darkData, s
113
114    cond = 1
115    while bool(cond):
116        acquire = ''
117        winsound.Beep(freq, duration)
118        acquire = int(raw_input('Do you want to acquire at an other camera
119                                position (yes = 1, no = 0) ? '))
120        if acquire == 1:
121            cond = 0
122        elif acquire == 0:
123            cond = 0
124        else:
125            print 'please answer with 0 or 1 for no or yes, respectively'
126
127    ##Stop the acquisition
128    cam.stop_acquisition()
129    cam.close_device()
130    print 'Acquisition finished'

```

---

### A.2.3 functionsXimea.py

```

1 import numpy as np
2 import pyfits
3 import os
4 import scipy.optimize as opt
5 #%% Functions
-----
6
7
8 #Create and save .fits from numpy array
9 def saveImg2Fits(date,folderPath,Detector,data,stdData,pos,nbrAveragingImg):
10
11     #date : datetime at which the data where taken
12     #folderPath : where to save the data$
```

```

13     #Detector : name of detector (ex:Ximea)
14     #data : np.array containing the image
15     #stdData: np.array containing the error on each pixel
16     #pos : the position of the camera on the sliding holder in mm
17
18     imgHdu = pyfits.PrimaryHDU(data)
19     stdHdu = pyfits.ImageHDU(stdData,name = 'imgStdData')
20     hdulist = pyfits.HDULList([imgHdu,stdHdu])
21
22     if not os.path.isdir(folderPath):
23         os.makedirs(folderPath)
24
25     hdulist.writeto(folderPath +
26                     date.strftime('%Y%m%d%H%M%S')+'_'+Detector+'_'+pos+'.fits')
27
28
29
30
31
32
33
34
35
36
37
38
39
40
41
42
43
44
45
46
47
48
49
50
51
52
53
54
55
56
57
58
59
60
61
62
63
64
65
66

```

---

```

#Detector : name of detector (ex:Ximea)
#data : np.array containing the image
#stdData: np.array containing the error on each pixel
#pos : the position of the camera on the sliding holder in mm

imgHdu = pyfits.PrimaryHDU(data)
stdHdu = pyfits.ImageHDU(stdData,name = 'imgStdData')
hdulist = pyfits.HDULList([imgHdu,stdHdu])

if not os.path.isdir(folderPath):
    os.makedirs(folderPath)

hdulist.writeto(folderPath +
                date.strftime('%Y%m%d%H%M%S')+'_'+Detector+'_'+pos+'.fits')

def acquireImg(cam,img,nbrImgAveraging):
    imgData = np.zeros([1024,1280])
    stdData = np.zeros([1024,1280])
    for iImg in range(nbrImgAveraging) :
        #print iImg
        cam.get_image(img)
        imgTmpData = img.get_image_data_numpy()
        imgData[:,:] += imgTmpData
        stdData += imgTmpData*imgTmpData

    stdData =
        np.sqrt((stdData-imgData*imgData/nbrImgAveraging)/(nbrImgAveraging-1))/(np.sqrt(nbrImgAveraging))
    imgData = imgData/nbrImgAveraging

    return [imgData,stdData]

def determineUnsaturatedExposureTime(cam,img,exposureLimit,precision):
    exposureTimes = exposureLimit
    if cam.get_acquisition_status() == 'XI_OFF':
        cam.start_acquisition()

    while np.absolute(np.diff(exposureTimes))>precision:
        expTime2check = int(np.round(np.nanmean(exposureTimes)))
        print 'Try expTime : %d [us]\n' %expTime2check
        cam.set_exposure(expTime2check)
        data = acquireImg(cam,img,10)[0]

        if np.sum(data)>250:
            exposureTimes[1] = int(np.ceil(np.nanmean(exposureTimes)))
        else:
            exposureTimes[0] = int(np.floor(np.nanmean(exposureTimes)))
        print 'exposure time between %d and %d \n' %(exposureTimes[0],exposureTimes[1])

    return int(np.floor(np.nanmean(exposureTimes)))

def TwoDGaussian((x, y), A, yo, xo, sigma_y, sigma_x):
    g = A*np.exp( - ((x-xo)**2/(2*sigma_x**2) + ((y-yo)**2)/(2*sigma_y**2)))
    return g.ravel()

def acquirePSFCentroid(cam,img,initial_guess):

```

```

67 #create the matrix grid of the detector CCD
68
69 data = acquireImg(cam,img,200)[0]
70 centroid = getPSFCentroid(data,initial_guess)
71 return centroid
72
73 def getPSFCentroid(data,initial_guess):
74
75     x = np.linspace(0,1280,1280)
76     y = np.linspace(0,1024,1024)
77     x, y = np.meshgrid(x, y)
78     print 'fitting'
79     popt,pcov = opt.curve_fit(TwoDGaussian, (x,y), data.ravel(), p0 =
        initial_guess)
80     print 'fitting done'
81     return [popt[2],popt[1]]
82
83
84 def cropAndCenterPSF(data,stdData,size,initial_guess):
85     Xextent = np.size(data,1)
86     Yextent = np.size(data,0)
87
88     centroid = getPSFCentroid(data,initial_guess)
89
90     minMarge =
91         np.min([centroid[0],centroid[1],Xextent-centroid[0],Yextent-centroid[1]])
92
93     if minMarge>size/2:
94         return cropAroundPSF(data,stdData,centroid,size,size)
95     elif minMarge<size/2:
96         return cropAroundPSF(data,stdData, centroid,2*minMarge,2*minMarge)
97
98 def cropAroundPSF(data,stdData,centroid,sizeX,sizeY):
99
100    pxX =
101        [int(np.floor(centroid[0])-np.ceil(sizeX/2)),int(np.floor(centroid[0])+np.ceil(sizeX/2))]
102    pxY =
103        [int(np.floor(centroid[1])-np.ceil(sizeY/2)),int(np.floor(centroid[1])+np.ceil(sizeY/2))]
104
105    dataCropped = data[pxY[0]:pxY[1],pxX[0]:pxX[1]]
106
107    stdDataCropped = stdData[pxY[0]:pxY[1],pxX[0]:pxX[1]]
108
109    return [dataCropped,stdDataCropped]
```

---

# Appendix B

## IDL Code

### B.1 ONERA phase diversity

#### B.1.1 Diversity.pro

---

```

1 ;+
2 ;FUNCTION
3 ;      DIVERSITY(PSF,DEFOCUS,LAMBDA,FDIST,PXSIZE,THRESHOLD,MODE[,D1=,D2=,JMAX=,/KECK,/LARGEHEX,/SHOW]
4 ;
5 ; A function to retrieve the phase from a set of several in-focus and
6 ; out-of-focus PSF (at least two PSF) using a phase diversity algorithm.
7 ;
8 ; =====
9 ; ===== Copyrights : PLEASE DO NOT DISTRIBUTE OUTSIDE OF WMKO =====
10 ; ===== The central tool, decoconj_marg.pro is a property of =====
11 ; ===== Laurent Mugnier et al. at ONERA, Paris, France =====
12 ;
13 ;INPUTS name | type | unit
14 ;
15 ; PSF | REAL 2D SQUARE ARRAY DIM = [N,N,M] | FREE
16 ; A suite of M PSF acquired along the optical axis. It is best to have
17 ; at least one PSF close to the focal plane. The PSF must have been
18 ; cleaned from bad pixels, cosmic etc, and back-ground
19 ; subtracted. Each PSF must be square (DIM NxN) and an even size.
20 ;
21 ; NOTE ON PSF MATRIX SIZE N : N must be at least equal to 118. This is
22 ; required to ensure the minimum spatial resolution in the pupil plane
23 ; when reconstructing the phase. Indeed, there is a specification on
24 ; this spatial resolution which is coming from the AO OTF
25 ; computation, and the smallest size for the PSF is the one above.
26 ;
27 ; DEFOCUS | REAL VECTOR WITH M COMPONENTS | MILLIMETERS
28 ; Defocus distance for PSF above. Must be of course of the same length as
29 ; the number M of PSF. For instance [0,3,5] for a set of 3 PSF. Positive
30 ; value means the PSF is after the telescope focal plane, along the
31 ; optical axis, in the direction of light propagation.
32 ; ****
33 ; THE IDEAL VALUE FOR DZ IS DZ = LAMBDA * 8 * (F/D)^2, IN ABSOLUTE
34 ; VALUE, BUT IT DOES NOT HAVE TO BE EXACTLY THIS VALUE. HAVING PSF IN
35 ; INTERMEDIATE PLANES CAN HELP BUT IS NOT MANDATORY.
36 ; NOTE THAT DZ CAN BE NEGATIVE (PSF TAKEN ON BOTH SIDES OF THE FOCAL PLANE).
37 ; ****
38 ;
39 ; LAMBDA | REAL SCALAR > 0 | MICRONS

```

---

```

40 ; The central wavelength of the filter associated with the PSF
41 ; acquisition. We ignore the filter width here, so we assume
42 ; it's a rather narrow filter. Of course if we have a laser
43 ; beam then the lambda to give is the laser lambda, and there is
44 ; no filter.
45 ; >>>>> DO NOT USE ANY OTHER VALUE OTHERWISE THE COMPUTATION <<<<<
46 ; >>>>> IS TOTALLY MESSED UP - EVEN IF IT WILL CONVERGE !! <<<<<<
47 ;
48 ; FDIST | REAL SCALAR > 0 | METERS
49 ; Telescope optics focal distance. (150 m for Keck telescopes).
50 ;
51 ; PXSIZE | REAL SCALAR > 0 | ASEC/PX
52 ; Focal plane camera angular pixel size.
53 ;
54 ; THRESHOLD | REAL SCALAR > 0 | 1
55 ; A relative convergence threshold for the phase reconstruction.
56 ; This value must be at least 1e-3.
57 ;
58 ; MODE | CHAR STRING | -
59 ; The computation basis mode. There are two options:
60 ;
61 ; > MODAL, where the basis of the reconstructed phase are the Zernike
62 ; polynomials. This mode assumes that the telescope pupil is
63 ; circular (or an annulus), and you will be asked to enter the
64 ; pupil diameters, and the number of Zernike polynomials you want
65 ; to take into account.
66 ;
67 ; > ZONAL, where the basis are the pixels of the matrix that is being
68 ; used as the support to reconstruct the phase. The pixel size
69 ; depends on the PSF matrix size (DIMPSF), the sky pixel size
70 ; (PXSIZE), and the wavelength, and is computed from
71 ;     dpx = LAMBDA*1e-6/(DIMPSF*PXSIZE)
72 ; where of course units have to be homogeneous.
73 ;
74 ; This mode works in principle with any sort of pupil
75 ; shape. Now for the Keck application, we only allow for either an
76 ; annular pupil (for instance we used circular pupil masks in the
77 ; camera) or the full hexagonal telescope pupil.
78 ;
79 ; It is interesting to run the code on both modes (modal/zonal)
80 ; when the pupil is circular. Do not be surprised if the
81 ; reconstructed phase does not look exactly the same in the two
82 ; cases. The phase reconstruction is always a procedure which is very
83 ; sensitive to a lots of sometime badly known parameters, for instance
84 ; the noise level, and other funny things...
85 ;
86 ; ****
87 ; THE OTHER INPUTS DEPEND ON THE MODE
88 ; ****
89 ;
90 ;OPTIONAL INPUTS name | type | unit | default value
91 ;
92 ; ****
93 ; If MODE = 'MODAL' the following conditions and inputs are required:
94 ; ****
95 ;
96 ; Pupil shape must be a disk or an annulus.

```

```
97 ;
98 ; D1 = value | REAL SCALAR > 0 | METERS | none
99 ; Telescope primary mirror external diameter.
100 ; Syntax: D1=value.
101 ;
102 ; D2 = value | REAL SCALAR >= 0 | METERS | none
103 ; Telescope primary mirror central obscuration diameter.
104 ; Syntax: D2=value.
105 ;
106 ; JMAX = value | REAL SCALAR > 0 | 1 | 45
107 ; The last Zernike polynomial j-index to consider in the reconstruction.
108 ; Syntax: JMAX=value.
109 ;
110 ; ****
111 ; If MODE = 'ZONAL' the following conditions and inputs are required:
112 ; ****
113 ;
114 ; -----
115 ; If the pupil is an annulus
116 ; -----
117 ;
118 ; D1 = value | REAL SCALAR > 0 | METERS | none
119 ; Telescope primary mirror external diameter.
120 ; Syntax: D1=value.
121 ;
122 ; D2 = value | REAL SCALAR >= 0 | METERS | none
123 ; Telescope primary mirror central obscuration diameter.
124 ; Syntax: D2=value.
125 ;
126 ; JMAX = value | REAL SCALAR > 0 | 1 | 45
127 ; **** OPTIONAL INPUT ****
128 ; The last Zernike polynomial j-index to consider in the modal
129 ; reconstruction of the zonal reconstructed phase. Do not try to
130 ; project on too many modes !
131 ; Syntax: JMAX = value.
132 ;
133 ; -----
134 ; If the pupil is the Keck telescope primary mirror
135 ; -----
136 ;
137 ; 1/ Set the keyword /KECK,
138 ; 2/ make the parameter file 'KeckSegmentedPupilArchitecture.sav',
139 ;     available in the directory where you run the code.
140 ;
141 ;KEYWORD
142 ;
143 ; /KECK reconstruct the phase for Keck hexagonal pupil.
144 ;
145 ; /LARGEHEX set if the pupil is the large hexagonal mask of NIRC2 @ KECK.
146 ;
147 ; /SHOW to display the in/out-of-focus OTF and the final phase.
148 ;
149 ;OUTPUT NAME | TYPE | UNIT
150 ;
151 ; A structure variable, with the following components (depending on
152 ; the computation mode and the pupil)
153 ;
```

```

154 ; .PHASE | REAL 2D ARRAY [DIMREC,DIMREC] | RAD
155 ; The reconstructed phase, in the pupil plane, projected in M2 plane,
156 ; and without tip-tilt.
157 ;
158 ; .LAMBDA | REAL SCALAR | MICROMETERS
159 ; The wavelength associated with the phase diversity PSF.
160 ;
161 ; .WAVEFRONT | REAL 2D ARRAY [DIMREC,DIMREC] | MICROMETERS
162 ; The reconstructed wavefront = PHASE*LAMBDA/(2*dpi),
163 ; in the primary mirror plane. We need it when we want to use the
164 ; static phase for another LAMBDA.
165 ;
166 ; .DIMREC | INTEGER SCALAR | 1
167 ; Phase matrix size.
168 ;
169 ; .DXP | REAL SCALAR | M
170 ; Phase matrix pixel size.
171 ;
172 ; .MASKPUPIL | BYTE 2D ARRAY | 1
173 ; The pupil mask, 1 inside, 0 outside.
174 ;
175 ; >>>> IF /KECK KEYWORD NOT SET
176 ; .A_J | REAL VECTOR DIM = 187 | MICROMETERS
177 ; The Zernike coefficients of the reconstructed phase, starting
178 ; with the defocus coefficient a4, up to a_JMAX.
179 ; PISTON AND TIP-TILT COEFFICIENTS ARE NOT GIVEN.
180 ;
181 ; .J | INTEGER VECTOR OF LENGTH (JMAX-3) | 1
182 ; The Zernike j-indexes associated with .AJ, from j=4 to j=JMAX.
183 ; PISTON AND TIP-TILT COEFFICIENTS ARE NOT GIVEN.
184 ;
185 ; >>>>> Only in MODAL mode :
186 ; .HIGHPHASE | REAL 2D ARRAY | RAD
187 ; The reconstructed phase without the defocus polynomial (Z4).
188 ;
189 ;EXTERNAL CUSTOM ROUTINES AND OTHER REQUIRED FILES
190 ;
191 ; coogrid.pro
192 ; discft.pro
193 ; hexaft.pro
194 ; hexagon.pro
195 ; indzer.pro
196 ; mathft.pro
197 ; pixmatsize.pro
198 ; psfotftsc.pro
199 ; polzer.pro
200 ; rectft.pro
201 ; tvsg.pro
202 ; valid_input.pro
203 ;
204 ; deco_conjmarg-IDLv7.0.6.sav - the phase diversity codes compiled.
205 ;
206 ; for KECK project : KeckSegmentedPupilArchitecture.sav
207 ; for KECK project : LargeHex.sav
208 ;
209 ;DEV NOTES
210 ;

```

```

211 ; Laurent Jolissaint, HEIG-VD, Switzerland, May 2, 2013.
212 ; Oct 01, 2013 LJ included Keck telescope pupil option.
213 ; Oct 18, 2013 LJ added pupil mask to the output structure variable
214 ; Dec 18, 2013 LJ added projection into the Zernike basis, in zonal mode.
215 ; May 16, 2014 LJ rotation of the hexagonal pupil to have the
216 ;           elevation axis oriented horizontally, as it should.
217 ; Jun 17, 2014 LJ there was a typo and a unit error for DEFOCUS.
218 ; Jun 17, 2014 LJ added a reconstruction of the phase map from the
219 ;           projected Zernike coefficients, for checking.
220 ; Jul 14, 2014 LJ made it possible to use more than 2 PSF on input.
221 ; Jul 14, 2014 LJ improved projection onto annular Zernike basis.
222 ; Jul 15, 2014 LJ changed input PXSIZE unit from asec to microns.
223 ; Sep 30, 2015 LJ changed KECK pupil orientation, now aligned with
224 ;           focal plane detector (NIRC2 for instance).
225 ; Sep 30, 2015 LJ removed projection onto the Zernike basis, replaced
226 ;           with a match of the reconstructed phase resolution
227 ;           with the AO structure function resolution.
228 ; Oct 01, 2015 LJ reorganized code, added a reconstructed wavefront
229 ;           to the output.
230 ; May 12, 2016 LJ added LARGEHEX option for KECK.
231 ; May 12, 2016 LJ restored PXSIZE unit to asec instead of mu (that was
232 ;           wrong).
233 ; May 18, 2016 LJ reset the setting of the phase matrix size to an
234 ;           optimum, different from KECK requirement.
235 ; May 18, 2016 LJ reintroduced projection onto the Zernike basis (but not
236 ;           in KECK mode).
237 ; Jun 08, 2016 LJ fully removed the constraint on the spatial
238 ;           frequency sampling in the pupil plane. It is better
239 ;           to use the value adapted to the input PSF and adapt
240 ;           the scaling of the final phase, if needed, using REBIN.
241 ; Jun 09, 2016 LJ simplified options in MODAL mode.
242 ; Jun 12, 2016 LJ allowed JMAX input in ZONAL mode.
243 ; Jun 12, 2016 LJ set the optical axis in between the 4 central pixels in
244 ;           order
245 ;           to follow the same convention than deco_conjmarg.
246 ; Jun 13, 2016 LJ removed the segments gaps for Keck pupil mask.
247 ; Jun 16, 2016 LJ implemented PSF noise reduction by filtering out the
248 ;           OTF above the telescope OTF domain definition.
249 ; Jul 11, 2016 LJ added /SHOW to display the OTF and the final phase.
250 ; Sep 10, 2016 LJ LARGEHEX option had an error in the pupil
251 ;           definition.
252 ; Sep 21, 2016 LJ I forgot to set a central obscuration in /KECK mode.
253 ; Nov 17, 2016 LJ computation of the defocus in radian done in double
254 ;           precision, because w/o this it was making a little
255 ;           but disturbing difference with L. Mugnier root
256 ;           code deco_conjmarg.pro
257 ; Nov 30, 2016 LJ added a few warnings for pixel size and wavelength.
258 ;
259 ;BUGS write to laurent.jolissaint@heig-vd.ch
260 ;-
261 FUNCTION
        DIVERSITY,PSF,DEFOCUS,LAMBDA,FDIST,PXSIZE,THRESHOLD,MODE,D1=D1,D2=D2,JMAX=JMAX,KECK=KECK,LARGE
262
263 ;*****
264 ;CHECK INPUTS

```

```

265 ;*****
266 if n_params() ne 7 then message,'THIS FUNCTION REQUIRES 7 INPUTS AND
267   SEVERAL OPTIONAL INPUTS'
268 VALID_INPUT,'DIVERSITY.PRO','PSF',PSF,'real',3,'no','free','free'
269 ss=size(PSF)
270 if ss[1] ne ss[2] then message,'PSF MATRICES MUST BE SQUARE AND EVEN SIZES'
271 if ss[1] mod 2 ne 0 then message,'PSF MATRICES MUST BE SQUARE AND EVEN
272   SIZES'
273 VALID_INPUT,'DIVERSITY.PRO','DEFOCUS',DEFOCUS,'real',[1,ss[3]],'no','free','free'
274 VALID_INPUT,'DIVERSITY.PRO','LAMBDA',LAMBDA,'real',0,'no','++','free'
275 VALID_INPUT,'DIVERSITY.PRO','FDIST',FDIST,'real',0,'no','++','free'
276 VALID_INPUT,'DIVERSITY.PRO','PXSIZE',PXSIZE,'real',0,'no','++','free'
277 VALID_INPUT,'DIVERSITY.PRO','THRESHOLD',THRESHOLD,'real',0,'no','++','free'
278 VALID_INPUT,'DIVERSITY.PRO','MODE',MODE,'string',0,'no',[zonal,modal,ZONAL,MODAL],'
279 if size(D1,/type) ne 0 then
280   VALID_INPUT,'DIVERSITY.PRO','D1',D1,'real',0,'no','++','free'
281 if size(D2,/type) ne 0 then
282   VALID_INPUT,'DIVERSITY.PRO','D2',D2,'real',0,'no','0+','free'
283 if size(JMAX,/type) ne 0 then
284   VALID_INPUT,'DIVERSITY.PRO','JMAX',JMAX,'integer',0,'no','++',1
285 if strlowlcase(MODE) eq 'modal' then if size(JMAX,/type) eq 0 then
286   message,'JMAX INPUT IS MANDATORY IF MODE=MODAL'
287 if strlowlcase(MODE) eq 'zonal' then begin
288   if not keyword_set(KECK) and not keyword_set(LARGEHEX) then if
289     fix(size(D1,/type) ne 0)+fix(size(D2,/type) ne 0) ne 2 then $
290       message,'IF MODE = ZONAL, EITHER GIVE THE PUPIL DIAMETERS D1 & D2
291         **OR** SET THE KEYWORDS /KECK OR /LARGEHEX'
292   if keyword_set(KECK) or keyword_set(LARGEHEX) then if fix(size(D1,/type)
293     ne 0)+fix(size(D2,/type) ne 0) ne 0 then $
294     message,'IN /KECK OR /LARGEHEX MODES, D1 AND D2 ARE NOT REQUIRED',
295   endif
296   if PXSIZE gt 100 or PXSIZE lt 0.01 then print,'WARNING: THE PIXEL SIZE
297     LOOKS ODD - CHECK IT. COMPUTATION CONTINUES ANYWAY.'
298
299 ;*****
300 ;SETTINGS
301 ;*****
302 rad2asec=180*3600.d!/dpi
303 asec2rad=1.d/rad2asec
304 dimmat=n_elements(PSF[*,0,0])
305 dfp=PXSIZExasec2rad/(LAMBDA*1e-6)
306 dxp=1.d/dfp/dimmat
307 xyrt=COOGRID(dimmat,dimmat,scale=(dimmat-1)*0.5*dxp)
308
309 ;*****
310 ;BUILD PUPIL MASK
311 ;*****
312 if keyword_set(KECK) then begin
313   restore,'KeckSegmentedPupilArchitecture.sav'
314   D1=mir.DEXTMAX
315   D2=2.65d
316   hexa=HEXAGON(mir.ssz,xyrt.x,xyrt.y)
317   maskpupil=bytarr(dimmat,dimmat); Below, I have an 'or' instead of a '+'
318   because I want maskpupil to be 0 or 1
319   for i=0,mir.tns-1 do maskpupil = maskpupil or
320     shift(hexa,mir.pos[0,i]/dxp,mir.pos[1,i]/dxp)
321   maskpupil=rotate(maskpupil,6)

```

```

310     hexa=HEXAGON(10.39,xyrt.x,xyrt.y) ; this is to remove the segment gaps
311     maskpupil=maskpupil or hexa
312     maskpupil=maskpupil*(xyrt.r ge 0.5*D2)
313 endif
314 if keyword_set(LARGEHEX) then begin
315   restore,'LargeHex.sav'
316   D1=2*b
317   maskpupil=hexagon(2*b,xyrt.x,xyrt.y)*(1-rotate(hexagon(2*a*2/sqrt(3),xyrt.x,xyrt.y),6))
318 endif
319 if not keyword_set(KECK) and not keyword_set(LARGEHEX) then begin
320   maskpupil=xyrt.r le 0.5*D1
321   if D2 gt dpx then maskpupil=maskpupil*(xyrt.r ge 0.5*D2)
322 endif
323 dimrec=fix(D1/dpx)
324 if dimrec mod 2 eq 1 then dimrec=dimrec+1
325 masklarge=maskpupil
326 if dimrec gt dimmat then message,'THERE IS AN ISSUE WITH THE PIXEL SIZE OR
THE WAVELENGTH - CHECK THE UNITS'
327 maskpupil=maskpupil[dimmat/2-dimrec/2:dimmat/2+dimrec/2-1,dimmat/2-dimrec/2:dimmat/2+dimrec/2-1]
328
329 ;*****
330 ;PREPARE PSF
331 ;*****
332 ; setting the sky OTF frequencies beyond the telescope OTF domain to 0
333 ; to minimize the noise content in the PSF
334 if keyword_set(KECK) then begin
335   ps=PIXMATSIZE(mir0,PXSIZE,dimmatt,LAMBDA)
336   tscpsf=(PSFOTFTSC(mir,ps)).psf
337   tscpsf[1:dimmatt-1,1:dimmatt-1]=rotate(tscpsf[1:dimmatt-1,1:dimmatt-1],1)
338 endif else tscpsf=abs(MATHFT(masklarge,dx=dpx,ic=dimmatt/2,jc=dimmatt/2))^2
339 tscotf=MATHFT(tscpsf,dx=PXSIZE*asec2rad,ic=dimmatt/2,jc=dimmatt/2)
340 ww=where(abs(tscotf) lt max(abs(tscotf))*1e-4) ; Telescope OTF footprint
            selection
341 ;sky PSF filtering
342 images=PSF
343 skyotf=PSF*dcomplex(0,1)
344 for i=0,n_elements(images[0,0,*])-1 do begin
345   tmp=MATHFT(images[*,*,i],dx=PXSIZE*asec2rad,ic=dimmatt/2,jc=dimmatt/2)
346   tmp[ww]=0
347   skyotf[*,*,i]=tmp
348   images[*,*,i]=double(MATHFT(skyotf[*,*,i],dx=PXSIZE*asec2rad,ic=dimmatt/2,jc=dimmatt/2,/inverse)
349   images[*,*,i]=images[*,*,i]/mean(images[*,*,i])
350 endfor
351
352 ;optionally displaying the OTF
353 if keyword_set(SHOW) then begin
354   rw,800,400,0
355   tmp=abs(skyotf[*,*,0])
356   for i=1,n_elements(images[0,0,*])-1 do tmp=[tmp,abs(skyotf[*,*,i])]
357   shade_surf,tmp
358 endif
359
360 ;*****
361 ;STARTING RECONSTRUCTION
362 ;*****
363 restore,'C:\Users\Jojo\Desktop\PdM-HEIG\Science\OneraCode\deco_conjmarg-IDLv7.0.6.sav',
364 defoc_array_a4=1d3*DEFOCUS/(16.d*sqrt(3.d)*(FDIST/D1)^2)*2.d!*dpi/LAMBDA

```

```

365 pupdiamPX=D1/dxp
366 ;
367 ;*****
368 ;OPTION MODAL RECONSTRUCTION
369 ;*****
370 if strlowcase(MODE) eq 'modal' then begin
371
372 ai_align = dblarr((n_elements(images[0,0,*])-1)*2)
373 ai_init = dblarr(JMAX-3) ; from Z_4 to Z_{nbmodes+1}
374 sigma2 = 1.0           ; noise variance initial guess / pixel
375
376 DECO_CONJMARG, objet_rec, a_rec, $
377             IMAGES = images, $
378             SIGMA2 = sigma2, $
379             OBJ_REGUL_TYPE = 'none', $
380             PSF_TYPE = 'ai', $
381             PARAMPSF_GUESS = ai_init, $
382             DEFOC_ARRAY_A4 = defoc_array_a4, $
383             PUP_DIAM = pupdiamPX, $
384             DOUBLE = 1B, $
385             METHODE = 'conj', $
386             PUP_MASQ = maskpupil, $
387             AI_ALIGN = ai_align, $
388             /VMLM, FSEUIL = THRESHOLD ,/LEQ
389
390 ;build the phase
391 ;
392 ;get Zernike basis
393 zernike=POLZER(dimrec,D1/dxp,4,JMAX-3)
394 ;
395 phase=dblarr(dimrec,dimrec)
396 for i=0,JMAX-4 do phase=phase+a_rec[i]*zernike[*,*,i]*maskpupil
397 highphase=dblarr(dimrec,dimrec)
398 for i=1,JMAX-4 do highphase=highphase+a_rec[i]*zernike[*,*,i]*maskpupil
399
400 return,{phase:phase,highphase:highphase,a_j:a_rec*LAMBDA/2!/dpi,j:indgen(JMAX-3)+4,dxp:dxp
401             maskpupil:maskpupil,lambda:LAMBDA,wavefront:LAMBDA/2!/dpi*phase,dimrec:n_elements(p
402
403 endif
404 ;
405 ;*****
406 ;OPTION ZONAL RECONSTRUCTION
407 ;*****
408 if strlowcase(MODE) eq 'zonal' then begin
409
410 psf_hyper=600.0 ; this parameter can be adjusted to optimize the
411                 computation but this values works best
412 phase_init = dblarr(dimrec, dimrec)
413 sigma2 = 1.0D
414 itmax = 5000L
415
416 DECO_CONJMARG, objet_rec, phase, $
417             IMAGES = images, $
418             SIGMA2 = sigma2, $
419             NOISE_TYPE = 'ls', $
420             OBJ_REGUL_TYPE = 'none', $
421             PSF_TYPE = 'phase', $
```

```

421     PSF_REGUL_TYPE = 'expifi', $
422     PSF_HYPER = psf_hyper, $
423     PARAMPSF_GUESS = phase_init, $
424     DEFOC_ARRAY_A4 = defoc_array_a4, $
425     PUP_DIAM = pupdiamPX, $
426     DOUBLE = 1B, $
427     ITMAX = itmax, $
428     METHODE = 'conj', $
429     PUP_MASQ = maskpupil, $
430     /VMLM, FSEUIL = THRESHOLD
431
432 if not keyword_set(KECK) and not keyword_set(LARGEHEX) then begin
433   ;project reconstructed phase onto the Zernike basis to get the
434   ;coefficients
435   ;
436   ;get Zernike basis
437   if not keyword_set(JMAX) then JMAX = 45
438   n_modes=JMAX-3
439   zernike=POLZER(dimrec,D1/dxp,4,n_modes)
440   ;
441   ;compute annular pupil Zernike polynomials covariance matrix
442   ;
443   zercov=ZERNIKE_SPATIAL_COVARIANCE_ANNULAR_PUPIL(D2/D1,4,JMAX)
444   ;get B vector
445   b_rec=dblarr(n_modes)
446   for i=0,n_modes-1 do
447     b_rec[i]=total(maskpupil*phase*zernike[*,*,i])*(dxp/(0.5*D1))^2/!dpi
448   ;get solution
449   a_rec=invert(zercov,/double)#b_rec*LAMBDA/2/!dpi
450   return,{phase:phase,dxp:dxp,maskpupil:maskpupil,dimrec:dimrec,lambda:LAMBDA,wavefront:LAMBDA}
451 endif
452
453 return,{phase:phase,dxp:dxp,maskpupil:maskpupil,dimrec:dimrec,lambda:LAMBDA,wavefront:LAMBDA/2}
454
455 endif
456
457 end

```

---

## B.2 Shack-Hartmann Acquisition Code

### B.2.1 readAndAverageSHdata.pro

```

1 function readAndAverageSHdata, folderPath
2
3 fileExt='*.csv'
4
5 files = file_search(folderPath+fileExt)
6
7 r = readshwfsdata(files[0])
8
9 NFiles = n_elements(files)
10
11 for ifile = 1,Nfiles-1 do begin
12
13   rtmp = readshwfsdata(files[ifile])

```

---

```

14
15   r.wavefront = r.wavefront+rtmp.wavefront
16   r.zernike[3,*] = r.zernike[3,*]+rtmp.zernike[3,*]
17
18 endfor
19
20 r.wavefront = r.wavefront / NFiles
21 r.zernike[3,*] = r.zernike[3,*] / Nfiles
22
23 return, r
24 end

```

---

## B.2.2 readSHWFSdata.pro

---

```

1 function readSHWFSdata, filePath
2
3 openr, f, filePath, /GET_LUN
4
5 iLine = 0
6 line =
7
8
9 coefficient = []
10 index = []
11 order = []
12 frequency = []
13 wavefront = []
14
15 while ~EOF(f) do begin
16   readf, f, line
17   iLine += 1
18
19   ;get the zernike coefficient
20   if strmatch(line,'* ZERNIKE FIT *') then begin
21     subheaderNbrLines = 5
22     for isHd =1,subheaderNbrLines do begin
23       readf, f, line
24       iLine += 1
25     endfor
26
27     readf, f, line
28     iLine += 1
29     sLine = strsplitsplit(line,',',,/EXTRACT)
30
31     while stregex(sLine[0],'[0-9]+') ne -1 and ~EOF(f) do begin
32       index = [[index],[long(sLine[0])]]
33       order = [[order],[long(sLine[1])]]
34       frequency = [[frequency],[long(sLine[2])]]
35       coefficient = [[coefficient],[double(sLine[3])]]
36       readf, f, line
37       iLine += 1
38       sLine = strsplitsplit(line,',',,/EXTRACT)
39     endwhile
40   endif
41

```

---

```
42 if strmatch(line,'*\/*\* WAVEFRONT \*/*\*') then begin
43   subheaderNbrLines = 11
44   for isHd =1,subheaderNbrLines do begin
45     readf, f, line
46     iLine += 1
47   endfor
48   readf, f, line
49   iLine += 1
50   sLine = strsplit(line,',',/EXTRACT)
51   nel = n_elements(sLine)
52   while stregex(sLine[0], '[0-9]+') ne -1 and ~EOF(f) do begin
53     waveform = [[waveform],[double(sLine[1:nel-1])]]
54     readf, f, line
55     iLine += 1
56     sLine = strsplit(line,',',/EXTRACT)
57   endwhile
58
59   endif
60 endwhile
61 free_lun, f
62
63 zernike = [index,order,frequency,coefficient]
64
65 return, {zernike:zernike,wavefront:wavefront}
66
67 end
```

---





## Appendix C

# Optical Component Datasheets

### C.1 Pigtailed laser diode

**THORLABS**

**Pigtailed Laser Diode, SMF**

**Description**

Thorlabs' Single Mode Pigtailed Laser Diodes are standard TO-packaged diodes that have been pigtailed to a 1 m long single mode fiber with an FC/PC connector. Each unit is tested before shipment. Please refer to the unit-specific test datasheet for optimal operating parameters.

**Specifications**

LPS-635-FC Specifications		LPS-635-FC Specifications		
		Min	Typ.	Max
LD Reverse Voltage (Max)	2 V	625 nm	635 nm	640 nm
PD Reverse Voltage (Max)	30 V	20 mA	50 mA	75 mA
Optical Output Power	2.5 mW (Typ.)	0.13 mW/mA	0.18 mW/mA	-
Operating Temperature	0 to 50 °C			
Storage Temperature	-10 to 65 °C			
Pin Code	9A			
Laser Diode	HL6320G			
Fiber	SM600			
Connector	FC/PC			

\*Temperature = 25 °C

**Drawing**

**Pigtail Bottom View:** Dimensions include 0.38", 0.75", 0.30", 0.59", Ø1.00", 0.15", 1.09", 1.28", Clearance Hole for #2 Hardware 2 Places, Diode Leads, and a note for 2.5 mm.

**Side View:** Dimensions include 1.28", 1.09", 0.15", Strain Relief Boot, Fiber 1 m of SM600, and Laser/Lens Housing.

**Diode Bottom View:** Dimensions include 2.5 mm and a note for 90°.

**Pin Diagram:** Shows PD (Positive) and LD (Negative).

**PIN CODE A:** Shows PIN CODE A.

**NOTICE:** To avoid equipment damage from static discharge: Wear ESD wriststrap when handling this device.

US, Canada, & South America: +1-973-300-3000 | France: +33 (0) 970 444 844 | Europe: +49 (0) 8131-5956-0 | UK & Ireland: +44 (0) 1353-654440  
Brazil: +55-16-3413 7062 | Scandinavia: +46-31-733-30-00 | Japan & Asia: +81-3-5979-8889 | China: +86 (0)21-60561122

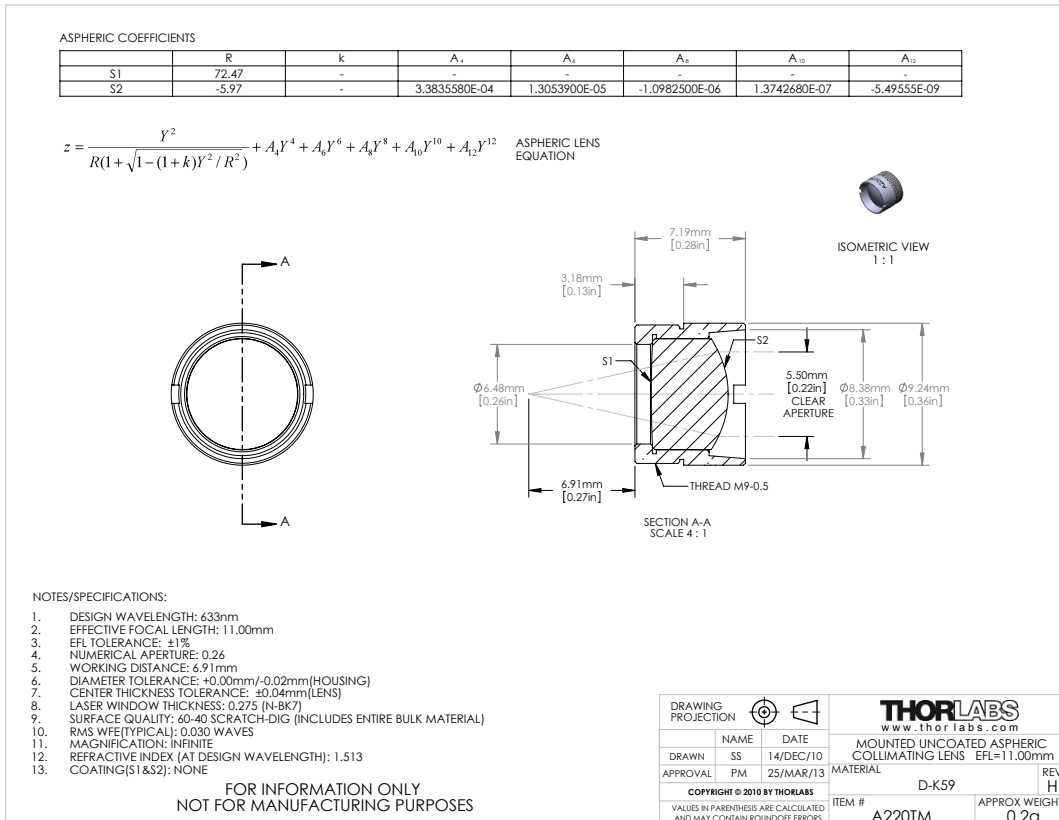
www.thorlabs.com

June 6, 2013  
5175-S01, Rev B

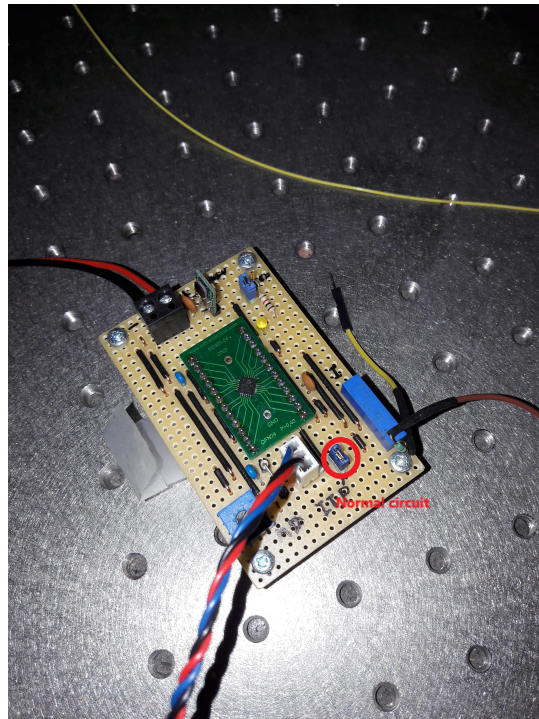
### C.1.1 Power supply modification

Unfortunately, for the phase diversity experiment, chapter , the power supplied by the Diode driver was too high and the Ximea camera was always saturated. So I modified the driver circuit and added a potentiometer and resistance to lower the current so that the detector do not reach the saturation.

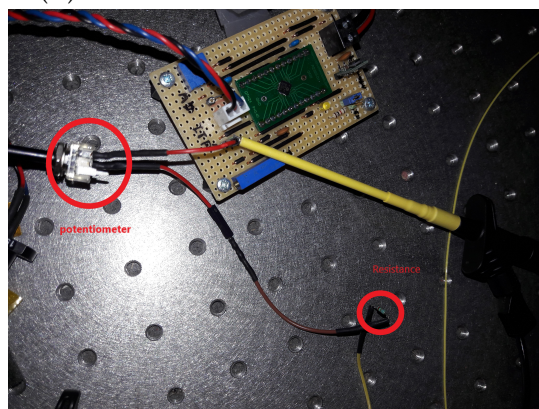
## C.2 Converging lens A220TM-A, f = 11 mm



Source : [www.thorlabs.com](http://www.thorlabs.com)



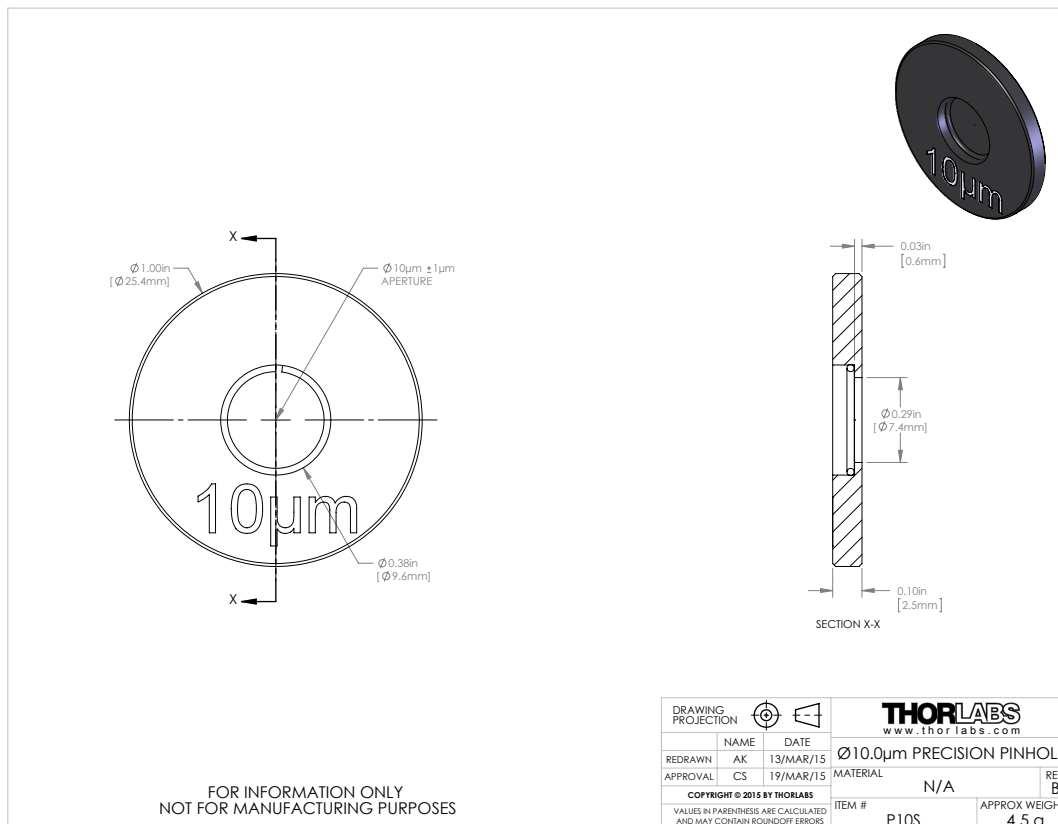
(A) LED driver without the modification



(B) LED driver with the resistance and the potentiometer

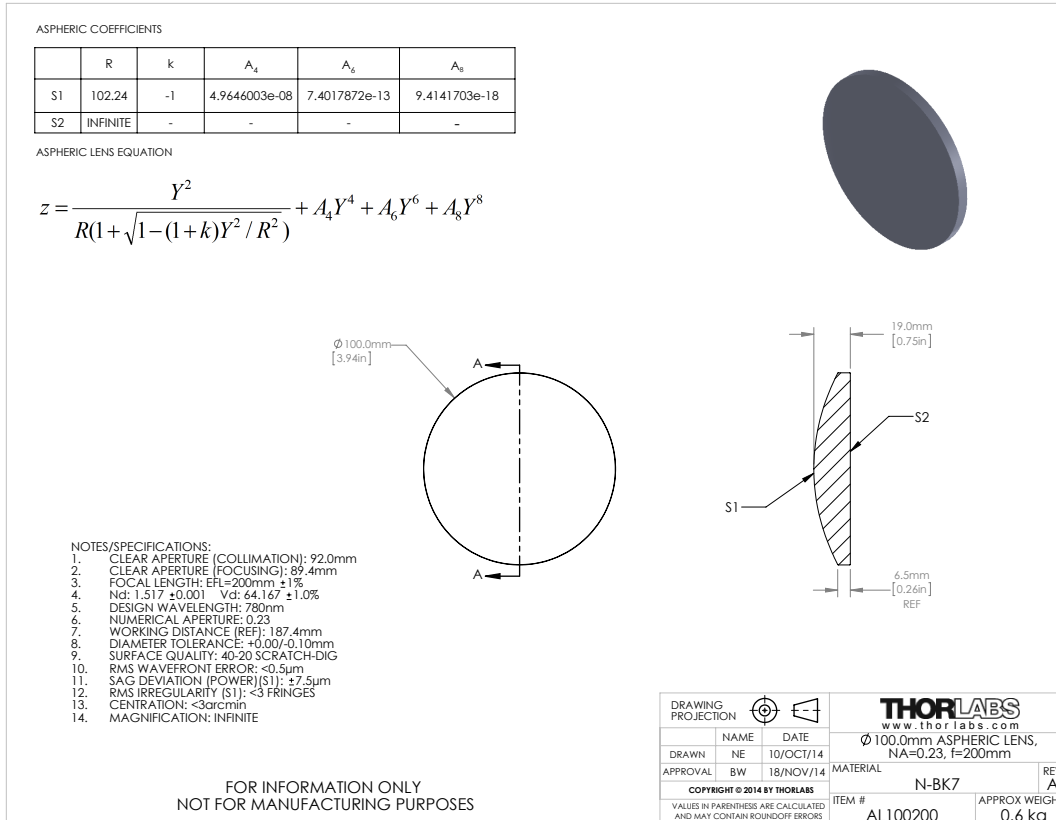
FIGURE C.1: LED driver

### C.3 Pinhole 10 $\mu\text{m}$



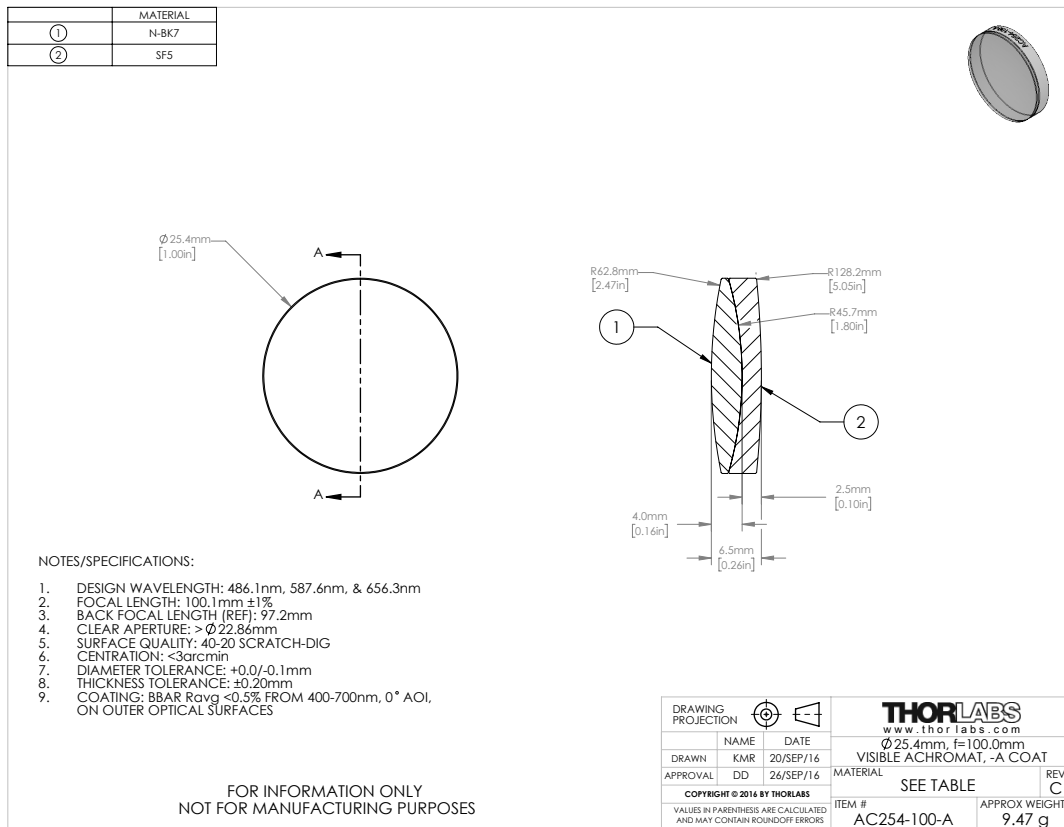
Source : [www.thorlabs.com](http://www.thorlabs.com)

## C.4 Converging lens AL100200, f = 200 mm



Source : [www.thorlabs.com](http://www.thorlabs.com)

## C.5 Converging lens AC254-100-A, $f = 100 \text{ mm}$



Source : [www.thorlabs.com](http://www.thorlabs.com)

## C.6 Ximea Camera, MQ013MG-E2



### Specifications:

<b>Resolution:</b>	1.3 MP 1280 × 1024 pixels
<b>Sensor type:</b>	CMOS Matrix B/W
<b>Sensor model:</b>	e2V EV76C560 ABT-EQV
<b>Sensor size:</b>	1/1.8"
<b>Sensor active area:</b>	6.9 × 5.5 mm
<b>Pixel size:</b>	5.3 µm
<b>Bits per pixel:</b>	8, 10
<b>Dynamic range:</b>	60 dB
<b>Frame rates:</b>	60 fps
<b>On-chip binning:</b>	1x1, 2x2
<b>Image data interface:</b>	USB 3.0
<b>Data I/O:</b>	GPIO IN, OUT
<b>Power requirements:</b>	0.9 Watt
<b>Lens mount:</b>	C or CS Mount
<b>Weight:</b>	26 grams
<b>Dimensions WxHxD:</b>	26 x 26 x 26 mm
<b>Operating environment:</b>	50 °C
<b>Customs tariff code:</b>	8525.80 30 (EU) / 8525.80 40 (USA)
<b>ECCN:</b>	EAR99

Source : [www.ximea.com/en/products/usb3-vision-cameras-xiq-line/mq013mg-e2](http://www.ximea.com/en/products/usb3-vision-cameras-xiq-line/mq013mg-e2)

## C.7 Shack-Hartmann wavefront sensor, WFS150-5C

### 8 Appendix

#### 8.1 Technical Data

##### 8.1.1 WFS150/300

Item #	WFS150-5C	WFS150-7AR	WFS300-14AR		
<b>Microlenses</b>					
Microlens Array	MLA150M-5C	MLA150M-7AR	MLA300M-14AR		
Substrate Material	Fused Silica (Quartz)				
Number of Active Lenslets	Software Selectable				
Max. Number of Lenslets	39 x 31	19 x 15			
<b>Camera</b>					
Sensor Type	CCD				
Resolution	max. 1280 x 1024 pixels, Software Selectable				
Aperture Size	5.95 mm x 4.76 mm				
Pixel Size	4.65 µm x 4.65 µm				
Shutter	Global				
Exposure Range	79 µs - 65 ms				
Frame Rate	max. 15 Hz				
Image Digitization	8 bit				
<b>Wavefront Measurement</b>					
Wavefront Accuracy <sup>1)</sup>	$\lambda/15$ rms @ 633 nm		$\lambda/50$ rms @ 633 nm		
Wavefront Sensitivity <sup>2)</sup>	$\lambda/50$ rms @ 633 nm		$\lambda/150$ rms @ 633 nm		
Wavefront Dynamic Range <sup>3)</sup>	> 100 $\lambda$ @ 633 nm		> 50 $\lambda$ @ 633 nm		
Local Wavefront Curvature <sup>4)</sup>	> 7.4 mm	> 10.0 mm	> 40.0 mm		
<b>External Trigger Input</b>					
Save Static Voltage level	0 to 30 V DC				
LOW Level	0.0 V to 2.0 V				
HIGH Level	5.0 V to 24 V				
Input current	> 10 mA				
Min Pulse Width	100 µs				
Min. Slew Rate	35 V / msec				
<b>Common Specifications</b>					
Optical Input	C-Mount				
Power Supply	<1.5 W, via USB				
Operating Temperature Range <sup>5)</sup>	+5 to +35 °C				
Storage Temperature Range	-40 to 70 °C				
Warm-Up Time for Rated Accuracy	15 min				
Dimensions (W x H x D)	32.0 mm x 40.4 mm x 45.5 mm				
Weight	0.1 kg				

<sup>1)</sup> Absolute accuracy using internal reference. Measured for spherical wavefronts of known RoC.

<sup>2)</sup> Typical relative accuracy. Achievable after, and with respect to a user calibration, 10 image averages

<sup>3)</sup> Over entire aperture of wavefront sensor

<sup>4)</sup> Radius of wavefront curvature over single lenslet aperture

<sup>5)</sup> non-condensing

All technical data are valid at  $23 \pm 5^\circ\text{C}$  and  $45 \pm 15\%$  rel. humidity (non condensing)



# Bibliography

- Blanc, Amandine (2002). "Identification de réponse impulsionnelle et restauration d'images: apports de la diversité de phase". PhD thesis. Université Paris XI UFR Scientifique d'Orsay.
- Bouxin, A. (2017). "Phasor diversity to measure the static aberrations of an optical system". MA thesis. HEIG-VD.
- F. Zernike, von (1934). "Beugungstheorie des schneidenverfahrens und seiner verbesserten form, der phasenkontrastmethode". In: *Physica* 1.7, pp. 689–704. ISSN: 0031-8914. DOI: [https://doi.org/10.1016/S0031-8914\(34\)80259-5](https://doi.org/10.1016/S0031-8914(34)80259-5). URL: <http://www.sciencedirect.com/science/article/pii/S0031891434802595>.
- Fontanella, J C (1985). "Wavefront sensing deconvolution and adaptive optics". In: *Journal of Optics* 16.6, p. 257. URL: <http://stacks.iop.org/0150-536X/16/i=6/a=002>.
- Gerchberg, R. W. and W. O. Saxton (1972). "A practical algorithm for the determination of phase from image and diffraction plane pictures". In: *Optik* 35.2, 237–250.
- Gonsalves, R. A. (1976). "Phase retrieval from modulus data". In: *J. Opt. Soc. Am.* 66.9, pp. 961–964. DOI: <10.1364/JOSA.66.000961>. URL: <http://www.osapublishing.org/abstract.cfm?URI=josa-66-9-961>.
- Gonsalves, Robert A. (1982). "Phase Retrieval And Diversity In Adaptive Optics". In: *Optical Engineering* 21, pp. 21–21–4. DOI: <10.1117/12.7972989>. URL: <http://dx.doi.org/10.1117/12.7972989>.
- Goodman, Joseph W. (1988). *Introduction to Fourier Optics*. Ed. by L. Cox and John M. Morris. 2nd. McGraw-Hill Companies, Inc.
- Hartmann (1900). "Bemerkungen über den Bau und die Justirung von Spektrographen". In: *Z. Instrumentenkde* 20, p. 47.
- Kolmogorov, A N (1968). "Local Strucure of Turbulence in an Incompressible Viscous Fluid at Very High Reynolds numbers". In: *Soviet Physics Uspekhi* 10.6, p. 734. URL: <http://stacks.iop.org/0038-5670/10/i=6/a=R02>.
- Mugnier, Laurent M., Amandine Blanc, and Jérôme Idier (2006). "Phase Diversity: A Technique for Wave-Front Sensing and for Diffraction-Limited Imaging". In: ed. by Peter Hawkes. Vol. 141. Advances in Imaging and Electron Physics. Elsevier, pp. 1–76. DOI: [https://doi.org/10.1016/S1076-5670\(05\)41001-0](https://doi.org/10.1016/S1076-5670(05)41001-0). URL: <http://www.sciencedirect.com/science/article/pii/S1076567005410010>.
- Noll, Robert J. (1976). "Zernike Polynomials and Atmospheric Turbulence". In: *J. Opt. Soc. Am.* 66.3, pp. 207–211. DOI: <10.1364/JOSA.66.000207>. URL: <http://www.osapublishing.org/abstract.cfm?URI=josa-66-3-207>.
- Obukhov, A. M. (1949). "Structure of the temperature field in turbulent flow". In: *Ser. Geograf. Geofiz.* 13.1, pp. 58–69.
- Paxman, Richard G., Timothy J. Schulz, and James R. Fienup (1992). "Joint estimation of object and aberrations by using phase diversity". In: *J. Opt. Soc. Am. A* 9.7, pp. 1072–1085. DOI: <10.1364/JOSAA.9.001072>. URL: <http://josaa.osa.org/abstract.cfm?URI=josaa-9-7-1072>.
- Ragazzoni, Roberto (1996). "Pupil plane wavefront sensing with an oscillating prism". In: *Journal of modern Optics* 43.2, pp. 289–293.

- Roddier, François (1988). "Curvature sensing and compensation: a new concept in adaptive optics". In: *Appl. Opt.* 27, pp. 1223–1225.
- Shack, R. V. and B. C. Platt (1971). "Production and use of a lenticular Hartmann screen". In: *Spring Meeting of the Optical Society of America*. Vol. 61, 656–660.
- Thorlabs (2017). *Principles of Spatial Filters*. Thorlabs. URL: [https://www.thorlabs.com/newgroupage9.cfm?objectgroup\\_id=1400](https://www.thorlabs.com/newgroupage9.cfm?objectgroup_id=1400).
- (2018). *Shack-Hartmann Wavefront Sensor*. Thorlabs. URL: [https://www.thorlabs.com/newgroupage9.cfm?objectgroup\\_id=2946](https://www.thorlabs.com/newgroupage9.cfm?objectgroup_id=2946).
- V.I. Tatarski, Richard A. Silverman (1961). *Wave Propagation in a Turbulent Medium*. Ed. by McGraw-Hill. McGraw-Hill.
- Wikipedia (2018). *Zernike polynomials*. Wikipedia. URL: [https://en.wikipedia.org/wiki/Zernike\\_polynomials](https://en.wikipedia.org/wiki/Zernike_polynomials).